MATRIX-ASSISTED LASER DESORPTION IONIZATION (MALDI) TANDEM MASS SPECTROMETRY (MS^n) USING A QUADRUPOLE ION TRAP

By

MATTHEW M. BOOTH

A DISSERTATION PRESENTED TO THE GRADUATE SCHOOL
OF THE UNIVERSITY OF FLORIDA IN PARTIAL FULFILLMENT
OF THE REQUIREMENTS FOR THE DEGREE OF
DOCTOR OF PHILOSOPHY

UNIVERSITY OF FLORIDA

1996

To my friends, my family, and my loving parents.

ACKNOWLEDGMENTS

I would first like to express my sincere gratitude to Dr. Rick Yost for allowing me to be a part of his research group, and for the freedom he gave me to pursue my own research ideas. He could always be counted on for critical insights into any project or for solutions to almost any problem that came up. I especially appreciate the flexibility he gave me in allowing me to work while completing my degree. I also would like to thank my committee members, Dr. Jim Winefordner, Dr. Bob Kennedy, Dr. Nigel Richards, and Dr. Sheldon Schuster, for the time they spent on my research.

Many Yost Group members were critical to the success of this project and in contributing to the fun I had working towards my degree. I first worked with Dr. Nate Yates when I came to UF, and this research eventually led to the work presented in this dissertation. I most appreciated the friendship of both him and his wife, Jan, and will never forget the camping trips in his Bus or the dinners at their apartment. Brody Guckenberger spent his first year at UF working with me on the construction of the MALDI QITMS instrument described in this dissertation. Most of the actual machine shop work required to modify the original Vestec instrument to accommodate the Finnigan QITMS was performed by him. Chris Reddick spent two years learning the fundamentals of MALDI (using a Finnigan LaserMAT TOF MS instrument), and he was of great assistance in the preparation of the samples that were analyzed for this dissertation. Scott Quarmby provided help in both the construction of the instrument and in discussions on both ion trap theory and data interpretation.

I would also like to credit several support personnel at UF who made it possible for me to work full-time at Environmental Science & Engineering while performing most of the research that went into this dissertation. Jeanne Karably and Donna Balkcom

were critical in helping me be at the right place at the right time with the right form in order to graduate. Joe Shalosky was the machine shop supervisor (although mechanical artist is probably a better title for him) who had a very large part in the construction of all instruments I had a part in while at UF. Most of the instruments I designed and constructed while at UF would not have even been attempted if Joe had not been there to make a critical part or supply some much needed advice on how best to make something. I must also thank Dr. David Powell for allowing me to work for him for a year in the chemistry department mass spectrometry laboratory. He was also always there when I needed someone to talk to (even if it was only ESE gossip).

I also need to thank my collaborator and good friend, Dr. Jim Stephenson. I never would have even considered returning to school to earn a Ph.D. if Jim had not blazed the trail for me. After three years with Finnigan, then four years at the University of Florida, we have been through a lot together. It is no exaggeration to say that none of this would have been possible without his help and encouragement. Thanks go to him and his wife, Tracy, these were the best times of my life.

Finally, I wish to thank my wife, Pauline, and son, Christopher, for the love and support they have given me. They truly are the most precious things that have every come into my life. I could not have done it without them!

TABLE OF CONTENTS

page

ACKNOWLEDGEMENTS iii

LIST OF TABLES vii

LIST OF FIGURES viii

ABSTRACT xiii

CHAPTERS

1. INTRODUCTION 1

Matrix-Assisted Laser Desorption Ionization (MALDI) 2
MALDI Matrices 4
MALDI Sample Preparation 6
Time-of-Flight Mass Spectrometers 8
Mass Resolution in MALDI TOF MS 11
The Quadrupole Ion Trap Mass Spectrometer 19
Fundamental Principles of Quadrupole Ion Trap Operation 19
Resonance Excitation and Resonance Ejection 26
Mass Range Extension in the Quadrupole Ion Trap Mass Spectrometer 27
MALDI Using a Quadrupole Ion Trap Mass Spectrometer 37
MALDI QITMS Using an External Ion Source 46
Overview of Dissertation 49

2. INSTRUMENTAL DESIGN AND CHARACTERIZATION OF A MALDI QUADRUPOLE ION TRAP MASS SPECTROMETER 55

Instrument Design 55
Instrument Simulation 64
Instrument Characterization 64
MALDI QITMS of a Synthetic Tetrapeptide (MRFA) 66
MALDI QITMS of Angiotensin II 72
Summary 87

3. THE ANALYSIS OF PHARMACEUTICAL COMPOUNDS USING A MALDI QUADRUPOLE ION TRAP MASS SPECTROMETER..... 88

Introduction..... 88
MALDI QITMS for the Structural Determination of Spiperone..... 88
Taxol (paclitaxel) and Cancer..... 99
MALDI QITMS and MS^2 of Taxol..... 103
MALDI QITMS for the Determination of Taxol in Rat Liver Tissue.. 107
Summary..... 108

4. CONCLUSIONS AND FUTURE WORK..... 114

REFERENCE LIST..... 117

BIOGRAPHICAL SKETCH..... 122

LIST OF TABLES

Table		page
2-1.	Scan table listing for the MALDI QITMS analysis of the synthetic tetrapeptide MRFA.	71
2-2.	Scan table listing for the MALDI QITMS analysis of angiotensin II.	79
3-1.	Scan table listing for the MALDI QITMS analysis of spiperone.	93

LIST OF FIGURES

Figure		page
1-1.	Representation of the MALDI process.	3
1-2.	Typical MALDI matrices used with a nitrogen laser.	5
1-3.	SEM micrograph of cytochrome C in a dihydroxybenzoic acid (DHB) matrix.	7
1-4.	MALDI TOF MS for the direct analysis of 14 salivary proteins.	9
1-5.	Linear Time-of-Flight Mass Spectrometer (TOF MS) used for MALDI analysis.	10
1-6.	MALDI TOF MS spectrum of Glucose Isomerase.	12
1-7.	MALDI TOF MS spectrum for a mixture of human and insulin mutants.	13
1-8.	Factors affecting the mass resolution in a TOF mass analyzer.	15
1-9.	Initial translational kinetic energy distributions for polypeptide ions.	17
1-10.	Reflectron Time-of-Flight Mass Spectrometer (TOF MS) used for MALDI analysis.	18
1-11.	Quadrupole Ion Trap Mass Spectrometer.	20
1-12.	Mathieu stability diagram for the quadrupole ion trap. Shaded region represents stable region of a,q values. Black circles indicate ions of successively higher mass lined up along the a=0 line.	23
1-13.	Diagram of the mass-selected instability scan (scan function) showing the RF amplitude as a function of time.	25
1-14.	Photograph of 20 μm aluminum particles in a quadrupole ion trap.	29
1-15.	Mathieu stability diagram, showing the point on the diagram where instability occurs when no axial modulation is used.	32

1-16. Scan function and ion signal for the mass-instability mode of operation where no axial modulation is used. Ejection corresponds to a q_{eject} of 0.908. 33

1-17. Mathieu stability diagram, showing the point on the diagram where instability occurs when using three different axial modulation frequencies to lower the q_{eject}. 34

1-18. Scan function and ion signal for the mass-instability mode of operation when using axial modulation to lower the q_{eject} to 0.906. This value corresponds to point A on figure 1-16. 35

1-19. Scan function and ion signal for the mass-instability mode of operation when using axial modulation to lower the q_{eject} to 0.454. This value corresponds to point B on figure 1-16. 36

1-20. Scan function and ion signal for the mass-instability mode of operation when using axial modulation to lower the q_{eject} to 0.0908. This value corresponds to point C on figure 1-16. 38

1-21. Relationship between the axial modulation frequency used during the mass analysis scan and the maximum detectable mass. 39

1-22. Instrumental configuration for performing MALDI inside of an ion trap. 41

1-23. MALDI QITMS spectrum of bovine insulin performed inside of the ion trap. 42

1-24. a). Laser desorption ionization (LDI) and b). MALDI QITMS spectra of spiperone performed inside of the ion trap. 44

1-25. MS/MS daughter spectrum of protonated spiperone 45

1-26. MALDI QITMS analysis of spiperone in a Matrigel matrix. 47

1-27. External ion source MALDI QITMS instrument using a modified GC ion source. 48

1-28. MALDI QITMS spectrum of bovine insulin using an external ion source. 50

1-29. MALDI QITMS spectrum of egg albumin using an external ion source. 51

1-30. MALDI QITMS instrument constructed at The Rockefeller University. 52

1-31. MALDI QITMS spectrum of bradykinin using the instrument constructed at The Rockefeller University. 53

2-1. Simulation of MALDI-produced egg albumin ions (m/z 43300) for the instrument used by Bier et al. Initial energy for this simulation was 126 eV, initial angle was 0 degrees, grid spacing was 0.05 mm/grid 57

2-2. Simulation of MALDI-produced egg albumin ions (m/z 43300) for the instrument used by Bier et al. Initial energy for this simulation was 126 eV, initial angle was 1 degree, grid spacing was 0.05 mm/grid 58

2-3. Simulation of MALDI-produced bovine insulin ions (m/z 5730) for the instrument used by Bier et al. Initial energy for this simulation was 17 eV, initial angle was 1 degree, grid spacing was 0.05 mm/grid 59

2-4. Vestec ResearcH™ MALDI TOF MS instrument used for this research. 61

2-5. MALDI QITMS instrument built for this research 62

2-6. SIMION simulation for bovine insulin using the design for the MALDI QITMS instrument built for this research. 65

2-7. MALDI QITMS spectrum for 20 pmol of the synthetic peptide MRFA. 68

2-8. Comparison of the MALDI analysis of MRFA on a). a Finnigan LaserMAT TOF MS instrument and b). on the MALDI QITMS instrument constructed for this research. 69

2-9. Scan function used for the MALDI QITMS analysis of the synthetic tetrapeptide MRFA. 70

2-10. MALDI QITMS spectrum for 20 pmol of angiotensin II. 74

2-11. Mechanism for the formation of the y_7^+ ion for angiotensin II. 75

2-12. Mechanism for the formation of the b_8^+ ion for angiotensin II. 76

2-13. Scan function used for the MALDI QIT MS/MS analysis of angiotensin II. 78

2-14. Sequential steps in the forward-and-reverse scan isolation procedure. 81

2-15. a). Mass-isolated MALDI QITMS specum ($[M + H]^+$ ion) for 20 pmol of angiotensin II, and b). MS/MS spectrum for this ion. 82

2-16. a). Mass-isolated MALDI QITMS specum ($[M + H]^+$ ion) for 20 pmol of angiotensin II, b). MS/MS spectrum for this ion, and c). MS/MS for the mass-isolated b_8^+ ion (MS^3 spectrum for the $[M + H]^+$ ion of angiotensin II). 84

2-17. a). Mass-isolated MALDI QITMS specum ($[M + H]^+$ ion) for 20 pmol of angiotensin II, b). MS/MS spectrum for this ion, and c). MS/MS for the mass-isolated y_7^+ ion (MS^3 spectrum for the $[M + H]^+$ ion of angiotensin II). 86

3-1. Spiperone, M.W. 395. 89

3-2. MALDI QITMS spectrum for 20 pmol of spiperone. 90

3-3. Scan function used for the MALDI QIT MS/MS analysis of spiperone 85

3-4. Stability diagram showing the path (-----) taken by the $[M + H]^+$ ion of spiperone during the two-step isolation sequence. 94

3-5. a). Mass-isolated MALDI QITMS spectrum ($[M + H]^+$ ion) for 20 pmol of spiperone, and b). MS/MS spectrum for this ion. 95

3-6. Possible fragments that produce the daughter ions seen in the spectrum for spiperone. 96

3-7. Series of mass-isolated spectra from the MS^n analysis of spiperone. 97

3-8. Possible fragment ions produced from the MS^n analysis of spiperone 100

3-9. Taxol (paclitaxel), M.W. 853. 101

3-10. MALDI QITMS spectrum for 20 pmol of Taxol. 104

3-11. a). Mass-isolated MALDI QITMS specum ($[M + H]^+$ ion) for 20 pmol of Taxol, and b). MS/MS spectrum for this ion. 106

3-12. MALDI QITMS spectrum for a thin slice of rat liver tissue incubated with Taxol. 109

3-13. Blow-up of four regions for the MALDI QITMS spectrum for a). a thin slice of rat liver tissue incubated with Taxol and b). 20 pmol Taxol standard. 110

3-14. a). The MALDI QITMS spectrum and b). MS/MS spectrum of Taxol incubated in a thin slice of rat liver tissue. 111

3-15. MALDI QIT MS/MS spectrum of Taxol in a). a standard and b). a thin slice of rat liver tissue incubated with Taxol. 112

Abstract of Dissertation Presented to the Graduate School
of the University of Florida in Partial Fulfillment of the
Requirements for the Degree of Doctor of Philosophy

MATRIX-ASSISTED LASER DESORPTION IONIZATION (MALDI) TANDEM MASS SPECTROMETRY (MS^n) USING A QUADRUPOLE ION TRAP

By

Matthew M. Booth

December 1996

Chairperson: Richard A. Yost
Major Department: Chemistry

The specific aim of this study was to develop a quadrupole ion trap mass spectrometer using a matrix-assisted laser desorption ionization (MALDI) source. Currently, mass analysis of MALDI-generated ions is most often performed using a time-of-flight (TOF) mass spectrometer due to its ability to record an entire spectrum for every laser shot, as well as its high mass range and simplicity. The major drawbacks for this type of mass analyzer are its poor mass resolution and lack of practical tandem mass spectrometric capabilities. By using a quadrupole ion trap, unit mass resolution for low-mass ions can be achieved, and tandem mass spectrometry can be performed for structural determination.

For this research, a Vestec ResearcH™ MALDI TOF instrument was modified by placing a quadrupole ion trap immediately after the MALDI source. An exit tube lens and dynode/electron multiplier were placed behind the exit endcap of the ion trap for ion detection. Finnigan ITS40™ electronics and Gatorware software (developed in our laboratory at the University of Florida) were used to control the ion trap for this

instrument. The commerically available Vestec system was chosen because it was designed specifically for MALDI TOF analyses.

The MALDI QITMS instrument designed and constructed for this research was used for the analysis of biological and pharmaceutical compounds. Two peptides (MRFA, a synthetic tetrapeptide, and Angiotensin II, an octapeptide) were analyzed to characterize the performance of this instrument and to demonstrate its utility for the analysis of peptides. The capability of this instrument for providing structural information using tandem mass spectrometry was demonstrated by performing MS^6 on Spiperone, an antipsychotic drug developed by Bristol-Meyers Squibb. Finally, the anticancer drug Taxol was analyzed in an incubated rat liver tissue sample to demonstrate the ability of MS^n for the detection of target compounds in the presence of a large number of interfering species.

CHAPTER 1
INTRODUCTION

It has traditionally been very difficult to generate intact gas-phase molecular ions from compounds that are large, polar, and/or thermally labile since they are usually solids and degrade or decompose when being exposed to thermal heating.[1] The vaporization and ionization that are required to perform a mass spectrometric analysis of these compounds demand a method of energy transfer to the material which is fast enough to avoid thermal degradation. Until 1988, the most successful methods of desorbing these sensitive compounds were secondary ion mass spectrometry (SIMS), which uses keV ions for desorption and ionization; fast atom bombardment (FAB), which uses keV neutral atoms; plasma desorption (PDMS) which uses MeV particles from the decay of radioactive compounds; and laser desorption (LDMS) which uses nanosecond-pulsed high-power laser beams.

Although lasers had been used for the desorption of organic ions, all early experiments revealed an upper limit to the size of molecules that could be desorbed as intact ions. This limit, which depends on molecular structure and laser parameters, was approximately 1000 Da for biopolymers and up to 9000 Da for synthetic polymers.[2] The laser desorption of molecules can occur either resonantly or nonresonantly. In the case of resonant desorption, the direct resonant excitation of the analyte molecules also puts energy into photodissociation channels. For nonresonant desorption, the high irradiances required for desorption occur very close to the point of plasma generation, which also destroys large organic molecules.

Matrix-Assisted Laser Desorption Ionization (MALDI)

In 1985, the Hillenkamp research group at the University of Frankfurt tried to use a matrix to circumvent this problem, and first used the term matrix assisted laser desorption ionization (MALDI). In MALDI, the analyte is mixed with a large excess of either a solid or liquid matrix consisting of a small, highly absorbing species. Resonant desorption of the matrix occurs, with the entrained analyte also being desorbed. Since it is the matrix that interacts directly with the laser energy, the analyte molecules are spared from the excessive energy that would lead to their decomposition.[3] This also produces a dilution of the analyte molecules which prevents associations that would otherwise lead to complexes of masses too large to be desorbed and analyzed.

Using various matrices (most notably sinapinic acid), they showed the MALDI time-of-flight mass spectrum of a dipeptide, Trp-Trp (M.W. 390) in 1985, Gramicidin (M.W. 1900) in 1987 (at the University of Munster), bovine albumin (M.W. 67,000) in 1988, β-D-galactosidase (M.W. 116,900) in 1989, and cluster ions of a monoclonal antibody (M.W. 300,000) in 1990.[4-5]

In MALDI, the matrix molecules absorb the energy from the laser pulse and transfer it into excitation energy of the solid system (Figure 1-1).[6] A supersonic plume of matrix with entrained analyte is formed with a velocity of approximately 750 m/s (at the threshold energy). Rapid adiabatic cooling of the expanding dense gas plume occurs. Radical molecular ion intermediates of the matrix are formed by photoionization in the condensed phase. Collisions of highly excited matrix molecules and ground-state analyte molecules occur within the first tens of nanoseconds in the solid state or in the high-density intermediate state of the desorbing material cloud just above the surface, leading to even-electron quasi-molecular ions produced by proton transfer.

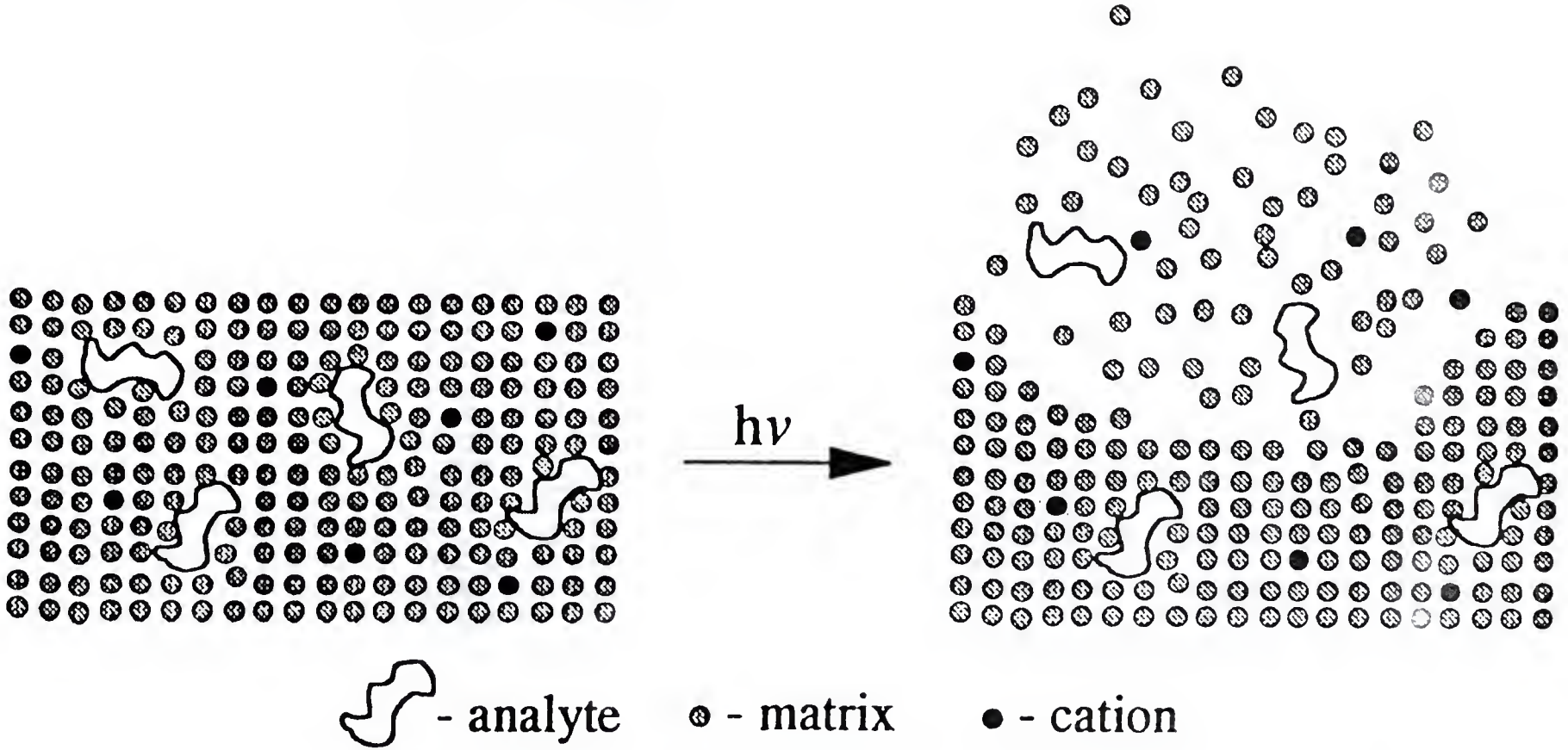

Figure 1-1. Representation of the MALDI process. After the sample containing the analyte and matrix is irradiated by a laser pulse (hv), a supersonic plume is formed.[3]

MALDI Matrices

In order for a matrix to be usable for MALDI, it must have several characteristics [7]:

1) The compound must strongly absorb the wavelength of the laser light. Using a nitrogen laser ($\lambda = 337$ nm), the molar absorptivity (ε) should be greater than 1000 L cm^{-1} mol^{-1}. Most of the compounds that are currently used as MALDI matrices when using a nitrogen laser contain a phenolic hydroxy group and a carbonyl function on an aromatic ring (Figure 1-2).
2) The matrix must contain -OH or -NH bonds for protonation. The excited state acidity of the matrix is involved in the MALDI analyte formation process.
3) The matrix and analyte must be soluble in the same solvent and should crystallize together (a matrix-isolated crystal containing the analyte must form).
4) The matrix must be stable under the vacuum conditions in the ion source of the mass spectrometer.
5) The matrix preferably does not form a large number of cluster ions or adduct ions with the analyte.

Although any compound that can perform a proton transfer under UV-irradiation is actually usable as a matrix for UV-MALDI MS, only a select few are used on a routine basis. The only differences that many matrices exhibit are in sensitivity, resolution, tendency to form adduct ions, and the solvent system. Furthermore, although it is possible to predict whether a candidate matrix material will absorb efficiently at the laser wavelength, it is not possible to predict if a compound will form a homogeneous solid (or liquid) solution with a given analyte molecule, particularly in the presence of ionic contaminants.

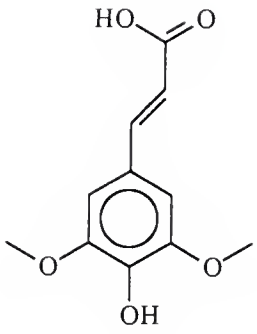

Sinapinic Acid

ε_{337}= 14600

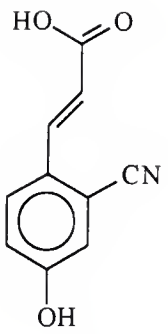

α-Cyano-4-hydroxy-cinnamic acid

ε_{337}= 21875

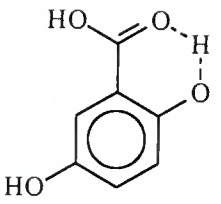

2,5-Dihydroxy-benzoic acid

ε_{337}= 4250

Figure 1-2. Typical MALDI matrices used with a nitrogen laser.[7]

MALDI Sample Preparation

Typical sample preparation for MALDI analysis is a very simple procedure:

1) Matrix solution: Make a saturated solution (5 to 10 g/L) of the matrix material in either pure water or a water/organic (ethanol, acetonitrile) solvent. Add 0.1% trifluoroacetic acid (TFA) to the solution for proteins with low solubility in water.
2) Sample solution: Make a 10^{-5} to 10^{-6} M aqueous solution of the analyte.
3) Add 5 uL of the matrix solution and 5 uL of the sample solution to a microcentrifuge tube and vortex. Add 1 uL of this mixture to the probe tip. Let this sample mixture dry at room temperature.

Using this preparation scheme, the typical sample amount loaded on the probe tip is in the range of 1 pmol or less, with the actual amount desorbed being in the amol range. In the case of sinapinic acid, care has to be taken to protect the matrix solution from light and to avoid heating in the evaporation step. Dried sinapinic acid preparations can furthermore be cleaned from precipitated water-soluble contaminants such as inorganic salts by immersing the dried sample in cold distilled water.

Depending on the matrix and the solvent used, the microscopic structure of the preparations may vary between rather homogeneous amorphous layers, a dense packing of tiny crystallites (e.g. sinapinic acid), or relatively large crystal needles grown from the rim of the droplet (e.g. Figure 1-3, showing an SEM micrograph of cytochrome C in a dihydroxybenzoic acid, DHB, matrix).[8] The most intense ion signals are usually associated with regions of the sample that appear crystalline, although this result depends on the matrix substance and the presence of buffers or detergents in the analyte sample.

A key feature of MALDI first noted by Beavis and Chait is that commonly used biological buffering agents, salts, and denaturants (for example phosphate, sodium, and

Figure 1-3. SEM micrograph of cytochrome C in a dihydroxybenzoic acid (DHB) matrix.[8]

urea) at concentrations up to several hundred millimolar do not have to be removed from the sample prior to analysis.[9-10] It is thought that crystallization of the matrix and analyte molecules occurs but not of water-soluble contaminants, which may explain the capability of some matrices to tolerate even a high excess of contaminants. This tolerance to contaminants is in direct contrast to all other MS techniques presently in use for the analysis of biological molecules. The ability to avoid purification prior to MS analysis is highly advantageous because a great deal of time and material is often lost at this step. As an example of the ability to analyze samples using MALDI without prior purification, Nelson and Vestal of Vestec Corp detected 14 proteins present in the direct analysis of a salivary sample (Figure 1-4).[11] Although MALDI is highly tolerant of many contaminants, sodium dodecylsulfate (SDS) contained in the sample can lead to a total quenching of the protein ion production and must be removed prior to the sample preparation.

Time-of-Flight Mass Spectrometers

MALDI has been used almost exclusively with time-of-flight (TOF) mass analyzers, which can record all of the ions from each ionization event and thus offer the possibility for higher sensitivity than scanning instruments. TOF mass spectrometers are relatively simple, inexpensive instruments with high sensitivity and virtually unlimited mass range. In a MALDI TOF mass spectrometer using a linear flight tube (Figure 1-5),[12] ions are formed in a short source region (s) by a pulse of laser light absorbed by the sample.[13] A positive voltage (V) placed on the backing plate imposes an electric field (E V/s) across the source region, which accelerates all of the ions to approximately the same kinetic energy. As the ions pass through the extraction grid they have velocities which depend inversely upon the square root of their mass. The ions then pass through a much

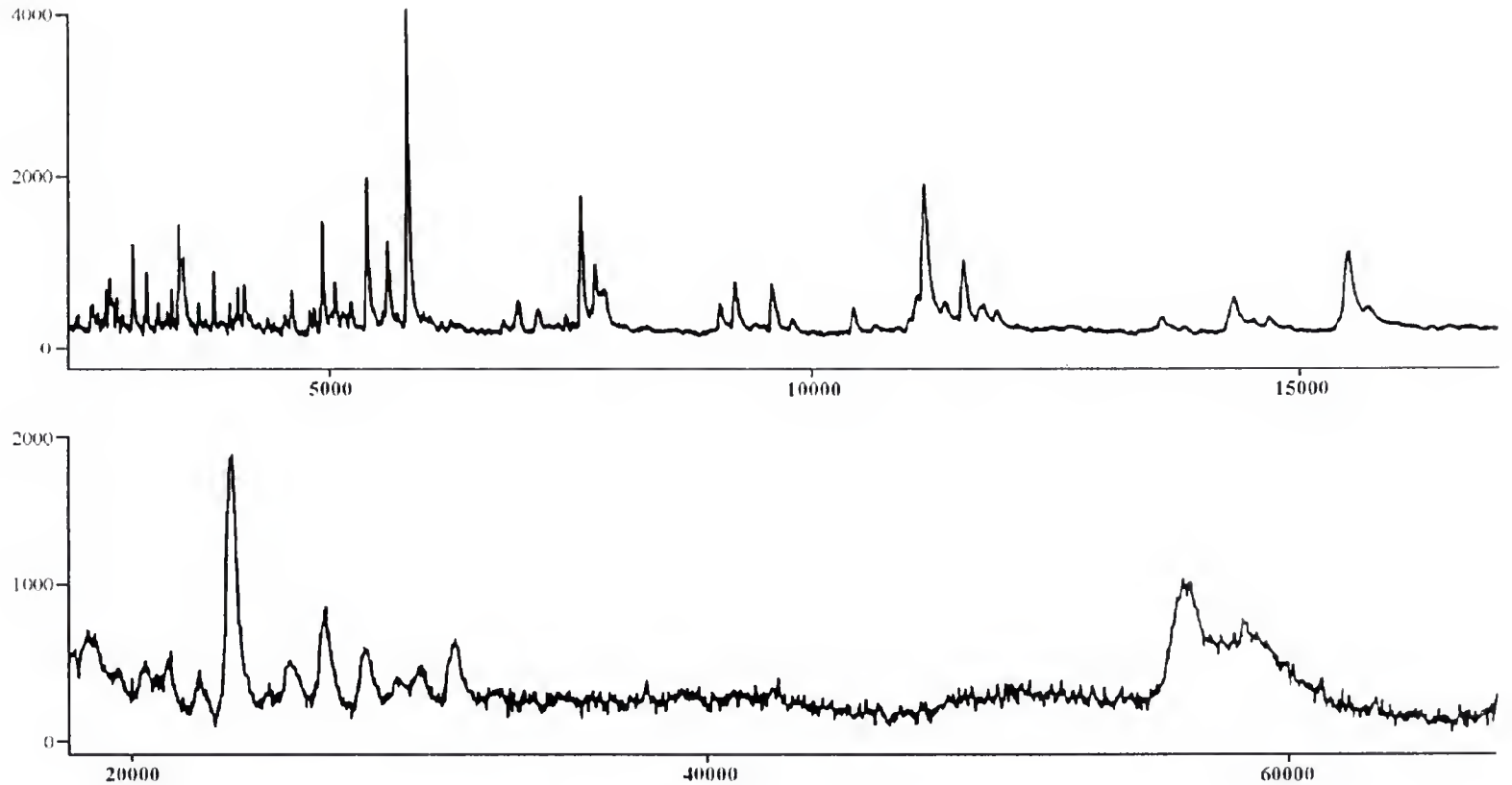

Figure 1-4. The MALDI Time-of-Flight Mass Spectrum of 14 salivary proteins.[11]

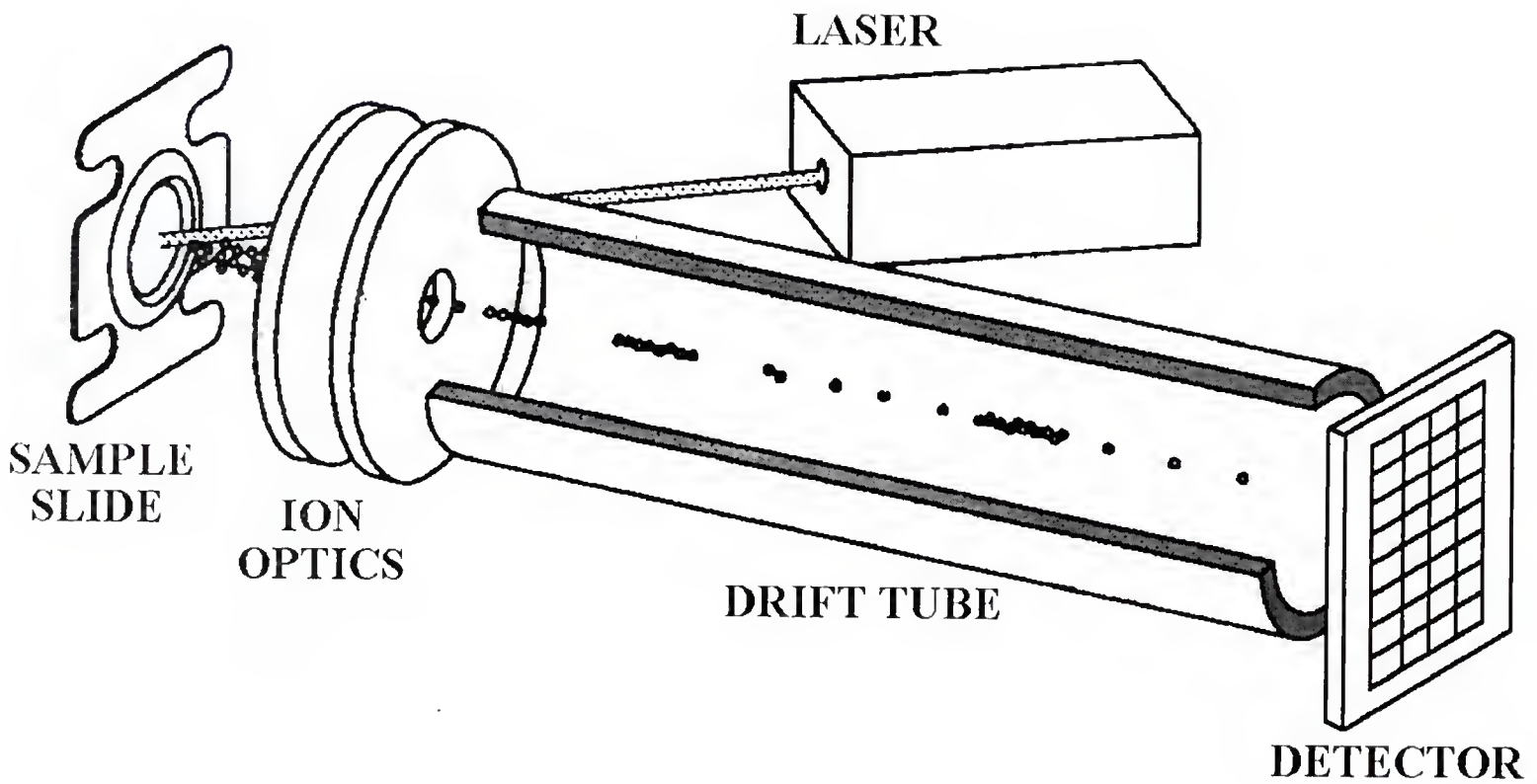

Figure 1-5. Linear Time-of-Flight Mass Spectrometer (TOF MS) used for MALDI analysis.[12]

longer drift region (D, typically 0.5 to 2 m) and arrive at the front plane of the detector. Because they spend most of their time in the drift region, their flight time measured at the detector is approximately $t = (m/2zeEs)^{1/2} D$. This time spectrum is then converted to a mass spectrum using a mass calibration routine.

Results for the analysis of glucose isomerase (Figure 1-6) show the typically simple spectra obtained when using MALDI, consisting predominately of $[M + H]^+$ and $[M + 2H]^{2+}$ ions.[14] Fragmentation of molecular ions due to the cleavage of covalent bonds in the protein backbone is not apparent from the spectra. Structural information from systematic fragmentations cannot be obtained directly (by fragment ion desorption), but can be obtained by taking advantage of metastable decay reactions. The ionization step seems to be extremely soft and no fragments are typically observed. The absence of fragment ions and the dominance of singly and doubly protonated intact protein ions make the interpretation of such spectra particularly straightforward.

Mass Resolution in MALDI TOF MS

In any mass spectrometer, mass resolution is defined as the separation of peaks of different masses (Δm) relative to the mass of interest (or more commonly, $m/\Delta m$).[15] The rather poor mass resolution obtained in MALDI TOF MS of large compounds has been realized as a drawback of the method from the very beginning.[16] This leads to an inability to resolve neighboring molecular ion signals in the high mass range and can lead to poor mass accuracy. The precision attainable by mass determination is limited, since peak broadening cannot be assumed to be absolutely reproducible, independent of substance and homogeneous. The importance of mass accuracy and resolution is demonstrated in Figure 1-7, where a mixture of human insulin and insulin mutants was

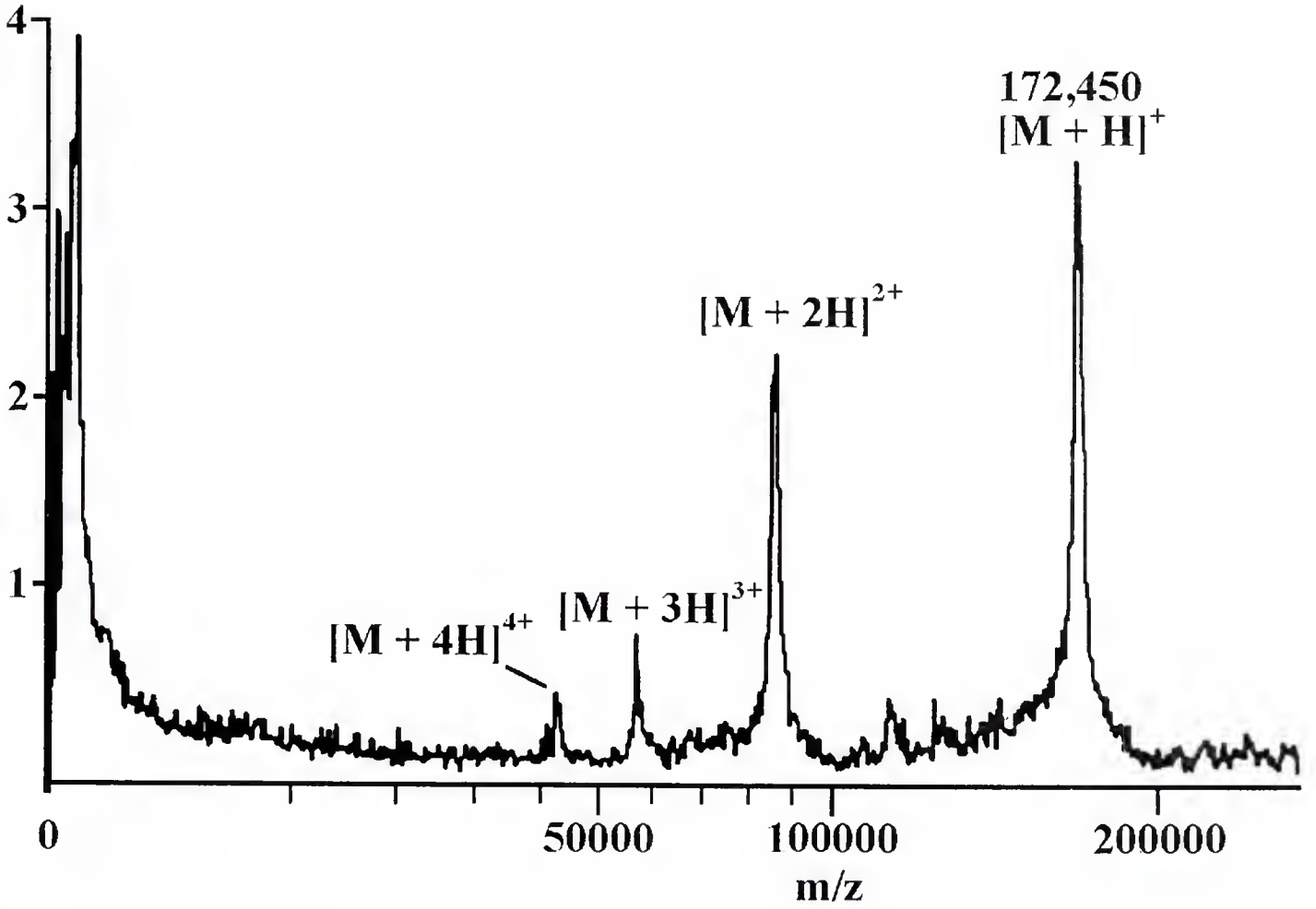

Figure 1-6. MALDI Time-of-Flight mass spectrum of Glucose Isomerase.[14]

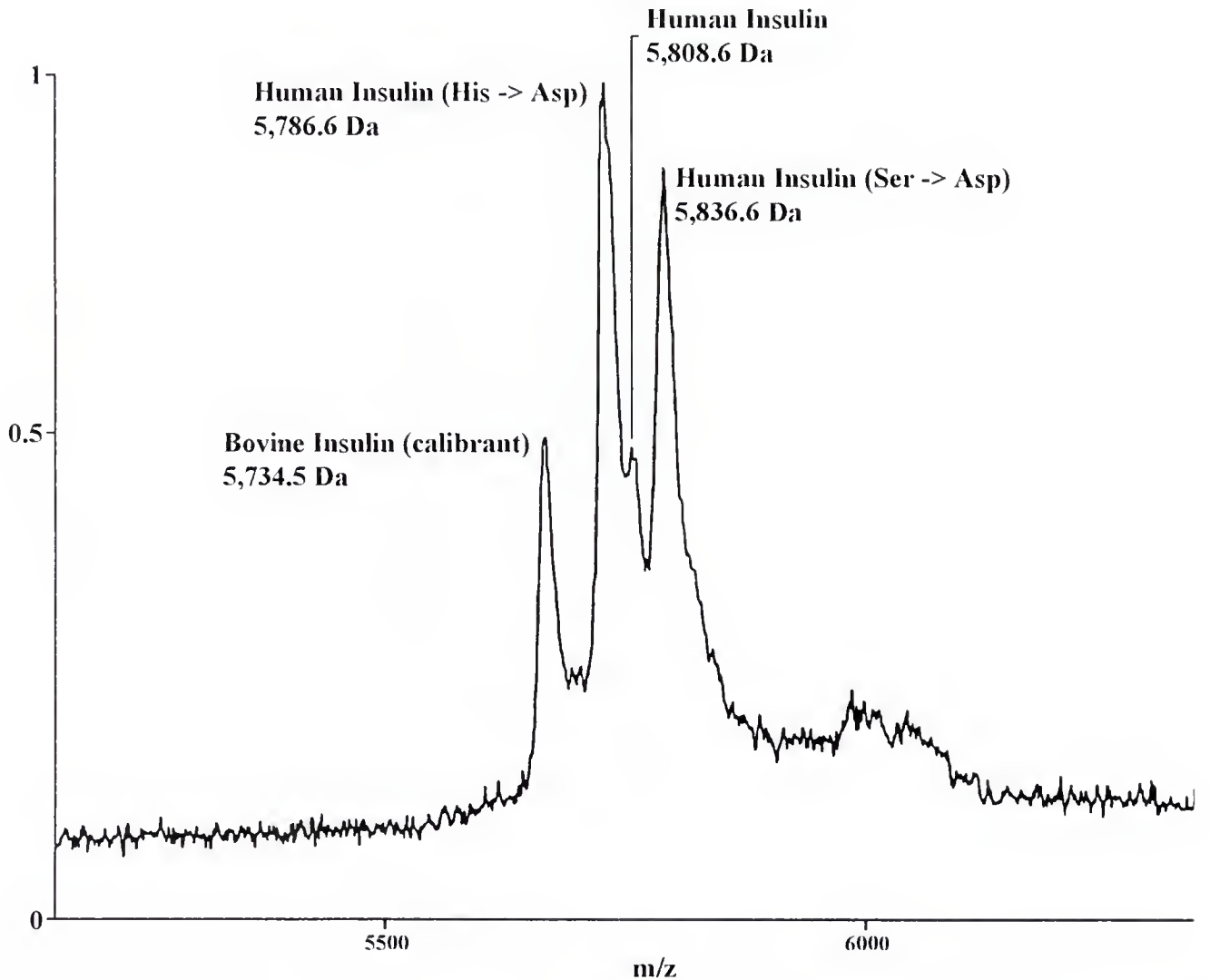

Figure 1-7. MALDI Time-of-Flight mass spectrum of a mixture of human and insulin mutants (Vestec Corporation, personal communication, 1993).

analyzed (Vestec Corporation, Personal Communication, 1993). Typical mass resolutions of $m/\Delta m$ = 600-1000 for linear TOF systems are observed, but the resolution degrades with mass (e.g. $m/\Delta m$ = 50 at m/z 75,000).

In a TOF mass spectrometer, peak widths (Δt) are determined by uncertainties in the temporal, spatial, and initial kinetic energy distributions. Each of these will now be discussed [17]:

Temporal distribution: A temporal distribution occurs when two ions of the same mass and initial kinetic energy are formed at different times in the ion source (Figure 1-8a). Because the ions have the same velocities, the time interval remains constant as they exit the drift tube and are recorded by the detector. For MALDI, ions desorb off of the probe surface within 20 μs.[18]

Spatial distribution: A spatial distribution occurs when ions of the same mass are formed at the same time with the same initial kinetic energy, but are formed in different locations in the extraction field (Figure 1-8b). Ions that are formed near the back of the source will be accelerated to higher kinetic energy than ions formed closer to the extraction grid. The ions formed at the rear of the source enter the drift region later, but have larger velocities so that they eventually pass the ions formed closer to the extraction grid and arrive at the detector sooner. For desorption techniques like MALDI, in which ions are formed from a smooth conducting surface parallel to the extraction grid rather than in the gas phase, the spatial distribution is greatly minimized.

Initial kinetic energy distribution: Ions formed with different initial kinetic energies will have different final velocities after acceleration and arrive at the detector at different times (Figure 1-8c). This is the most difficult initial condition to correct in a linear instrument, since increases in drift length increase peak widths along with the separation of peaks of different mass. Beavis and Chait[19] determined the velocity and translational kinetic energy distributions for polypeptide ions produced by MALDI. Using three

a). Temporal Distribution

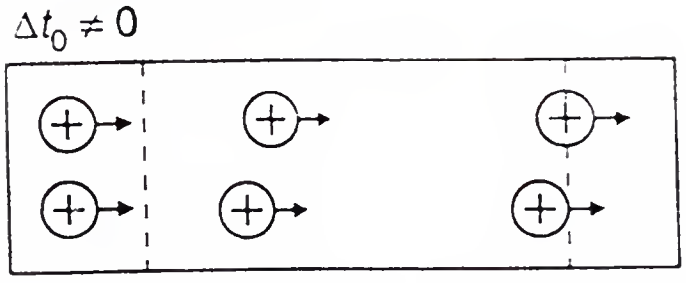

b). Spatial Distribution

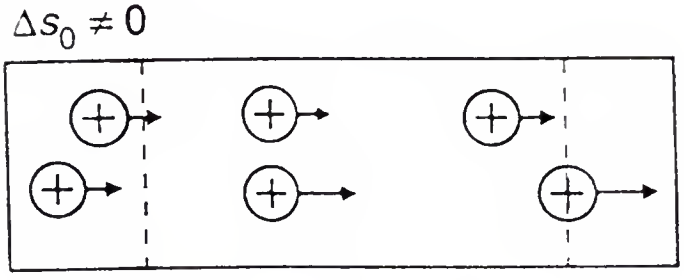

c). Kinetic Energy Distribution

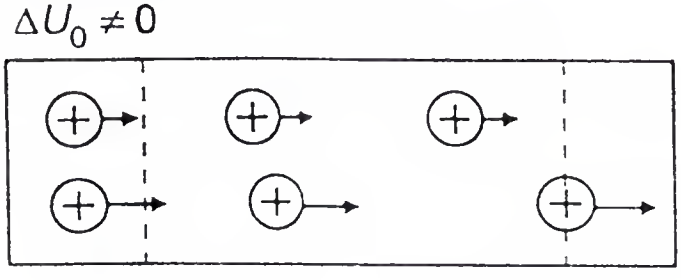

Figure 1-8. Factors affecting the mass resolution in a TOF mass analyzer.[17]

different polypeptides (angiotensin, M.W. 1030; insulin, M.W. 5730; and superoxide dismutase, M.W. 15590), they determined that these molecules all had very similar initial velocity distributions, independent of the molecule's mass, centered at approximately 750 m/s. Using this value as the most probable initial velocity, the average initial translational kinetic energies for polypeptide ions are directly proportional to the molecular mass

$$KE_{avg}\,(eV) = 0.003 * \text{mass (u)}$$

The initial translational kinetic energy distributions for the three polypeptide ions studied by Beavis and Chait are shown in Figure 1-9. For insulin, the average initial translational kinetic energy is 17 eV, with a distribution ranging from 5 eV to 25 eV. This large spread in initial translational kinetic energy is the limiting factor in the resolving power of a linear TOF mass spectrometer.

In order to deal with the initial translational kinetic energy distributions that lead to a reduction in mass resolution in linear time-of-flight mass spectrometers, a different geometry TOF MS was introduced by Mamyrin and coworkers in the early 1970s.[20] This instrument, called a Reflectron (Figure 1-10), incorporates a region containing both decelerating and reflecting electric fields. When ions having the same m/z ratio but different velocities enter the electric field region, those with a higher velocity (because of their higher initial kinetic energy) will penetrate further into the decelerating field before reflection than will those with lower velocities. By choosing appropriate reflection voltages, the fast and slow ions will reach the detector together, which will optimize the energy resolution.

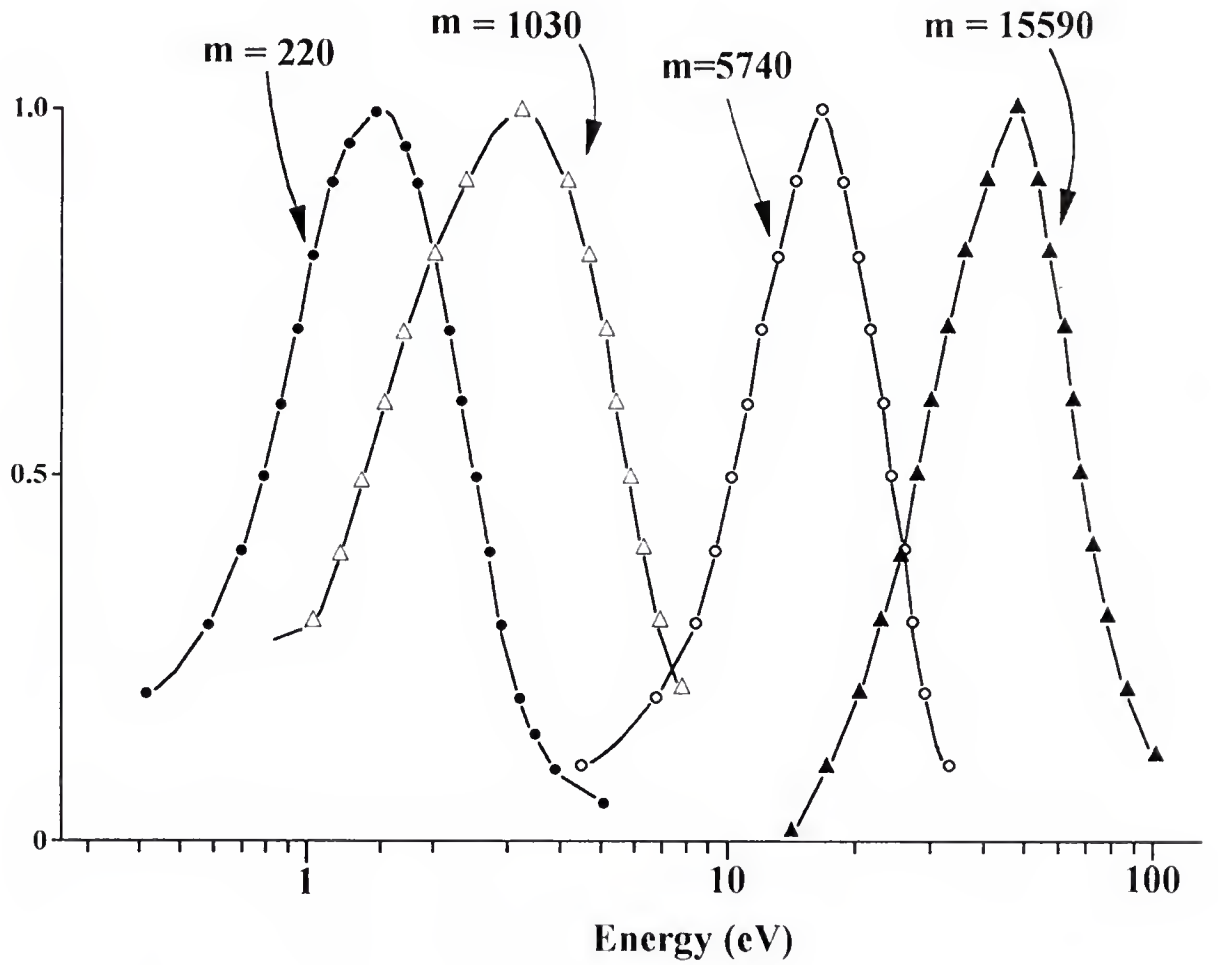

Figure 1-9. Initial translational kinetic energy distributions for polypeptide ions.[19]

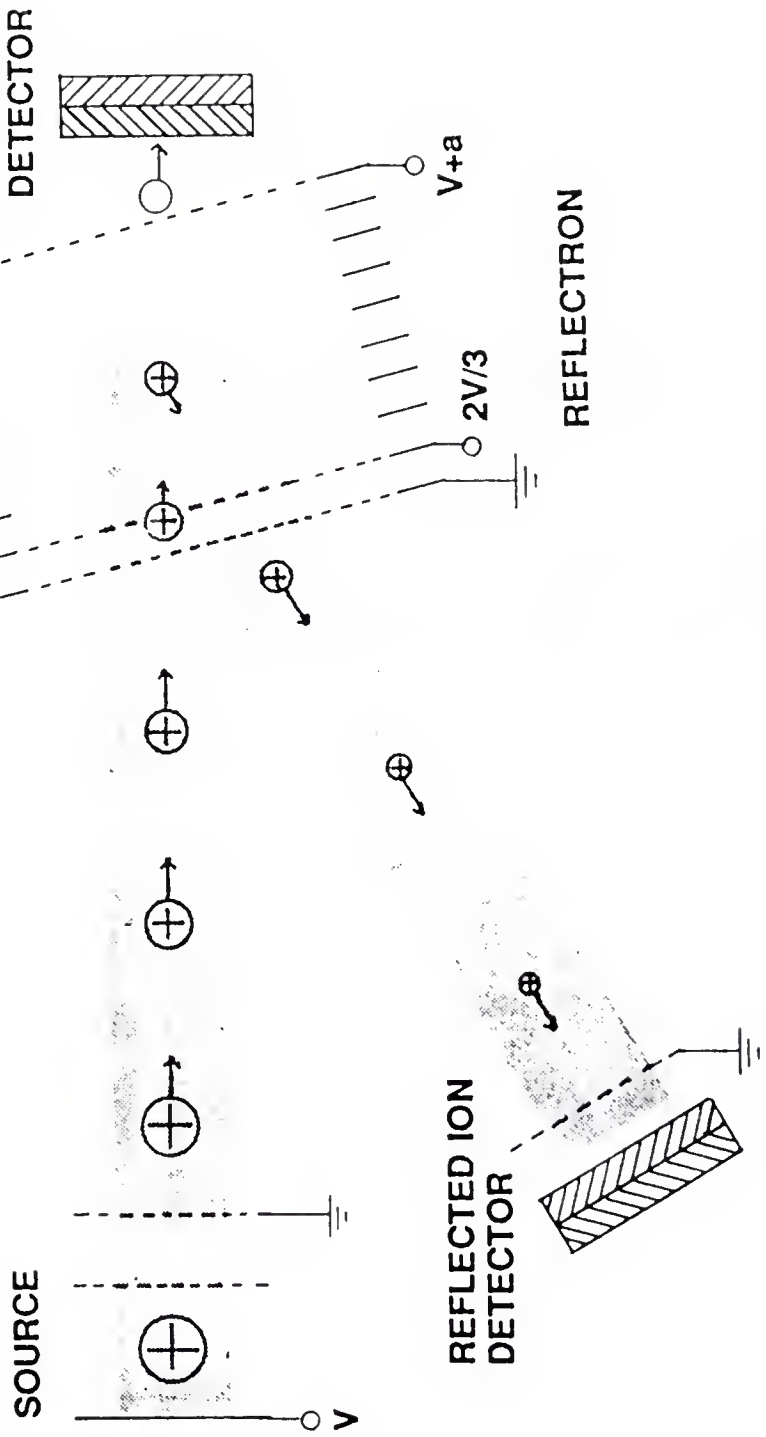

Figure 1-10. Reflectron Time-of-Flight Mass Spectrometer (TOF MS) used for MALDI analysis.[20]

The Quadrupole Ion Trap Mass Spectrometer

In 1953 Wolfgang Paul and his coworkers at the University of Bonn in Germany first described both the quadrupole mass filter and its three-dimensional analog, the quadrupole ion trap.[21] While the quadrupole mass filter has become the most common analyzer employed for mass spectrometry, until the 1980s the quadrupole ion trap was only used by chemists and physicists to study trapped ions. The first commercial quadrupole ion trap was introduced by Finnigan Corp. in 1984 as an inexpensive and sensitive mass spectrometric detector for gas chromatography. This instrument was based on a new method developed by George Stafford and his coworkers at Finnigan for selectively ejecting ions of increasing mass-to-charge ratio from the ion trap, known as mass-selective instability. The following discussion of the fundamental principles of the quadrupole ion trap is adapted from March and Hughes, 1989 (unless otherwise noted).[22]

Fundamental Principles of Quadrupole Ion Trap Operation

The quadrupole ion trap (Figure 1-11) consists of three electrodes of hyperbolic cross section: a central ring electrode and two endcap electrodes. The general mathematical equations used for the construction of the ring and endcap electrodes for a quadrupole ion trap are given by

$$\frac{1}{r_o^2}(r^2 - 2z^2) = 1 \qquad (1\text{-}1)$$

$$\frac{1}{2z_o^2}(r^2 - 2z^2) = -1 \qquad (1\text{-}2)$$

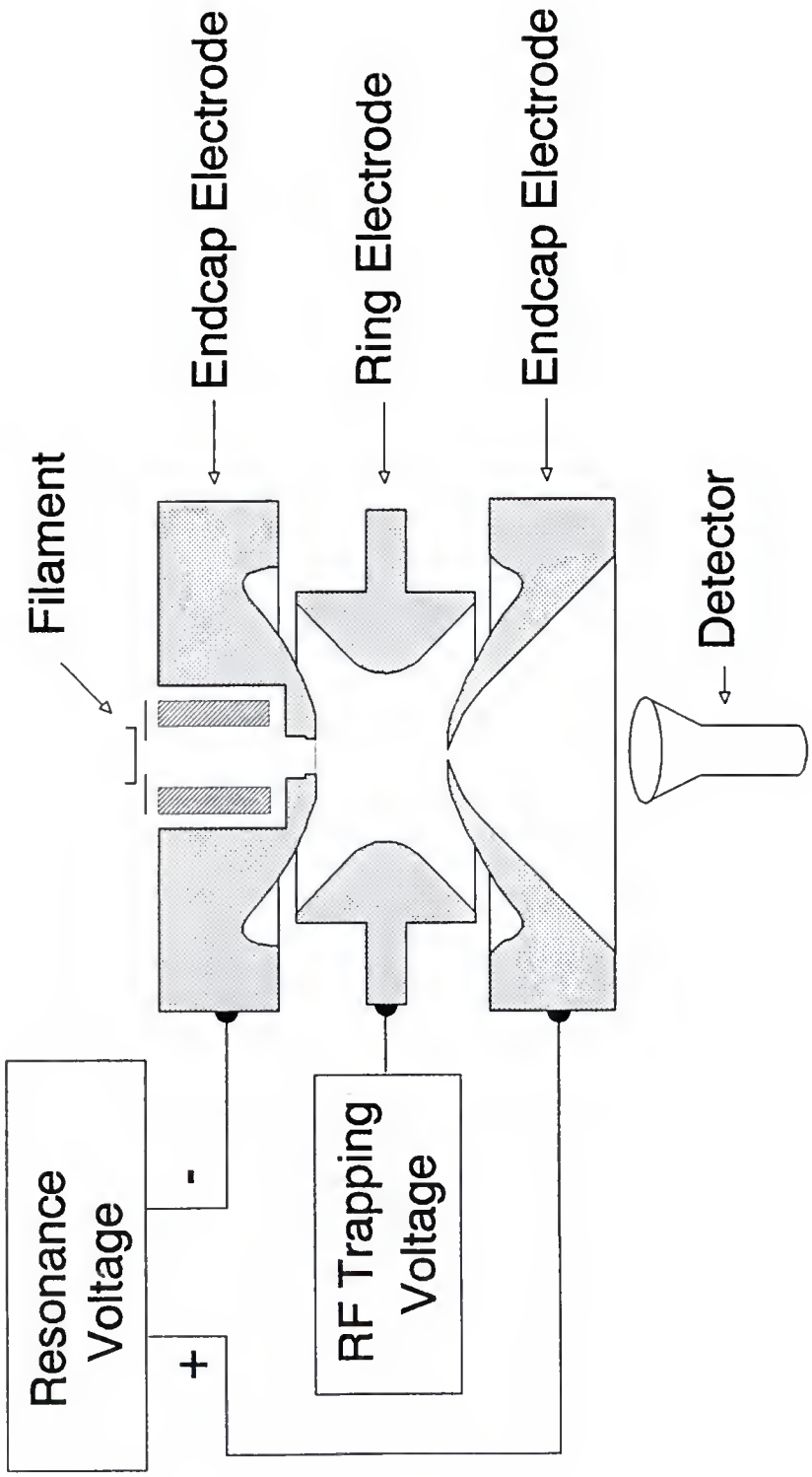

Figure 1-11. The quadrupole ion trap mass spectrometer.

where r_o is the radius of the ring electrode and z_o is the center-to-endcap distance. In the case of a pure quadrupolar field, the relationship between the ring radius and the endcap distance is given by

$$r_o^2 = 2z_o^2 \qquad (1\text{-}3)$$

Application of a radio-frequency (rf) potential to the ring electrode produces a quadrupolar electric field within the ion trap, with the force on an ion within the potential energy well formed by this field varying linearly with the ion's position from the center of the device. The potential at the center of an ion trap is given by

$$\Phi_o = \frac{U - V\cos\Omega t}{2} \qquad (1\text{-}4)$$

where U is the DC potential and $V\cos\Omega t$ is the rf potential (with V being the zero-to-peak amplitude and $\Omega/2\pi$ being the frequency in Hertz, Hz). For an ion trap employing an ideal quadrupolar trapping field, the potential at any point is given by

$$\Phi_2 = \Phi_o + \frac{\Phi_o}{r_o^2}(r^2 - 2z^2) \qquad (1\text{-}5)$$

Using equations 1-4 and 1-5 above, and setting the field strength at the exact center of the ion trap to zero (in order to satisfy Laplace's equation), the resulting equations for the motion of an ion in an ion trap can be given in terms of a radial (r) and axial (z) displacement

$$\frac{d^2r}{dt^2} + \frac{2e}{2mr_o^2}(U - V\cos\Omega t)r = 0 \qquad (1\text{-}6)$$

$$\frac{d^2z}{dt^2} + \frac{4e}{2mr_o^2}(U - V\cos\Omega t)z = 0 \qquad (1\text{-}7)$$

where m is the mass of interest and t is the time variable.

These two equations of ion motion are in the form of linear second-order differential equations, and the Mathieu equation can be used to obtain a solution which is given in terms of stability parameters a and q

$$a_u = a_z = -2a_r = \frac{-8eU}{m(r_o^2 + 2z_o^2)\Omega^2} \qquad (1\text{-}8)$$

$$q_u = q_z = -2q_r = \frac{-4eV}{m(r_o^2 + 2z_o^2)\Omega^2} \qquad (1\text{-}9)$$

These two equations are typically given as a_u and q_u, since analogous equations can be derived for a_r and q_r for ion motion in the radial direction. It should be noted that both Mathieu stability parameters are inversely proportional to the m/z for the ion of interest, and that a_u is proportional to the DC voltage and q_u is proportional to the rf voltage applied to the ring electrode. The range of a_u and q_u values that give rise to stable ion trajectories in both the radial and axial directions can be expressed in terms of a Mathieu stability diagram (Figure 1-12). It is evident from this diagram that there is a region where ions are stable with respect to radial motion in the ion trap and a region where ions are stable with respect to axial motion. When an ion has values of q_u and a_u that fall within the area of the diagram where these two regions overlap (the shaded portion of the stability diagram shown in Figure 1-12), it is stable within the body of the ion trap and is

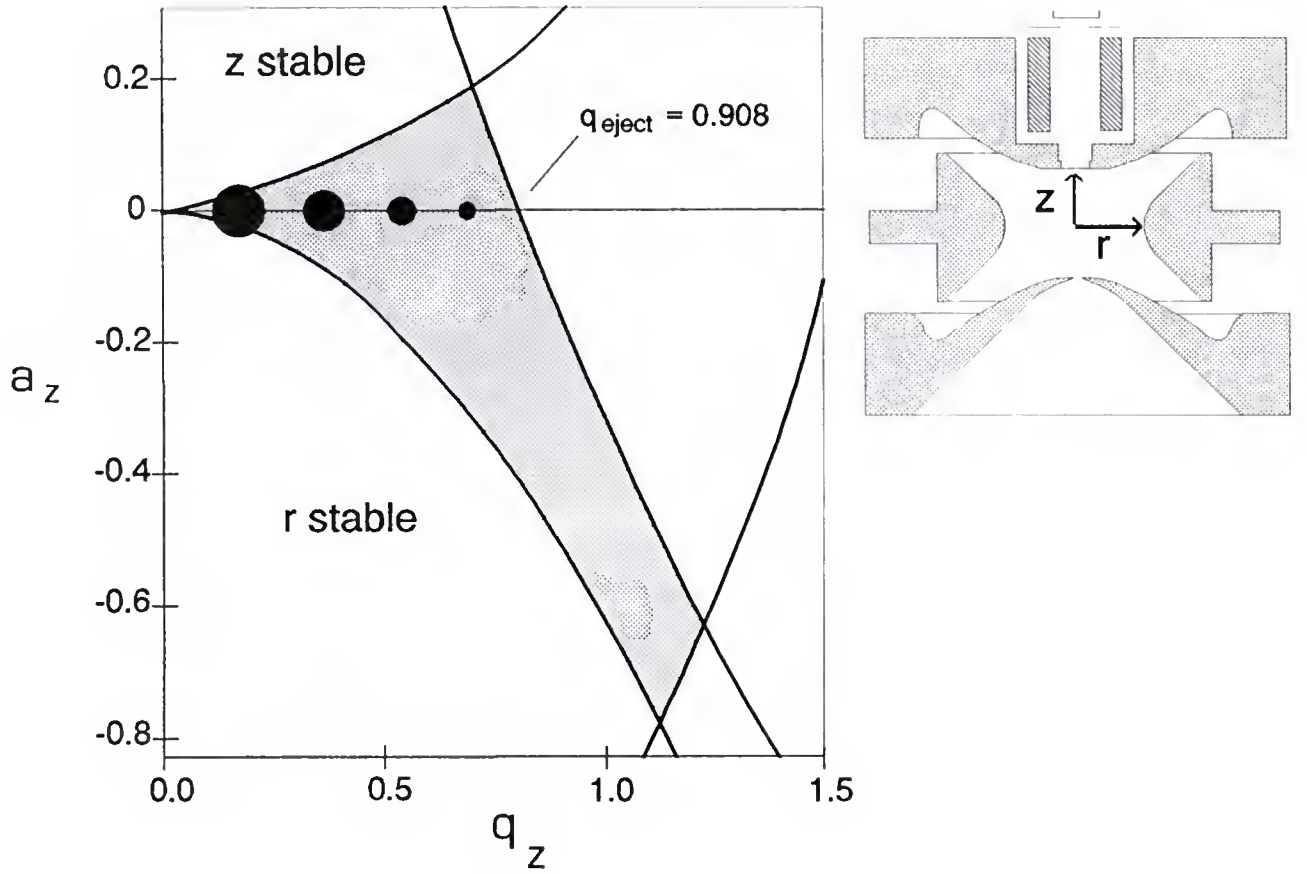

Figure 1-12. Mathieu stability diagram for the quadrupole ion trap. Shaded region represents stable region of a,q values. Black circles indicate ions of sucessively higher mass lined up along the a=0 line.

stored. Because of the inverse relationship between m/z and q_u, more massive ions will have a lower q_u value than less massive ions and will appear towards the left side of the stability diagram.

Mass analysis using the mass-selective instability mode of operation in the ion trap is given as

$$(m/z) = \frac{4V_{p\text{-}p}}{(r_o^2 + 2z_o^2)\ \Omega^2\ q_{eject}} \qquad (1\text{-}10)$$

where m/z is the mass-to-charge ratio of a given ion, V is the amplitude of the rf voltage applied to the ring electrode, r_o is the internal radius of the ring electrode, z_o is the distance from the center to the end-cap electrode, Ω is the angular component of the rf drive frequency, and q_{eject} is the point on the Mathieu stability diagram where ions become unstable under the influence of the rf-only field and are ejected into the detector. After a period of time where ions are created and stored in the ion trap, the amplitude of the rf voltage applied to the ring electrode is ramped from approximately 100 $V_{0\text{-}p}$ to 7500 $V_{0\text{-}p}$ in 110 ms (using a nominal scan rate of 5550 Da/s, scanning from 40 Da to 650 Da). As the amplitude of the rf voltage is increased, the q_z values for all ions stored in the ion trap will increase. Once the q_z value for any given ion exceeds 0.908 (which occurs from low m/z to high m/z in increasing fashion), the motion in the z-direction will be unstable, with one-half of the ions hitting the top endcap and one-half exiting through holes in the bottom (or exit) endcap, where they are detected by an electron multiplier. This is shown in Figure 1-13 as a scan function, which is a plot of the rf voltage versus time.

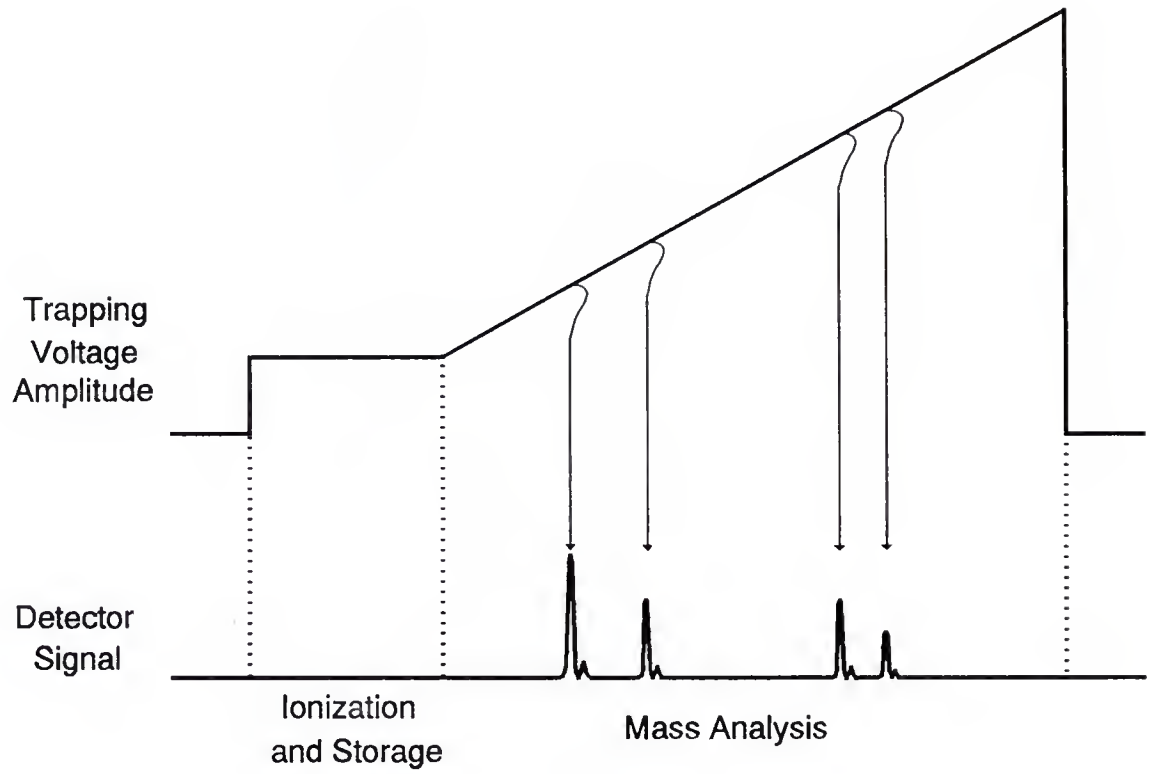

Figure 1-13. Diagram of the mass-selected instability scan (scan function) showing the RF amplitude as a function of time. The simulated spectrum for perfluorotributylamine demonstrates the timing sequence used to acquire a mass spectrum.

Resonance Excitation and Resonance Ejection

When Finnigan Corp. introduced the Ion Trap Detector (ITD) in 1983 as an inexpensive and sensitive mass spectrometric detector for gas chromatography, a 1.1 MHz ($\Omega/2\pi$), 0 $V_{0\text{-}p}$ to 7500 $V_{0\text{-}p}$ rf potential was placed on the ring electrode with no DC potential ($a_u = 0$), and the endcap electrodes were grounded. A significant advancement was made in the operation of the ion trap with the introduction of the Finnigan Ion Trap Mass Spectrometer (ITMS) in 1985. In this system, a DC potential could be applied to the ring electrode along with the rf potential, which allows for mass-selective isolation. In addition to this, a dipolar field could be created by the application of a low-voltage supplemental rf signal (530 kHz, typically 3 $V_{p\text{-}p}$ to 6 $V_{p\text{-}p}$) placed 180° out of phase across the endcap electrodes. For a fixed set of operating conditions, ions of each m/z have characteristic frequencies of motion in the axial and radial directions. When the amplitude of the rf placed on the ring electrode is ramped, ions of increasing m/z are brought into resonance with the supplemental rf signal applied to the endcaps. As the ions come into resonance with the supplemental signal, they absorb power (termed "resonance excitation"), resulting in an increase in the amplitude of their axial trajectories. If a very low voltage is used (typically 50 to 500 mV), the increase in ion trajectory may result in fragmentation due to energetic collisions with background gases (collision-induced dissociation, CID). When a much higher voltage (typically 1000 to 6000 mV) is used, the amplitude of an ion's axial trajectory will become so great that it will exit the ion trap and be detected by the electron multiplier. This is termed "resonance ejection" or "axial modulation".

Mass Range Extension in the Quadrupole Ion Trap Mass Spectrometer

For a quadrupole ion trap operated in the mass-selective instability mode, the maximum mass that can be detected is given by

$$(m/z)_{max} = \frac{4V_{max}}{(r_o^2 + 2z_o^2)\Omega^2 q_{eject}} \qquad (1\text{-}11)$$

where V_{max} is the maximum radio frequency (rf) voltage that can be applied to the ring electrode. Adding conversion factors to present this equation in terms of amu, volts, cm, and MHz gives the following expression for the maximum mass:

$$(m/z)_{max} = \frac{(4\ kg\ m^2\ s^{-2}\ C^{-1}) * (1.6022 \times 10^{-19}\ C) * (6.022 \times 10^{26}\ mol^{-1}) * V_{max}}{(r_o\ (cm)^2 + 2(z_o(cm^2)) * 10^{-4}\ m^2/cm^2 * ((\Omega\ (MHz))^2 * 4\pi^2 \times 10^{12})(Hz^2/MHz^2) * q_{eject}}$$

$$(m/z)_{max} = \frac{(0.09776) * V_{max}}{(r_o\ (cm))^2 + 2(z_o\ (cm)^2)) * (\Omega\ (MHz))^2 * q_{eject}} \qquad (1\text{–}12)$$

Using the operating conditions for the commercially available Finnigan ITS40 mass spectrometer (V_{max} = 15000 $V_{p\text{-}p}$, r_o = 1 cm, z_o = 0.792 cm, $\Omega/2\pi$ = 1.0485 MHz, q_{eject} = 0.908), the resulting maximum mass that can be detected is 651.6 amu:

$$(m/z)_{max} = \frac{(0.09776) * 15000\ V}{(1\ cm)^2 + 2(0.792\ (cm)^2)) * (1.0485\ MHz)^2 * 0.908} = 651.6 \qquad (1\text{-}13)$$

It must be noted that this is not the maximum mass that can be stored within the ion trap, but rather the maximum mass that can be ejected during a mass-selective instability scan and detected. As an example of this, 20 μm diameter aluminum particles were trapped by Wuerker, Shelton, and Langmuir (Figure 1-14 and detected using a camera.[23] It was calculated that the relative molecular mass of these particles was 6×10^{15} and that there were approximately 3×10^{5} charges on these particles, giving an m/z value of 2×10^{10}.

Using equation 1-12, the mass range of the ion trap can be extended, therefore, by any one of four ways

(i) by increasing the maximum rf voltage, V_{max},

(ii) by adjusting the dimensions of the trap (reducing r_o),

(iii) by decreasing the rf frequency, Ω, and

(iv) by selecting a different point on the stability diagram, q_{eject}, to cross from stability to instability rather than the normal q_{eject} value of 0.908.

Each of these methods for extending the mass range of the ion trap shall be now be discussed.

1) Operating at higher values of rf voltages (V_{max}).

The current maximum rf voltage used for the ion trap is 15,000 V_{p-p}. Any attempt to increase the mass range accessible to the ion trap by increasing this voltage would result in severe arcing between the ring and endcap electrode. This method has never been attempted.

2) Reducing the size of the ion trap (r_o, z_o).

Kaiser et al. evaluated the use of smaller ion traps to increase the accessible mass range.[24] The electrodes used for these studies conformed to the theoretical calculations for the

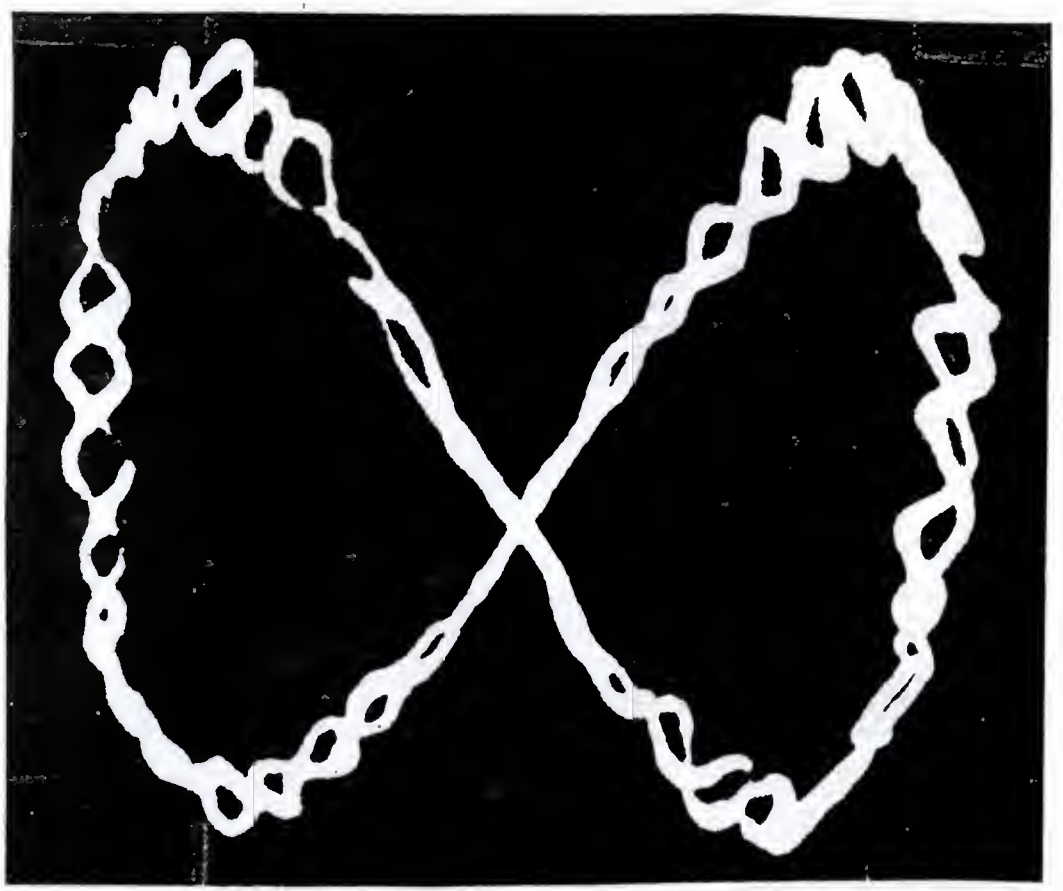

Figure 1-14. Photograph of 20 μm aluminum particles in a quadrupole ion trap.[23]

hyperbolic surfaces and spacing ($r^2 - 2z^2 = r_o^2$ for the end-cap electrodes and $r^2 - 2z^2 = -r_o^2$ for the ring electrode, and the spacing between the end caps and the ring electrode $r_o^2 = 2z_o^2$), with the dimensions scaled to produce an ion trap at half-, third- and quarter-sizes. Data produced using desorption ionization and ion injection using the reduced size ion traps showed that although the mass range was increased as expected, artifact signals of low intensity were evident. These artifact peaks were believed to be due to ions ejected prematurely because of imperfections in the rf field caused by the holes in the ion trap electrodes (which were not reduced in size).

3) Reduction of the rf drive frequency (Ω).

In addition to changing the standard crystal used to generate the waveform for the rf drive frequency, the air core coil (which is the tuned rf transformer on this system) has to be modified to reduce the rf drive frequency. This transformer is essentially a tuned LC circuit with a resonant frequency given as

$$f = 1/2\pi (LC)^{-½} \qquad (1\text{-}12)$$

where L is the inductance of the air core coil and C is the tuning capacitance of the system (which includes the capacitance between the ion trap ring electrode and the endcaps, the capacitance of any capacitors placed between the transformer coil's secondary tap and ground, and the stray capacitance of the coil assembly). Since it is extremely difficult to reduce the tuning capacitance of the system (C), the inductance of the transformer coil (L) needs to be substantially higher to reduce the resonant frequency to match the desired output frequency. In the work by Kaiser et al., a special coil consisting of a smaller diameter coil mounted inside and connected in series with a standard coil was used. This coil, used in conjunction with a lower frequency crystal,

allowed for an rf drive frequency 1.2 x lower (0.921 MHz), which led to an increase in mass range by a factor of 1.7 times. Since a reduction in the rf drive frequency (Ω) affects both the actual frequency placed on the ring electrode and the rf control DAC, the increase in the mass range is proportional to $(\Omega_{std}/\Omega_{new})^3$, where Ω_{std} is the drive frequency on the commercial ion trap system (1.0485 MHz) and Ω_{new} is the modified drive frequency.

4) Reduction in q_{eject}.

The last method to increase the mass range of the ion trap is to lower the q at which ions are ejected from the ion trap. This is accomplished by the use of axial modulation. As described above, a dipolar field is placed 180° out of phase across the endcap electrodes. As the ions come into resonance with this supplemental signal, they absorb power and their trajectories become axially unstable, at which point they exit the ion trap and are detected by the electron multiplier. At the standard axial modulation frequency used on the Finnigan ITS40 ion trap system (485 kHz), the mass spectral peak shapes are dramatically improved (particularly under space charge conditions).[25] Another consequence of this field is that the observed mass for a given ion decreases (e.g. the m/z 502 ion of perfluorotributylamine appears at m/z 498 in an uncalibrated system). Instead of the ion being ejected when it reaches the stability boundary (q_z = 0.908, shown in Figure 1-15 and the corresponding scan function with detected ion signal, Figure 1-16, it is ejected early (q_z = 0.906 for the Finnigan ITS40, corresponding to point **A** in Figure 1-17 and as a scan function and detected ion signal in Figure 1-18. When the q_{eject} point is further lowered (e.g., q_{eject} = 0.454, corresponding to point **B** shown in Figure 1-17, the ions are ejected much earlier than at the original q_{eject} of 0.908, and are hence ejected at a much lower rf voltage (Figure 1-19. Since the rf voltage can still be ramped to its maximum value of 7500 V_{0-p}, a much higher maximum mass can be ejected. This effect

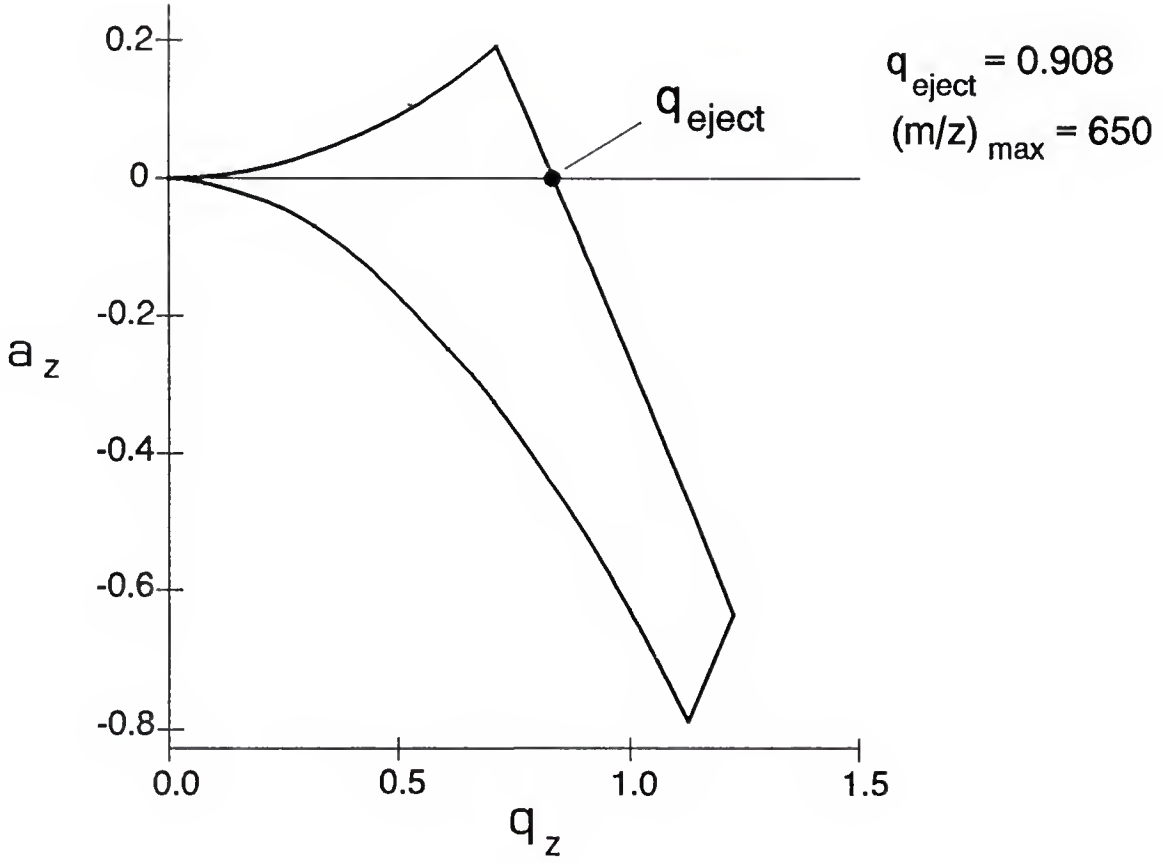

Figure 1-15. Mathieu stability diagram, showing the point on the diagram where instability occurs when no axial modulation is used.

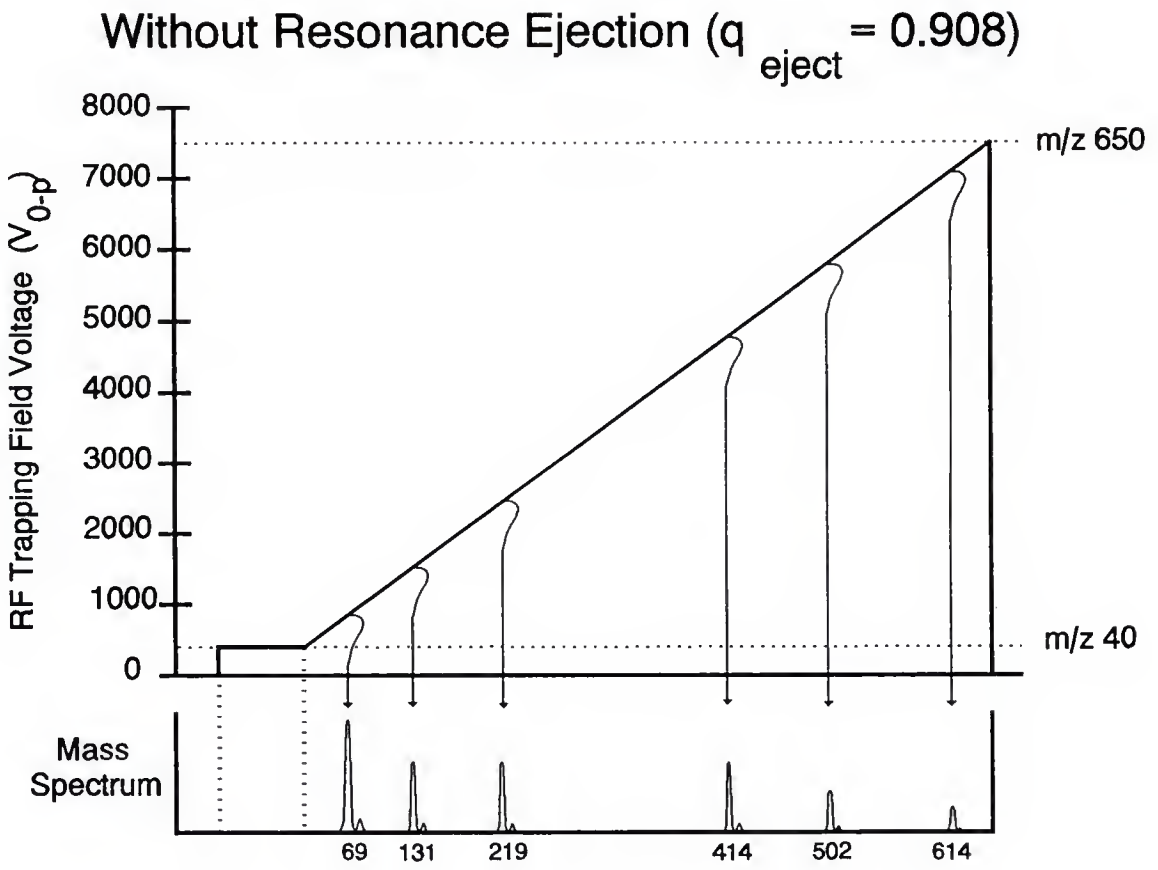

Figure 1-16. Scan function and ion signal for the mass-instability mode of operation where no axial modulation is used. Ejection corresponds to a q_{eject} of 0.908.

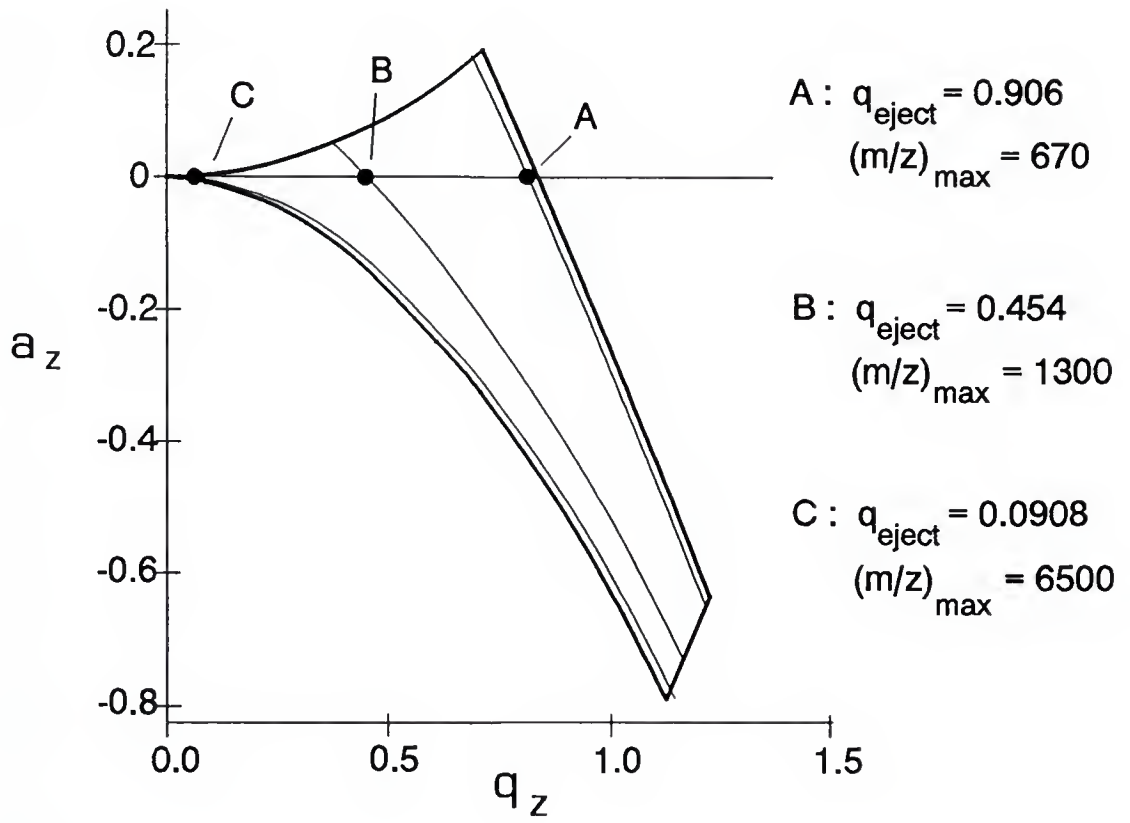

Figure 1-17. Mathieu stabillity diagram, showing the point on the diagram where instability occurs when using three different axial modulation frequencies to lower the q_{eject}.

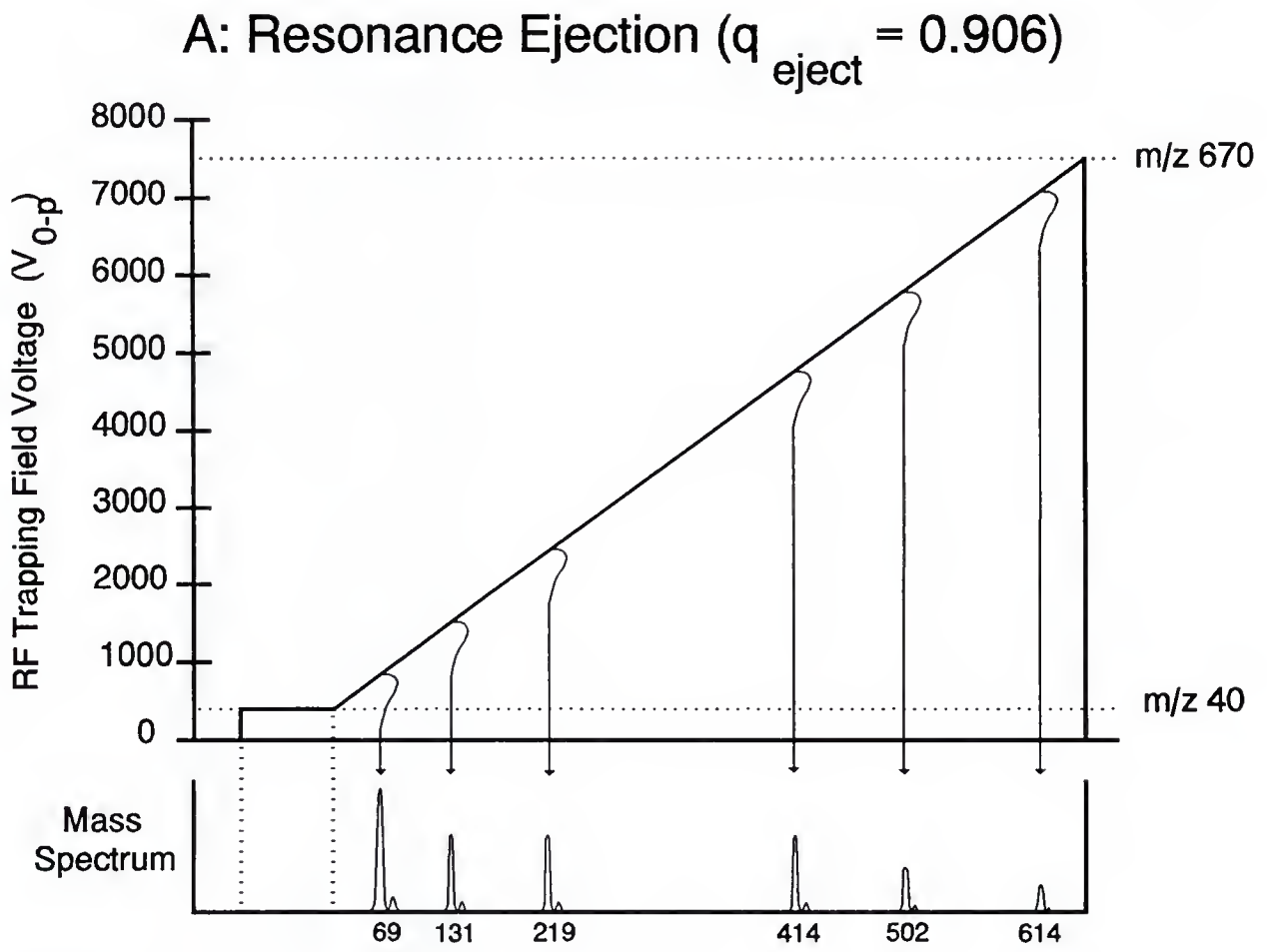

Figure 1-18. Scan function and ion signal for the mass-instability mode of operation when using axial modulation to lower the q_{eject} to 0.906. This value corresponds to point A on figure 1-16.

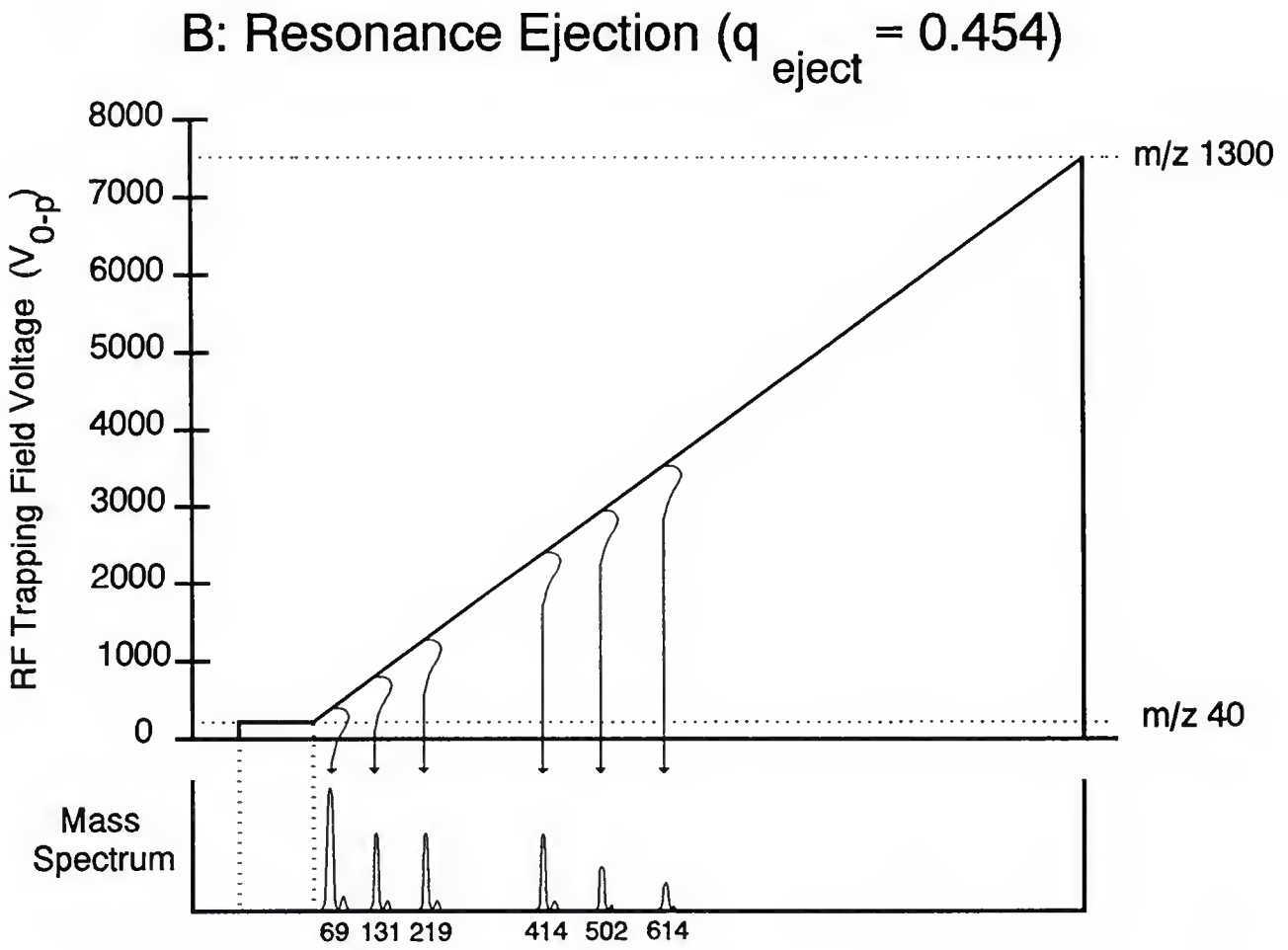

Figure 1-19. Scan function and ion signal for the mass-instability mode of operation when using axial modulation to lower the q_{eject} to 0.454. This value corresponds to point B on figure 1-17.

is even more exaggerated at a lower q_{eject} (e.g., $q_{eject} = 0.0908$, corresponding to point **C** in Figure 1-16, where the mass range is extended by a factor of 10 since the q_{eject} has been decreased by a factor of 10, shown as a scan function and detected ion signal in Figure 1-20 The mass range is effectively increased by this amount, and the new mass limit is given as

$$(m/z)_{new\ max} = (m/z)_{old\ max} * [(q_{old\ eject})/ q_{new\ eject})] \qquad (1\text{-}13)$$

The axial modulation frequency (ω) required to achieve a desired q_{eject} cannot be calculated directly, but must be obtained through β, which is related to the frequency of an ion

$$\omega = \beta\ \Omega/2 \qquad (1\text{-}14)$$

β is a complex function of a and q which can be approximated using the relationship

$$\beta^2 = a + [q^2/(2+\beta)^2\text{-}a\text{-}[q^2/(4+\beta)^2\text{-}a\text{-}[q^2/(6+\beta)^2\text{-}a\text{-}[...etc.]]]] + [q^2/(2-\beta)^2\text{-}a\text{-}[q^2/(4-\beta)^2\text{-}a\text{-}[q^2/(6-\beta)^2\text{-}a\text{-}[...etc.]]]] \qquad (1\text{-}15)$$

The relationship between the axial modulation frequency used during the mass analysis scan and the maximum mass detectable is shown in Figure 1-21.

MALDI Using a Quadrupole Ion Trap Mass Spectrometer

Mass analysis of MALDI-derived ions is most often carried out with time-of-flight (TOF) mass spectrometers due to their ability to record an entire spectrum for every single laser shot, as well as their high mass range and simplicity. As discussed earlier,

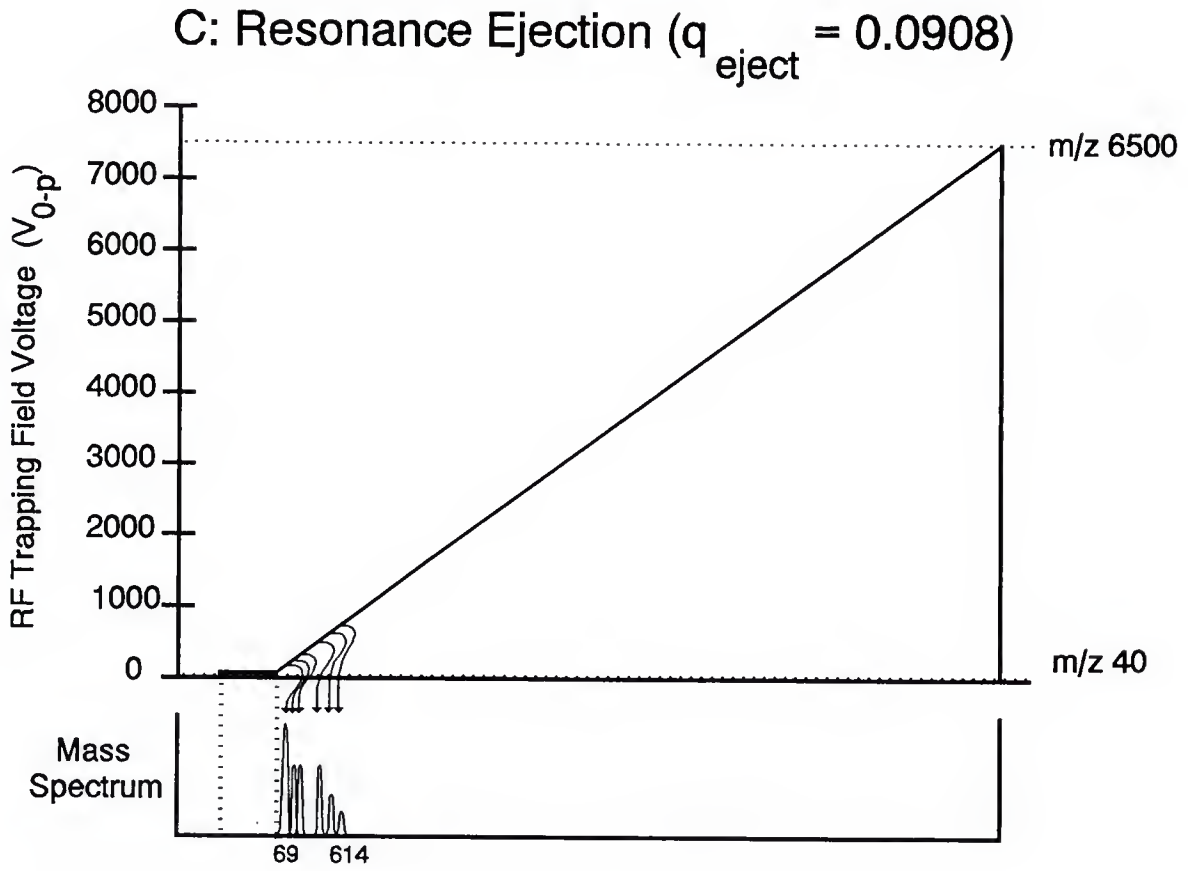

Figure 1-20. Scan function and ion signal for the mass-instability mode of operation when using axial modulation to lower the q_{eject} to 0.0908. This value corresponds to point C on figure 1-17.

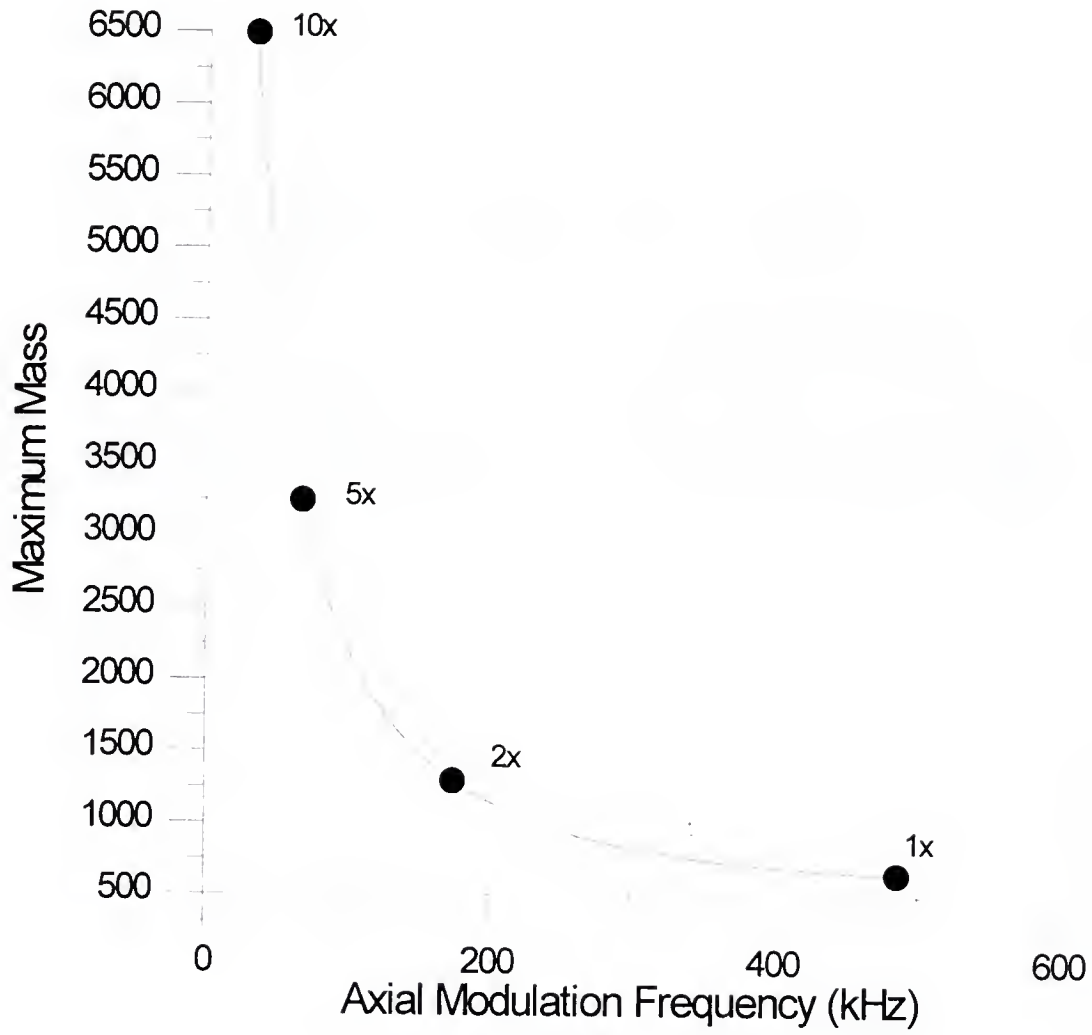

Figure 1-21. Relationship between the axial modulation frequency used during the mass analysis scan and the maximum detectable mass.

although the packet of ions produced by MALDI is well-suited for TOF mass analysis, the initial kinetic energy spread of the ions leads to poor mass resolution. Typically, mass resolutions of between 400 and 700 (m/Δm, full-width at half-maximum, fwhm) are observed for bovine insulin (M.W. 5733.5) using a TOF mass spectrometer with a linear flight tube and between 1000 and 3000 using a reflectron.[26] Another factor which degrades the mass resolution in MALDI TOF MS is metastable decay along the flight tube. This is particularly important when using a reflectron instrument, where it can seriously degrade peak widths and sensitivity.[27]

In order to overcome some of the disadvantages of using a TOF instrument with MALDI, a quadrupole ion trap mass spectrometer (QITMS) has been used with MALDI. Whereas the detection and ionization processes are coupled when using a TOF mass spectrometer with MALDI, when using a QITMS the MALDI-generated ions are stored inside of the ion trap prior to mass analysis.

The first attempt at using a QITMS for the mass analysis of MALDI-derived ions was shown by Heller et al. in 1989.[28] A Finnigan Corp. (San Jose, CA) ion trap detector (ITD) was modified by drilling a hole through the center of the ring electrode. An insertion probe lock was fitted to one side of the vacuum manifold and a flange with a ZnSe lens was fitted to the opposite side (Figure 1-22). MALDI was performed within the ion trap by placing a matrix/sample mixture on the tip of a stainless steel probe, inserting the sample probe through the probe lock and into the hole in the ring electrode so that it was flush with the surface of the ring electrode, and bringing in a laser beam through the other side of the ring electrode.

Using a design similar to this, Chambers et al.[29] showed the analysis of 163 pmol of bovine insulin (M.W. 5733.6) (Figure 1-23). Although the molecular ion for this compound can be seen, the sensitivity and resolution are very poor. This can be attributed to two factors: (i) neutrals produced by the laser desorption process are present

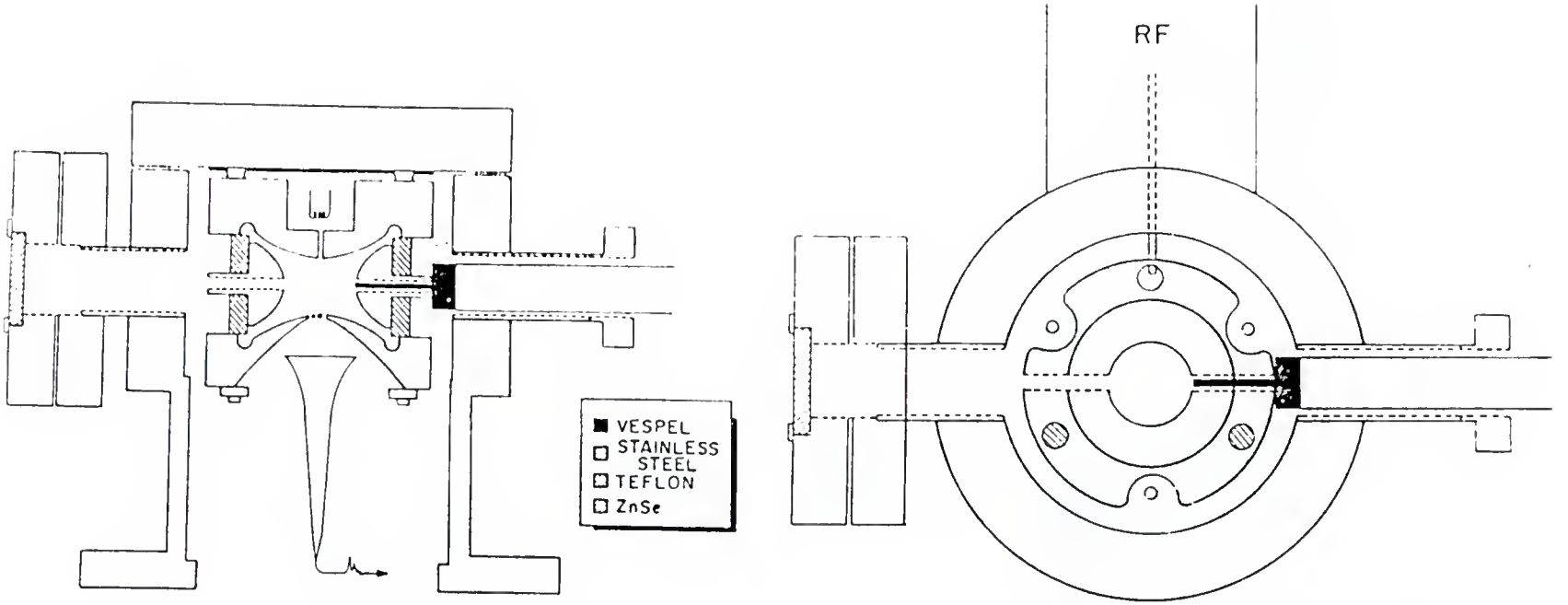

Figure 1-22. Instrumental configuration for performing MALDI inside of an ion trap.[28]

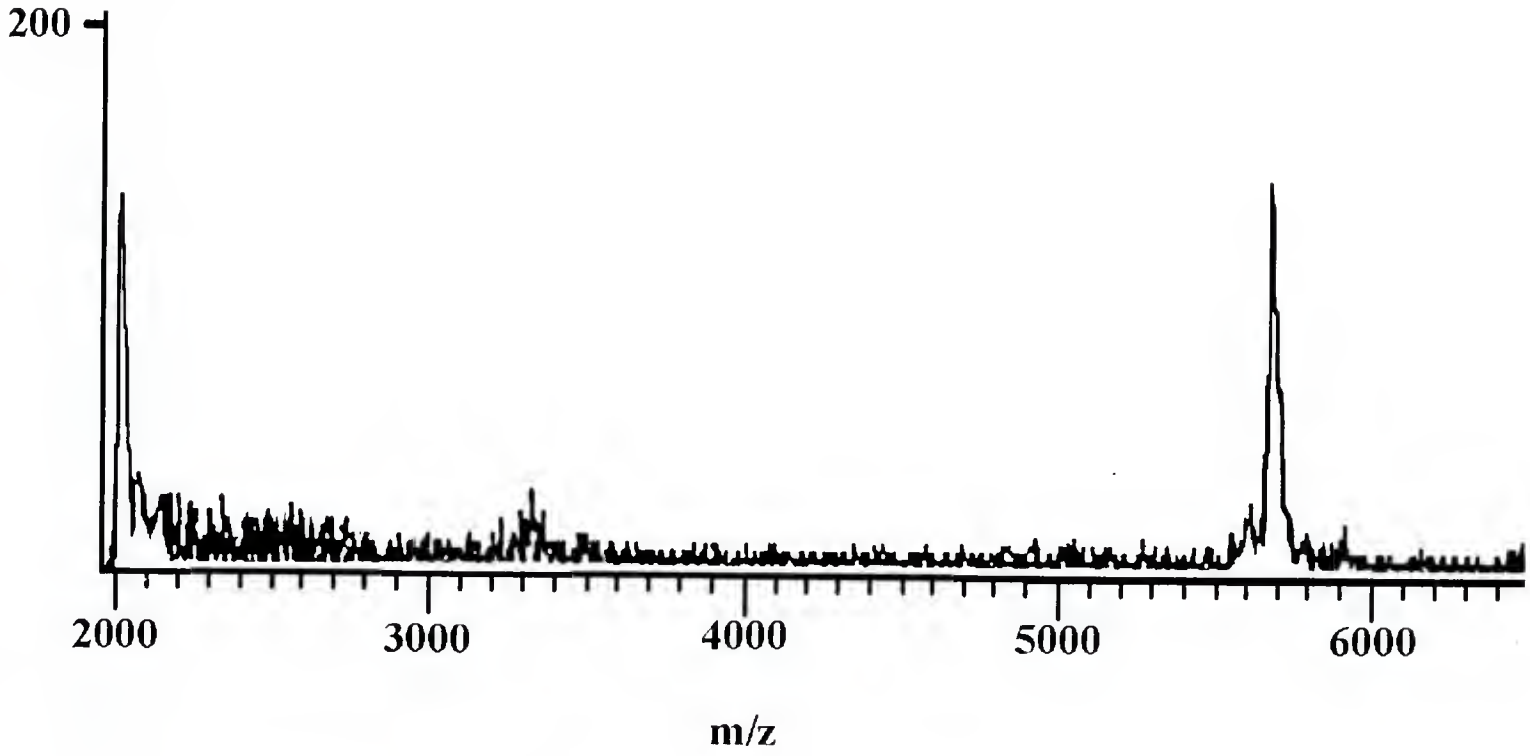

Figure 1-23. MALDI QITMS spectrum of bovine insulin performed inside of the ion trap.[29]

within the ion trap during the storage of the ions and (ii) the trapping efficiency of the MALDI-produced ions decreases with increasing mass due to the initial kinetic energy of the MALDI-produced ions. If an ion is produced with an initial kinetic energy greater than the potential well created by the radio-frequency trapping field inside of the ion trap, the ion will travel across the ring electrode without being trapped. Chambers et al. calculated a high-mass limit of m/z 9830 when performing MALDI inside the body of the QITMS.[30] This leads not only to an upper mass limit but also to a loss in sensitivity as the initial kinetic energy of an analyte increases (which increases linearly with mass).

This same instrumental configuration was used by Vargas and Yost[31] at the University of Florida for the analysis of spiperone, an antipsychotic drug developed by Bristol-Myers Squibb. Both laser desorption ionization (LDI) and MALDI were performed on this compound to demonstrate the differences between these two techniques. LDI was performed by applying 2 μL of a 0.1 μg/μL spiperone solution onto a probe tip. MALDI was performed by depositing 2 μL of a 0.1 mM spiperone solution onto a probe tip followed by an equal volume of a 100 mM nicotinic acid MALDI matrix solution. After air drying, the samples were analyzed by LDI (Figure 1-24a) and MALDI QITMS using a nitrogen laser (Figure 1-24b). The major ions seen in the LDI spectrum for this compound are low molecular weight fragment ions. As discussed earlier, the high irradiance required for nonresonant desorption (approximately 10^7 W cm^{-2}) is very close to the point of plasma generation, which leads to fragmentation of the molecule. MALDI, however, produces mainly $[M + H]^+$ ions, along with a small amount of adduct ions and fragment ions.

In addition to performing MALDI of spiperone, Vargas and Yost also performed tandem mass spectrometry on the MALDI-produced ions of this compound. Figure 1-25 shows the results for the MALDI MS/MS analysis for the m/z 396 ion of spiperone. The results for the tandem mass spectrometric analysis of this compound using MALDI were

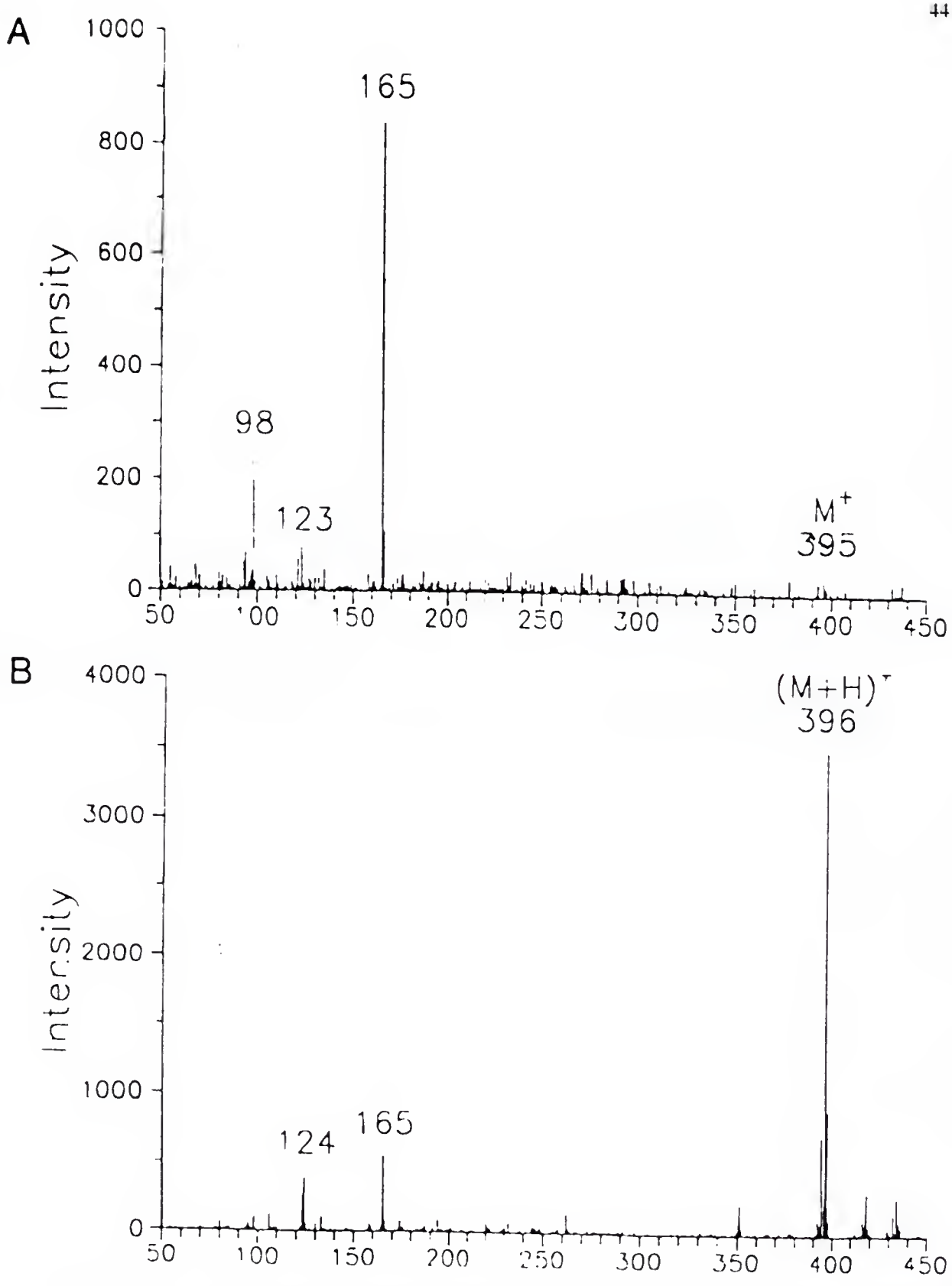

Figure 1-24. a). Laser desorption ionization (LDI) and b). MALDI QITMS spectra of spiperone performed inside of the ion trap.[31]

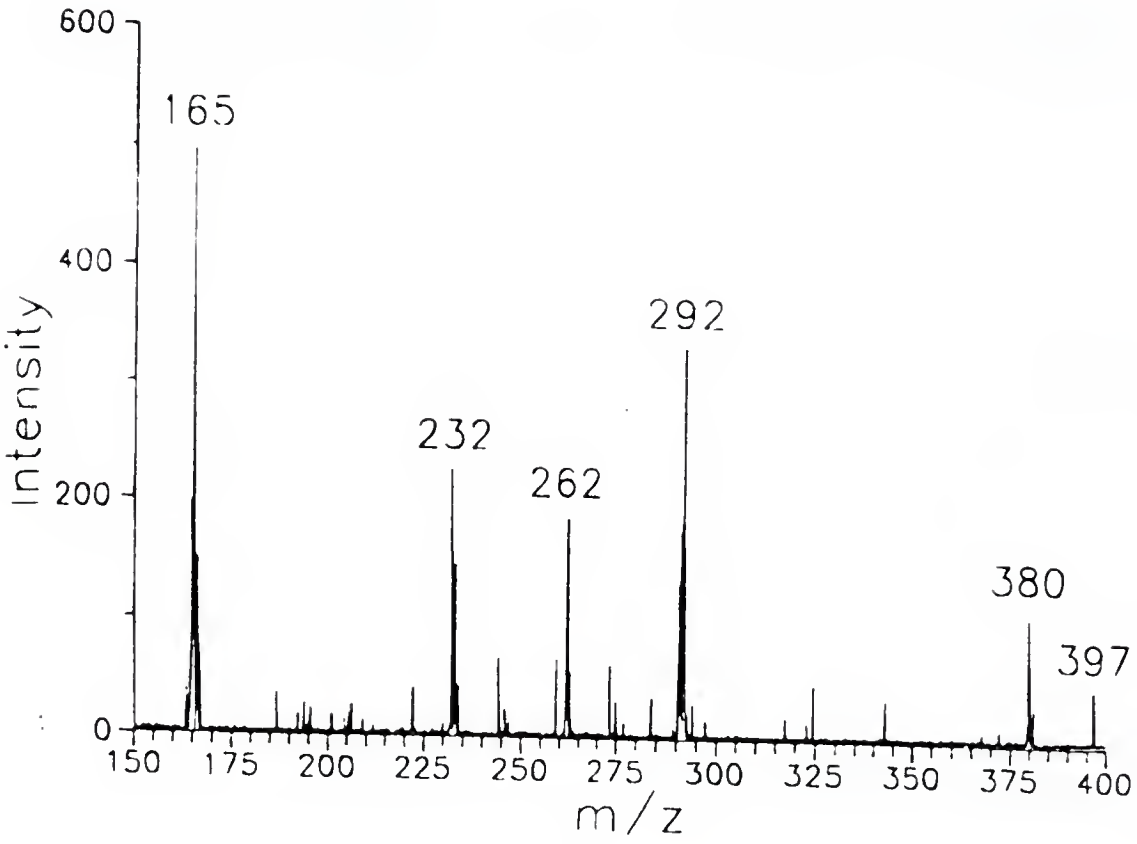

Figure 1-25. MS/MS daughter spectrum of protonated spiperone.[31]

similar to those obtained using other methods of sample introduction and mass analysis (e.g., solids-probe CI).[32]

Vargas and Yost also demonstrated the MALDI QITMS analysis of spiperone in a Matrigel matrix. Matrigel (Collaborative Research, Inc.) is mouse extracellular tissue used as a model biological matrix. 0.5 to 1 mg of spiperone was mixed in 1 mL of Matrigel, and 4 μL of this solution was deposited onto a probe tip followed by an equal volume of a 100 mM sinapinic acid MALDI matrix solution. After air drying, the samples were analyzed by MALDI QITMS (Figure 1-26). Unlike the MALDI QITMS analysis for spiperone analyzed with the matrix alone, addition of the Matrigel produced intense sodium and potassium adduct peaks, due to the presence of these cations in the Matrigel.

MALDI QITMS Using an External Ion Source

MALDI QITMS has also been performed using an external ion source. The advantages of using an external ion source instead of performing MALDI directly inside the ion trap are increases in sensitivity and resolution by not having the neutrals produced by the laser desorption process present in the ion trap during the storage of the ions. In addition, there is no upper mass limit due to the initial kinetic energy of the MALDI-produced ions.

The first MALDI QITMS instrument designed with an external ion source was constructed by Bier et al. of Finnigan.[33] They modified a GC/MS ion source so that a nitrogen laser beam at 337.1 nm was brought through a fiber optic and focused onto a sample probe (Figure 1-27). Desorbed ions were extracted from the source and injected into the ion trap for mass analysis. Using this design, they showed the analysis of 50

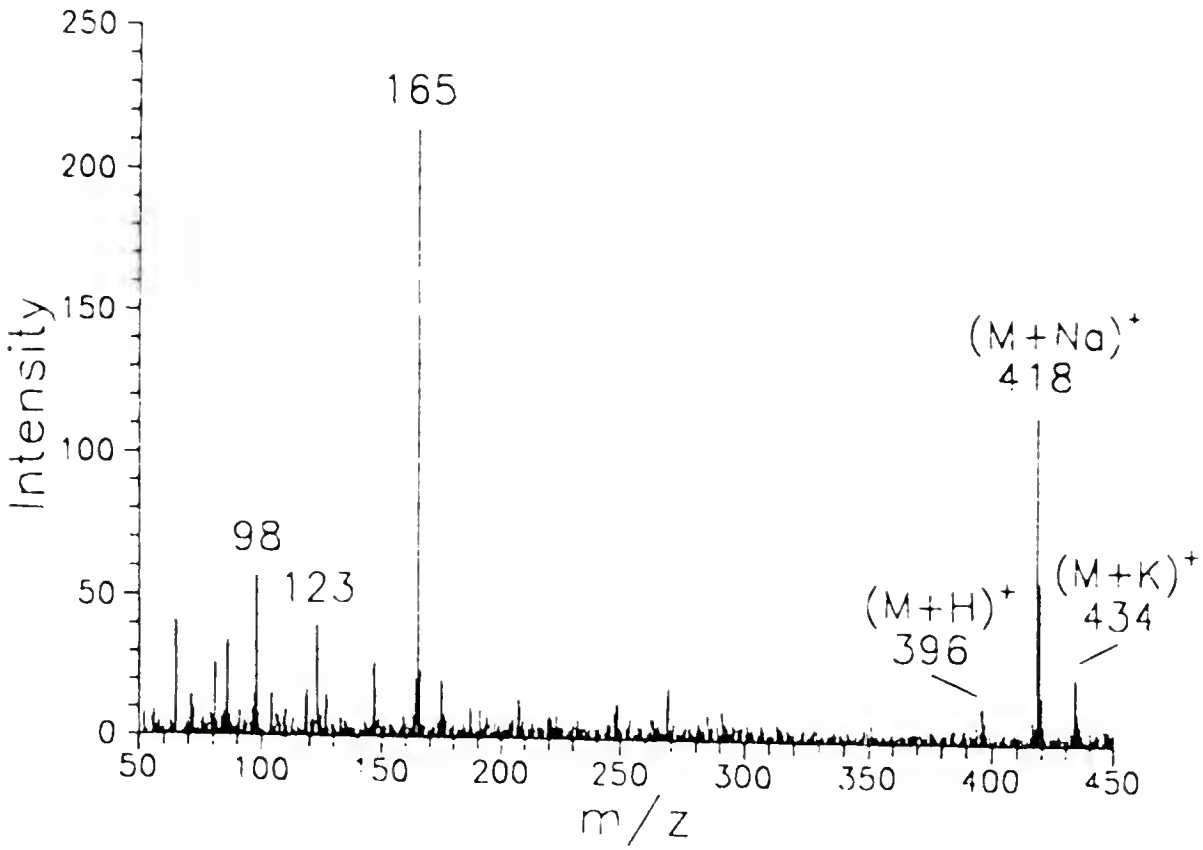

Figure 1-26. MALDI QITMS analysis of spiperone in a Matrigel matrix.[31]

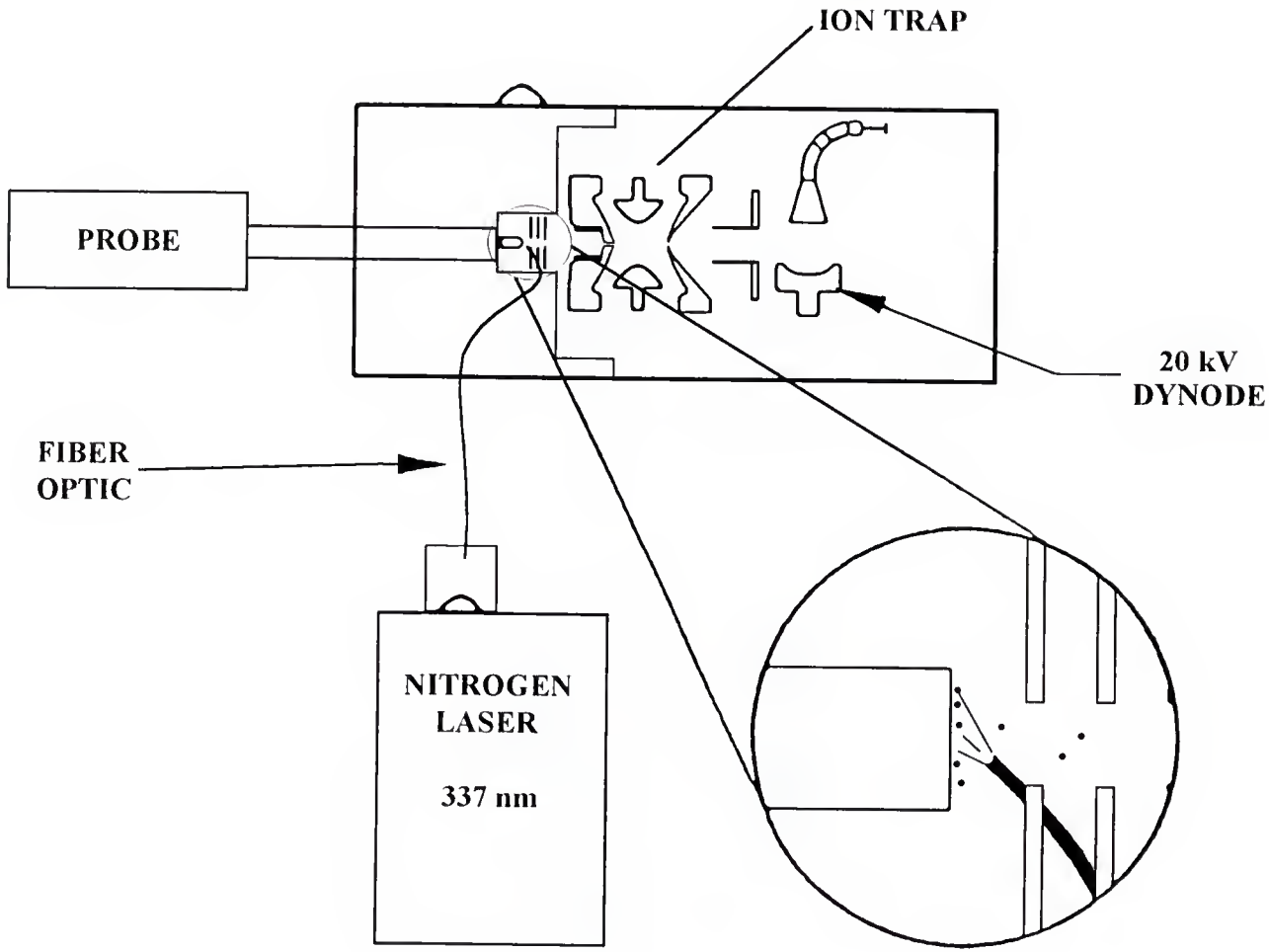

Figure 1-27. External ion source MALDI QITMS instrument using a modified GC ion source.[33]

pmol of bovine insulin (M.W. 5374) (Figure 1-28) and 600 pmol of egg albumin (M.W. 43300) (Figure 1-29). Although this instrument showed good results for the MALDI QITMS analysis of bovine insulin, the spectrum for the higher mass egg albumin showed a very poor signal-to-noise ratio and poor resolution.

At the same time that the MALDI QITMS instrument described in this dissertation was being designed and built at the University of Florida, the Chait group at the Rockefeller University was constructing a similar instrument.[34] This instrument consists of a sample probe plate, source ion extraction plate, three tube lenses, and the quadrupole ion trap with a channeltron detector fitted with a conversion dynode (Figure 1-30). Finnigan ITMS electronics were used to control the QITMS, with the addition of a scan rate reduction board (Ionstor, Oak Ridge, TN) for increased mass resolution experiments and an rf amplifier (Ionstor) used to increase the amplitude of the supplemental ac field for mass range extension. Results from this system included the MALDI QITMS spectra for 100 fmol of bradykinin (M.W. 1060.2) (Figure 1-31). As is typical with other ion traps used for MALDI analysis, fragment ions (typically seen as a loss of H_2O and NH_3, and loss of the C-terminal residue, in this case the amino acid arginine (R)) created upon injection are evident.

Overview of Dissertation

This chapter described the development, mechanism, and application of MALDI using both time-of-flight and ion trap mass spectrometers. Chapter 2 describes the design considerations for the MALDI QITMS instrument built for this dissertation, including simulations of both the modified-GC ion source MALDI QITMS instrument used by Bier et al. of Finnigan and the Vestec MALDI ion source MALDI QITMS instrument designed and constructed for this dissertation. The data for the two peptides

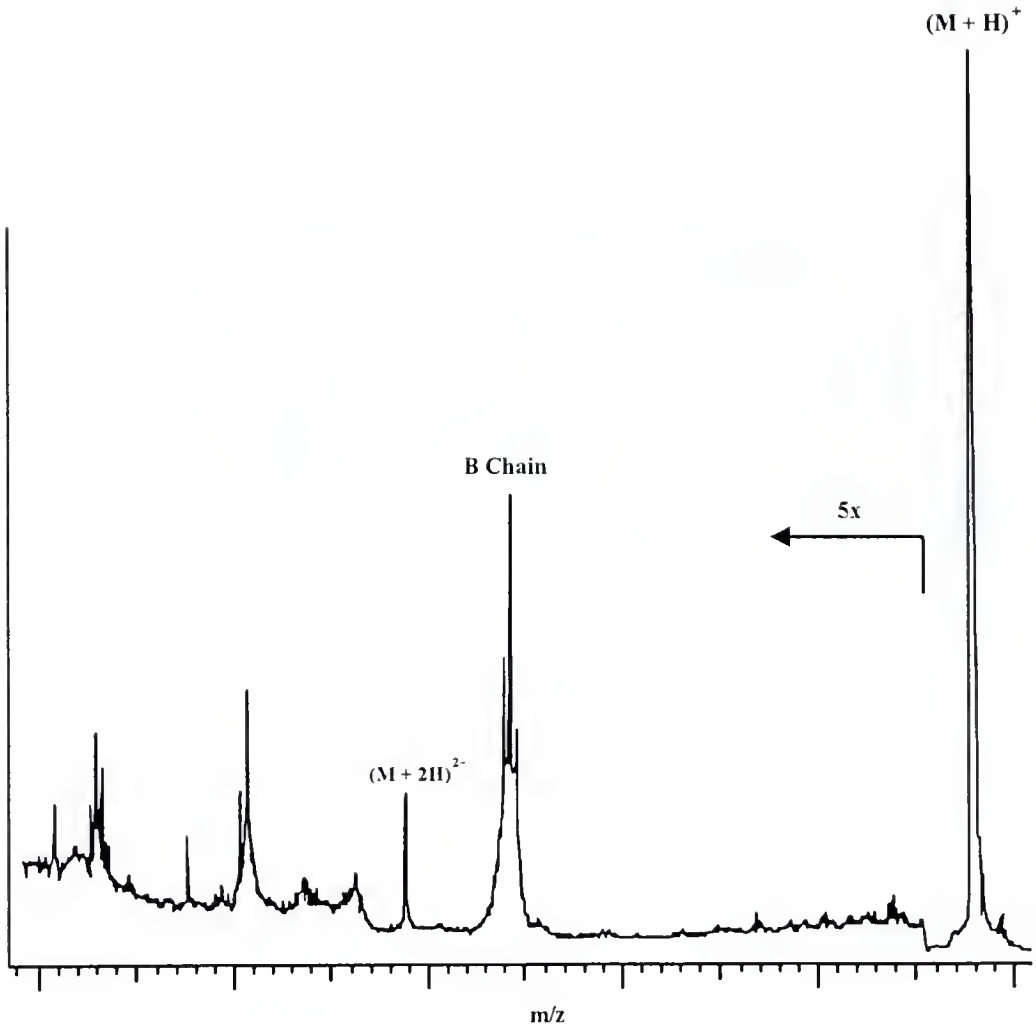

Figure 1-28. MALDI QITMS spectrum of bovine insulin using an external ion source.[33]

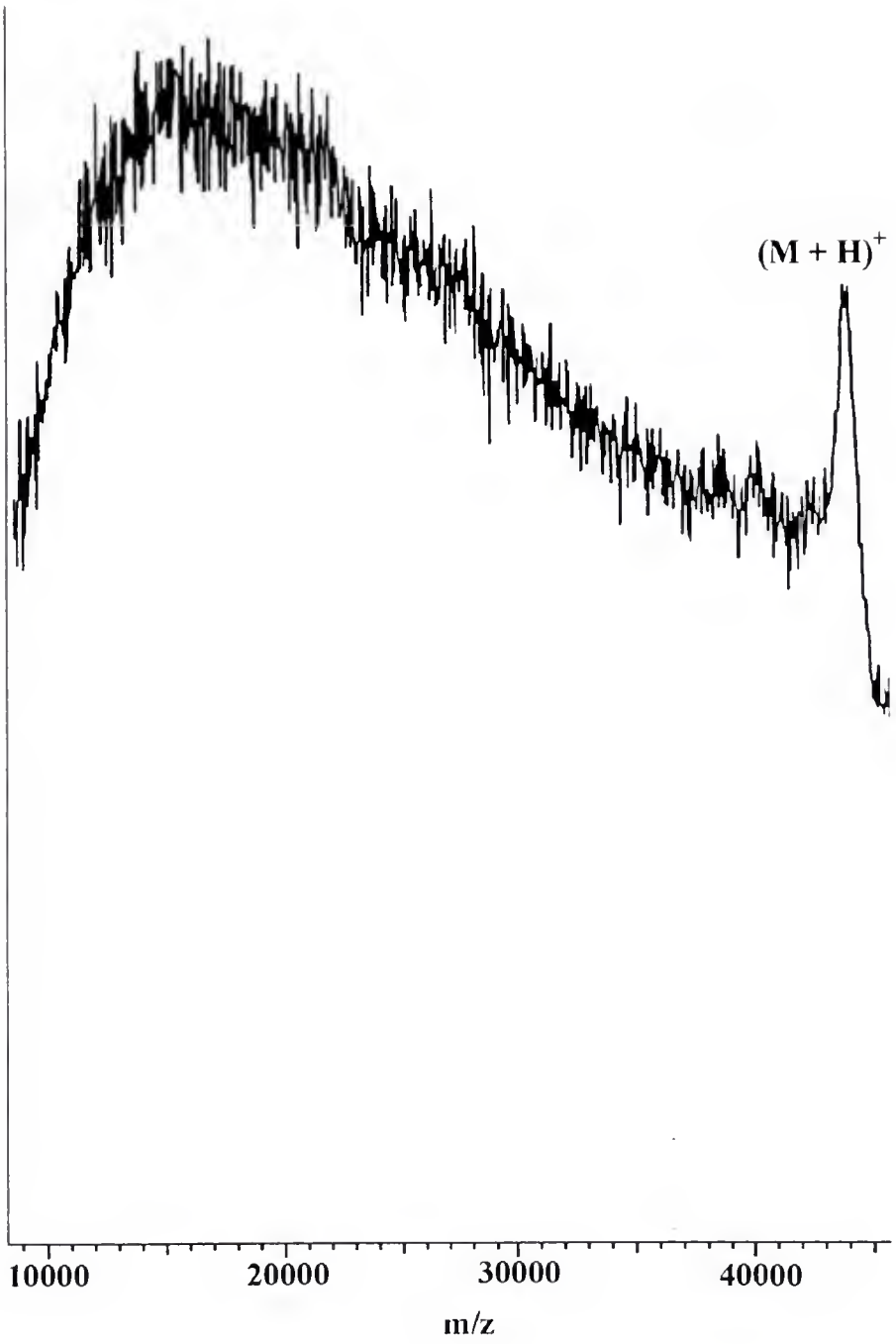

Figure 1-29. MALDI QITMS spectrum of egg albumin using an external ion source.[33]

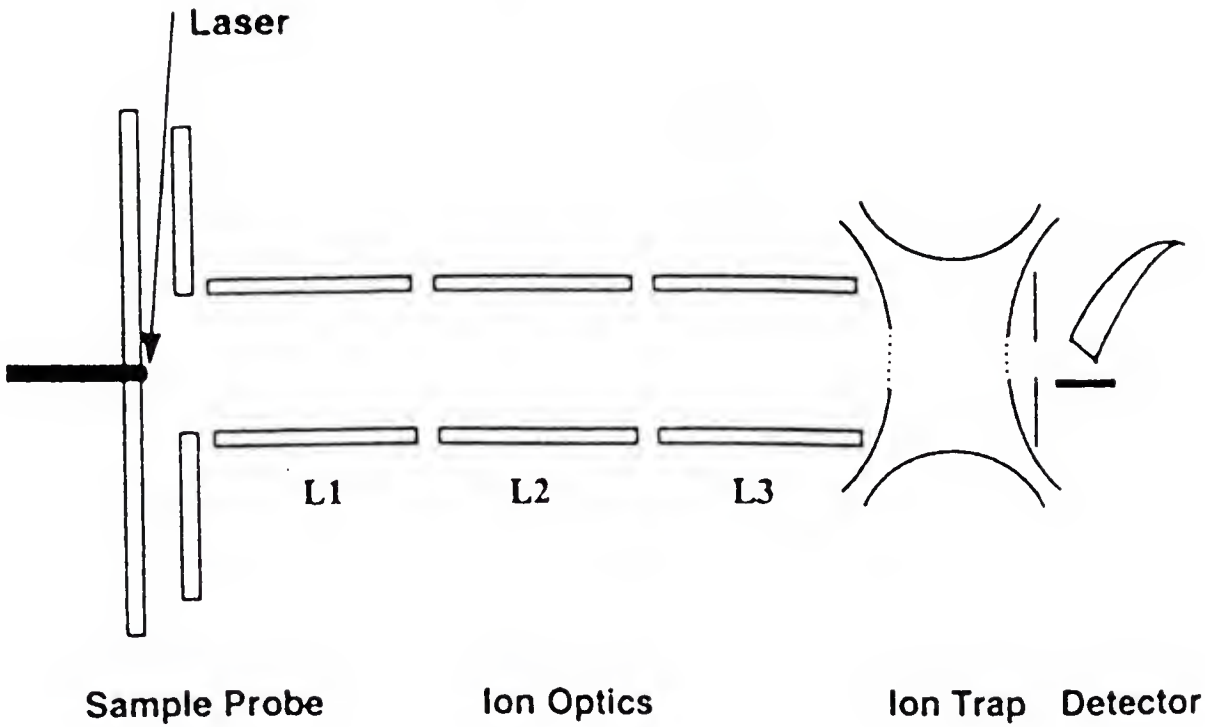

Figure 1-30. MALDI QITMS instrument constructed at The Rockefeller University.[34]

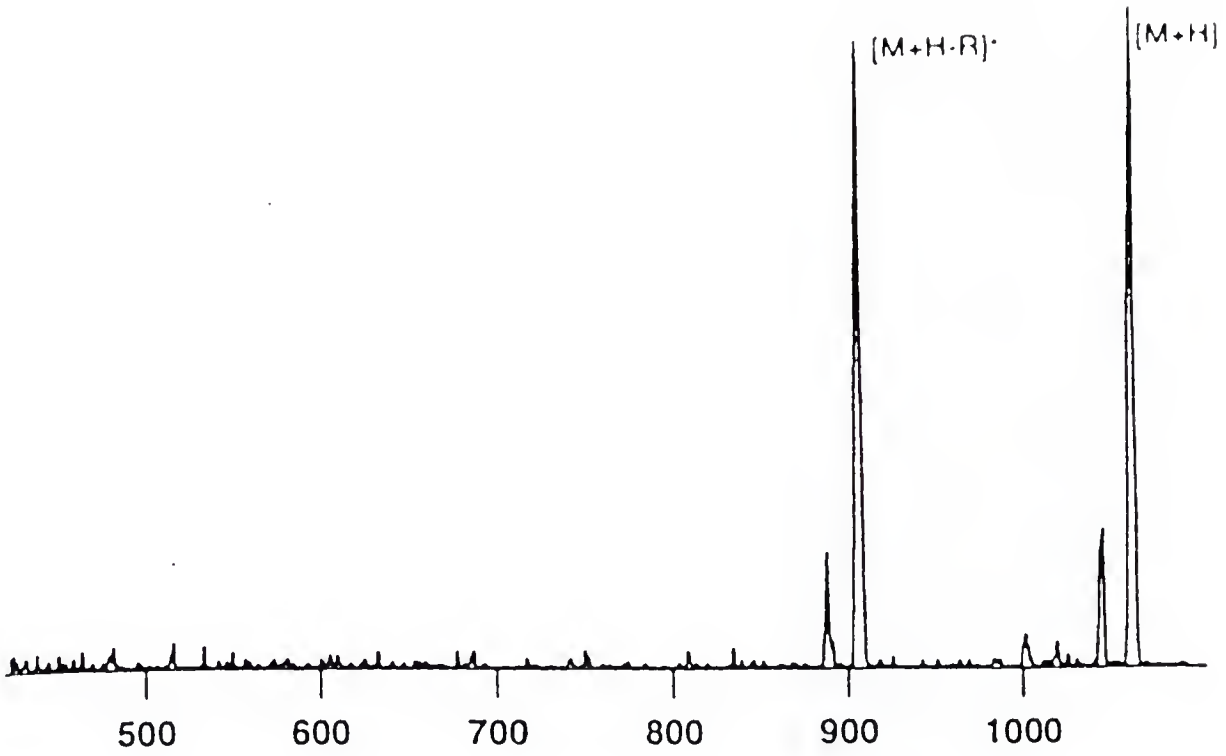

Figure 1-31. MALDI QITMS spectrum of bradykinin using the instrument constructed at the Rockefeller University.[34]

(MRFA and angiotensin II) analyzed for the characterization of this instrument are also included in this chapter. The MALDI QITMS instrument described in chapter 2 of this dissertation was used for the analysis of two pharmaceutical compounds: spiperone, an antipsychotic drug developed by Bristol-Myers Squibb, and the anticancer drug Taxol. Chapter 3 contains the results for the MALDI QITMS analysis of spiperone using MS and MS^n. A fragmentation map for this compound was generated using multiple stages of mass spectrometry, up to MS^6. Also contained in this chapter is the MALDI QITMS analysis of Taxol in an incubated rat liver tissue sample. This last analysis was performed to demonstrate the ability of MS^n for the detection of target compounds in the presence of a large number of interfering species. Chapter 4 concludes by summarizing the research described in this dissertation, and discusses the future work needed to use a MALDI QITMS instrument for the analysis of tissue samples.

CHAPTER 2
INSTRUMENTAL DESIGN AND CHARACTERIZATION OF A MALDI QUADRUPOLE ION TRAP MASS SPECTROMETER

Instrument Design

As discussed in the background section of this dissertation, the mass analysis of MALDI-generated ions has been demonstrated using a quadrupole ion trap. Successful instrument designs have been developed around the use of MALDI-generated ions produced inside of the ring electrode of the ion trap and using an external ion source along with ion injection into the ion trap. Since one of the ultimate goals of the research undertaken as part of this dissertation is to produce a microprobe instrument, imaging of the sample is critically important. Although an instrument which produces the MALDI-generated ions directly inside of the body of the ion trap can be used, the use of an external ion source allows for easier sample imaging and the potential to use a translatable sample stage (using an x-y positioner coupled to the sample probe). Because of these important features, a MALDI ion source externally coupled to an ion trap was the instrument configuration chosen for this project.

Although the limitations of using internally generated MALDI ions has been discussed by Glish et al., the use of a modified GC ion source to produce MALDI ions also leads to instrumental compromises. These limitations have a direct impact on the choice of the MALDI ion source that will be used for the research covered in this dissertation. In order to understand the limitations in using a modified GC ion source to produce MALDI ions, a study of the ion optics of the system used by Bier et al. was

performed using version 5.0 of the ion simulation program SIMION.[35] Accurate dimensions were taken of a Finnigan 4500 (TSQ70) ion source and a Finnigan ITS40 quadrupole ion trap, and these were used to generate a SIMION grid file. The voltages used to produce the MALDI QITMS data shown in Figure 1-27 and Figure 1-28 were supplied by Mark Bier (with no rf voltage placed on the ion trap and no collisions used for these simulations). Most probable velocities of 750 m/s (as described by Chait[20]) were used for these two different mass ions, which gave initial kinetic energies of 17 eV for bovine insulin and 126 eV for egg albumin. The results from the SIMION analysis of the modified GC ion source instrument used to produce the mass spectra of bovine insulin and egg albumin are shown in Figures 2-1, 2-2, and 2-3.

It is evident from Figures 1-27 and 1-28 that the resolution and signal-to-noise ratio (S/N) for egg albumin are very poor compared to that of bovine insulin. The poor performance of this system for the higher m/z compound is a direct result of the use of a modified GC source for performing MALDI. Even though this source had been modified (the lens spacers were better anodized to allow for higher voltages before arcing), only a limited range of voltages could be used to focus ions from the region where the nitrogen laser strikes the sample to where they enter the ion trap. The consequences of this are seen on ions with a significant radial velocity (that is, ions leaving the probe tip at an angle with respect to the ion trap. When the ion beam leaves the probe tip at an angle of 0° (directly towards the QITMS), the ions enter the ion trap regardless of mass (Figure 2-1). In MALDI, however, only a small percentage of the ions generated leave the probe tip at this angle.[36] Since this source is designed to be used with relatively low voltages, ions produced with radial velocities can not be well focused. Figure 2-2 shows the SIMION results for egg albumin when the ion beam leaves the probe tip at a 1° angle (corresponding to an ion leaving the probe tip with only a slight radial velocity). When compared to the 0° angle case (where the ion leaves the probe tip

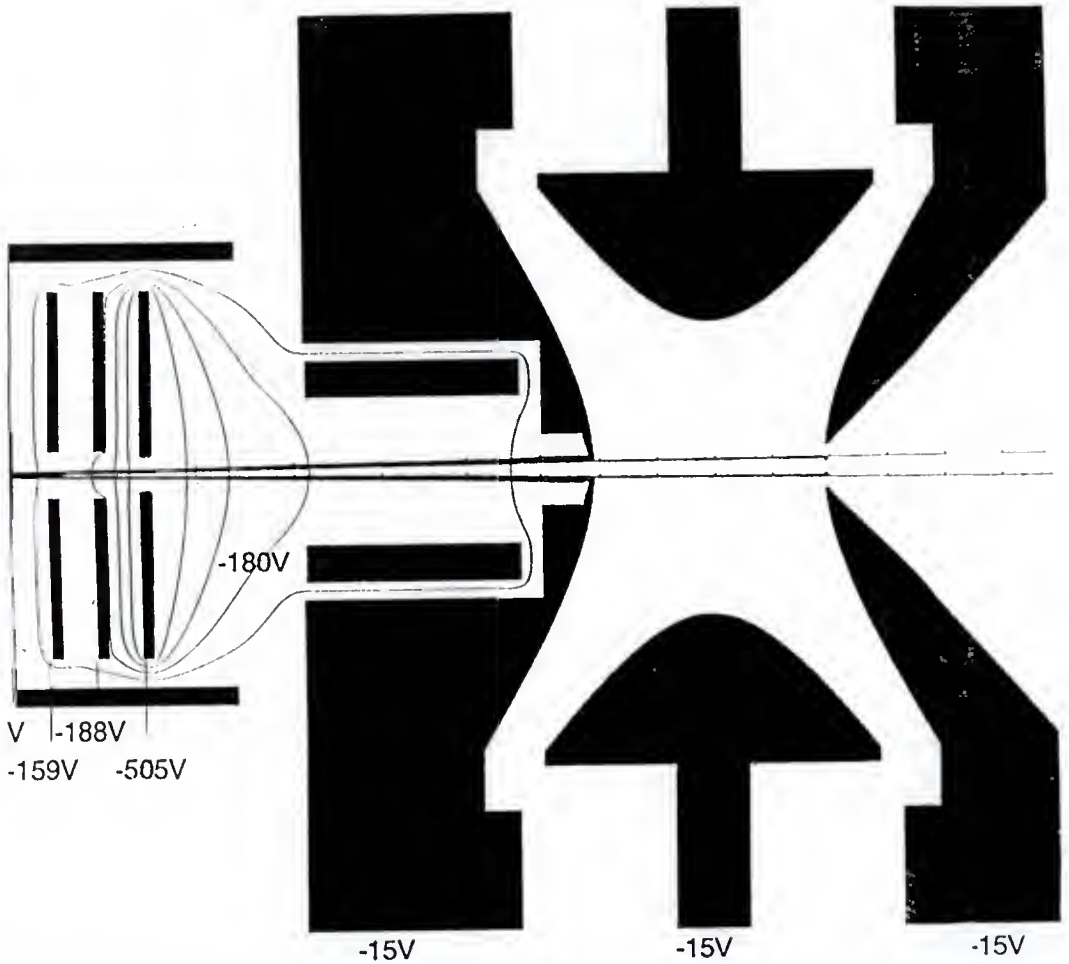

Figure 2-1. Simulation of MALDI-produced egg albumin ions (m/z 43300) for the instrument used by Bier et al..[32] The initial energy for this simulation was 126 eV, the initial angle was 0 degrees, and the grid spacing was 0.05 mm/grid.

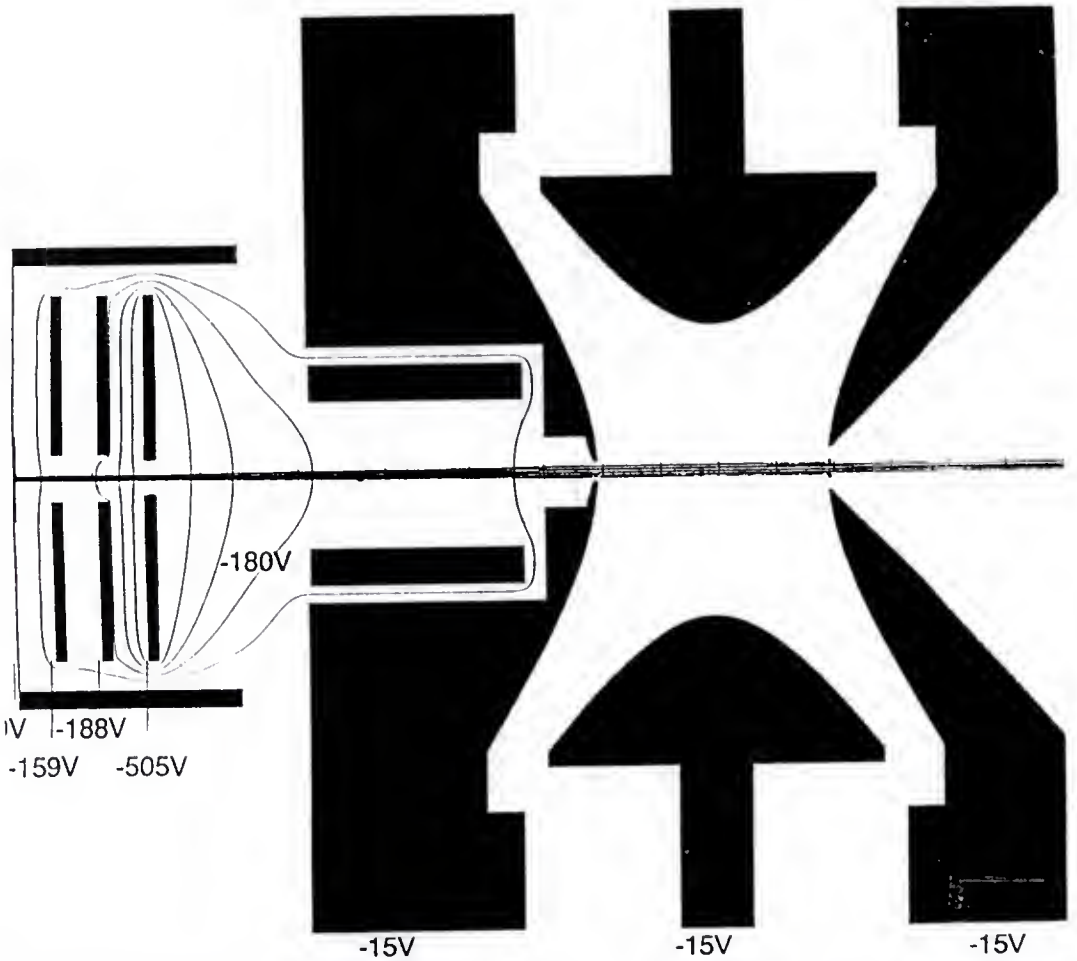

Figure 2-2. Simulation of MALDI-produced egg albumin ions (m/z 43300) for the instrument used by Bier et al..[33] The initial energy for this simulation was 126 eV, the initial angle was 1 degree, and the grid spacing was 0.05 mm/grid.

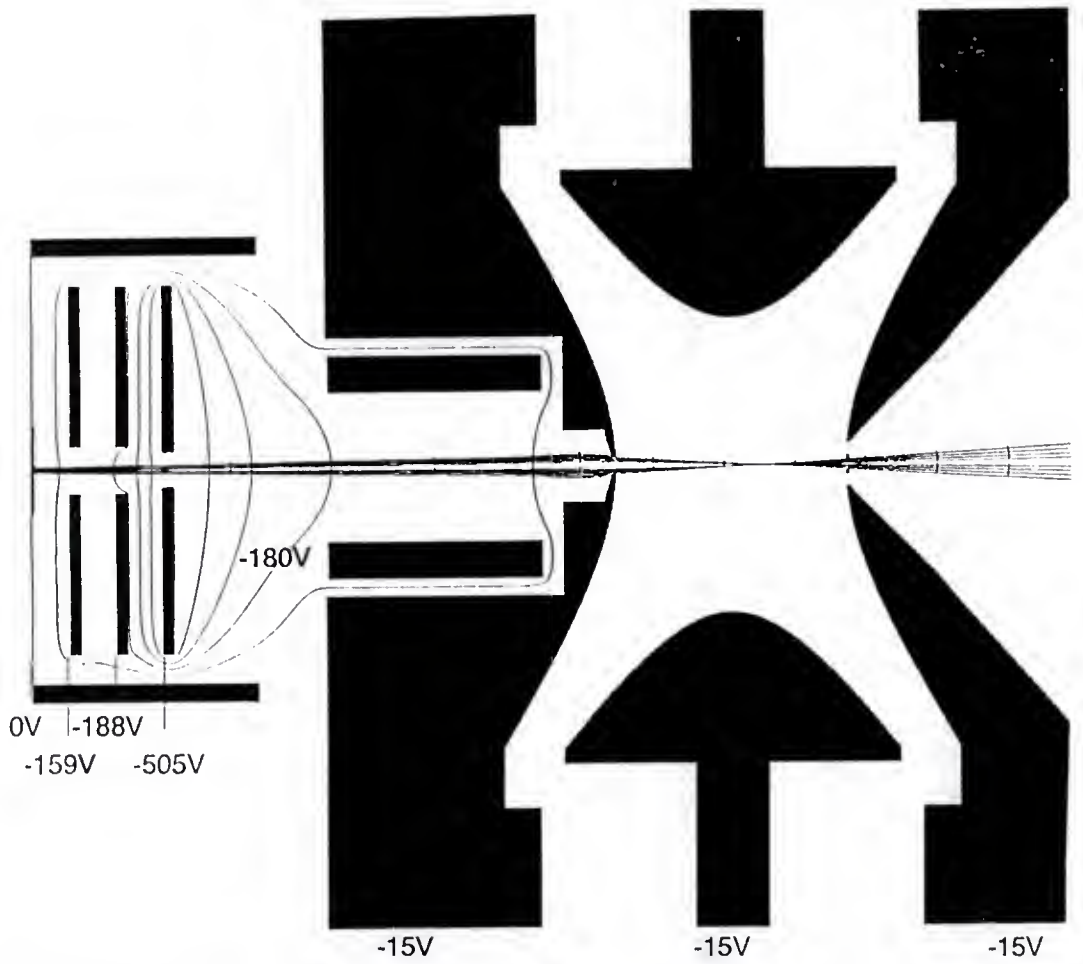

Figure 2-3. Simulation of MALDI-produced bovine insulin ions (m/z 5730) for the instrument used by Bier et al..[33] The initial energy for this simulation was 17 eV, the initial angle was 1 degree, and the grid spacing was 0.05 mm/grid.

with no radial velocity) as shown in Figure 2-1, there is a large loss in sensitivity due to a lack of focusing of the ion beam caused by the radial velocities present in the 1° angle case. In the case of a lower molecular weight molecule such as bovine insulin (Figure 2-3), some focusing does occur, leading to a much more intense mass spectrum. This is reflected in the data presented in Figure 1-28.

The SIMION results for the use of a modified GC ion source as a MALDI ion source shows the limitations in this type of instrument configuration (that is, limited ion source voltages due to the lens placement in the source). This type of source also is very difficult to operate, since the laser beam intensity is affected by the distance the fiber optic is inserted in the ion source and the distance from the probe tip to the end of the fiber optic. Sample imaging is also very difficult because of the compact size of the ion source.

For the MALDI quadrupole ion trap that was to be constructed for the research to be performed in this dissertation, a MALDI ion source taken from a commercially-available time-of-flight mass spectrometer (a Vestec ResearcH™ linear time-of-flight mass spectrometer) was chosen. This ion source was specifically designed for the MALDI analysis of proteins and polymers, and should perform this function much better than an ion source originally designed for another purpose (e.g. gas chromatography). A schematic of the original Vestec time-of-flight system is shown in Figure 2-4. The final design of the MALDI QITMS instrument is shown in Figure 2-5.

The vacuum chamber from the Vestec ResearcH™ was used for this instrument. The original Vestec MALDI sample probe and air-actuated probe inlet mechanism were removed from this chamber, and a standard Finnigan probe and bellows valve assembly were added to the flange that holds the MALDI ion source and ion trap. The much larger probe tip on the Finnigan probe allowed for easier placement of tissue samples on the

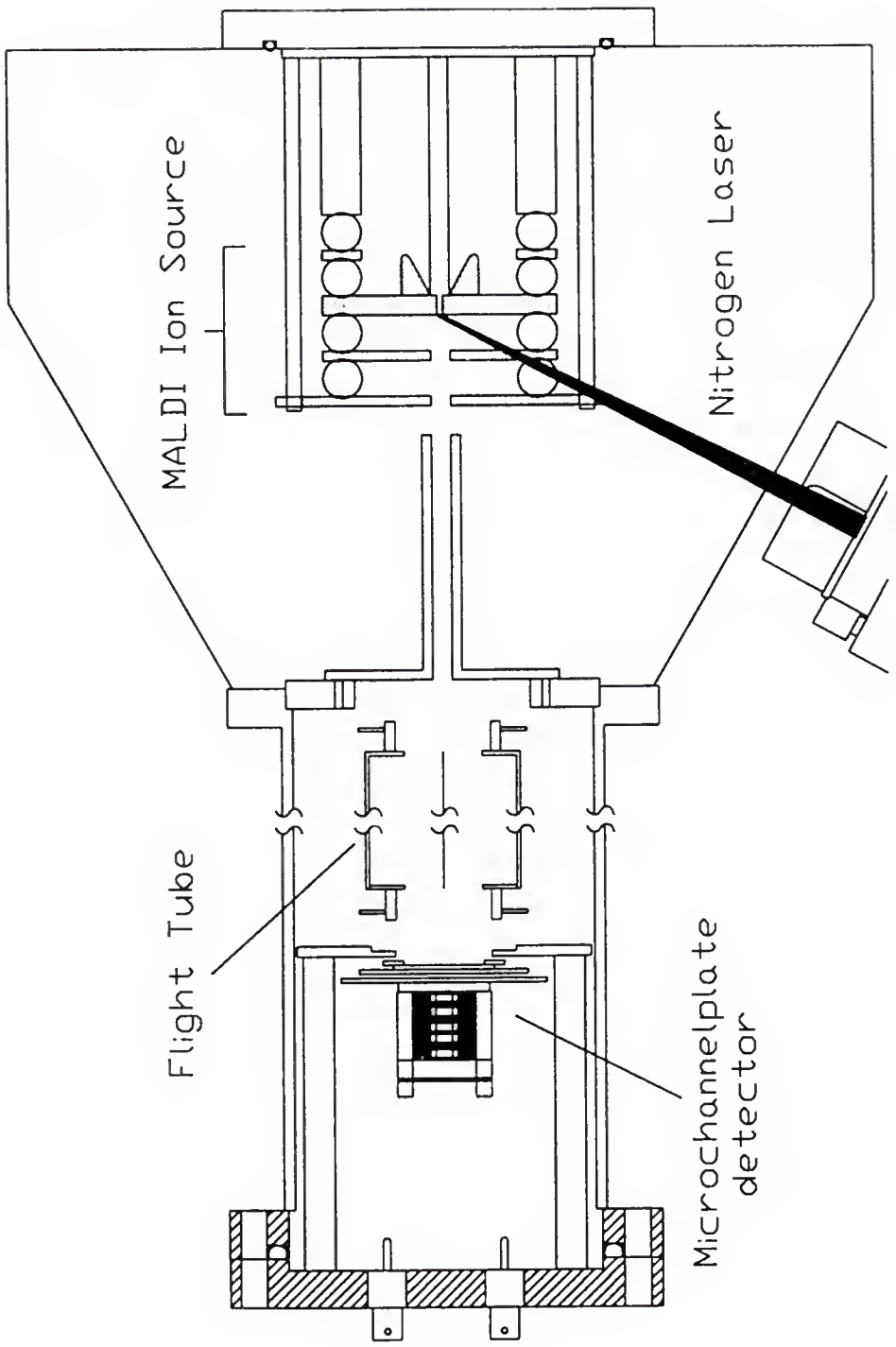

Figure 2-4. Vestec ResearcH™ MALDI Time-of-Flight MS instrument used for this research.

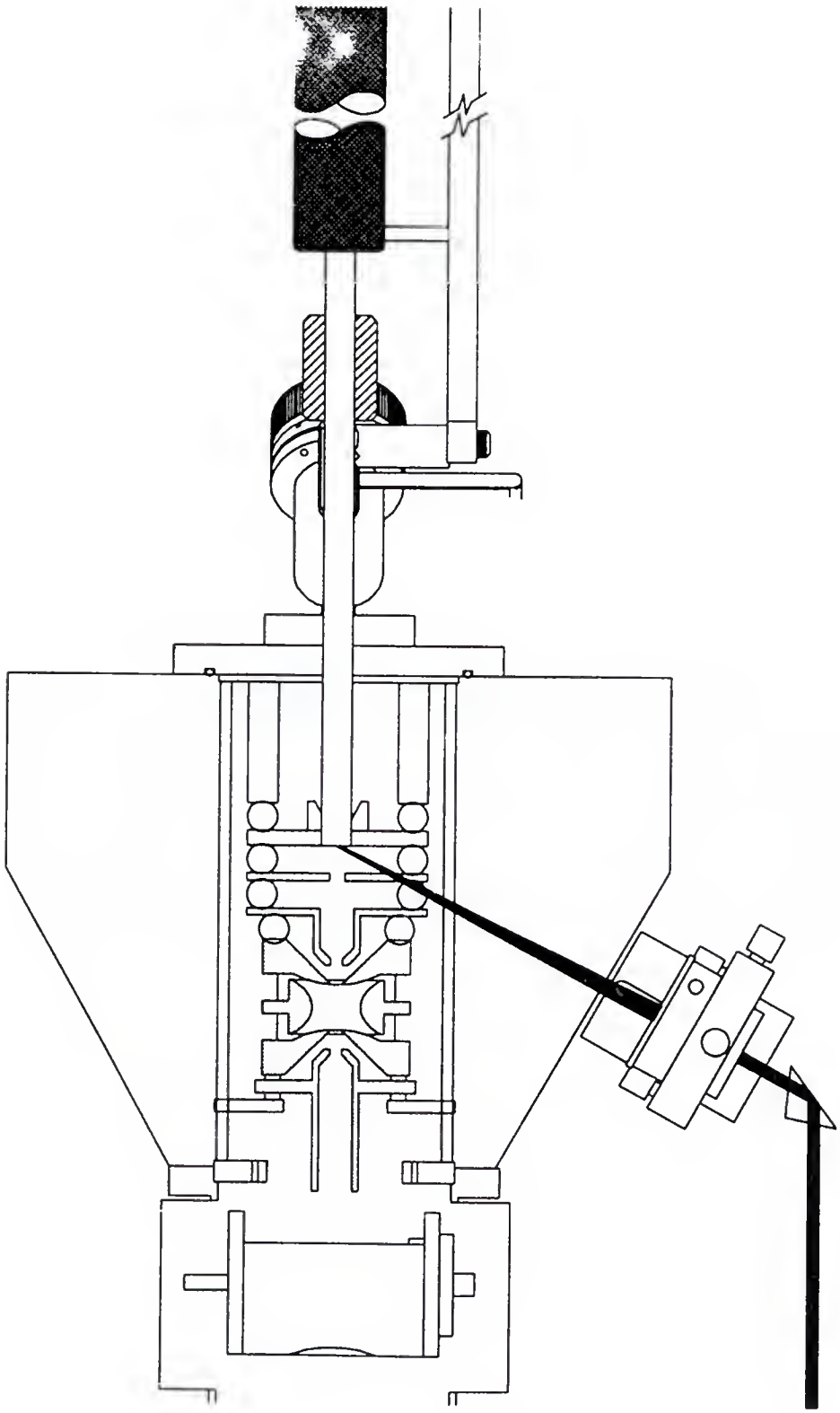

Figure 2-5. MALDI QITMS instrument built for this research.

surface of the probe, which allowed for a greater choice of the site where MALDI will be performed on the sample (since the site that the nitrogen laser will strike the sample can be controlled by the laser optics). Four stainless steel rods were added to the flange as an optical rail to facilitate alignment of the MALDI source and the ion trap. The flange opposite the laser window flange was modified to allow for the addition of an rf high voltage feedthrough for the ion trap ring electrode, a gas feedthrough for the helium buffer gas needed for cooling of the ions in the quadrupole ion trap, and four single-ended MHV feedthroughs rated to 1 kV (Insulator Seal Incorporated, Hayward, CA). Two of the high voltage feedthroughs were used for the axial modulation signal placed on the endcap electrodes of the ion trap, and two were used for the entrance and exit tube lenses of the ion trap. The high voltage feedthroughs that are standard on the Vestec system (rated at ±35 kV) were used for the sample lens and focusing lens of the MALDI ion source. The flight tube and MCP detector used for the MALDI TOF instrument were removed, and the vacuum chamber that attaches to the back of the MALDI source vacuum chamber was modified to allow for the mounting of a ±20 kV off-axis conversion dynode detector. A Finnigan ITS40 quadrupole ion trap with quartz spacers was used for this instrument, with the electronics from the ITS40 used to control the ion trap and detector.

The software used to control the quadrupole ion trap was Gatorware software, created by Tim Griffin of the Richard Yost research group at the University of Florida.[37] This software allows for the creation of the scan functions used for all of the MALDI QITMS analyses shown in this dissertation. Major features of this software are the ability to control axial modulation frequencies and voltages during each step of a scan table (allowing for software control of the mass range extension and CID parameters), the ability to use a TTL pulse to control the firing of the nitrogen laser, and the ability to

acquire profile data (as uncorrrected mass, acquisition DAC, and intensity) to disk for later processing (to allow for signal averaging and mass assignment).

Instrument Simulation

Before this instrument was constructed, the proposed design was simulated using SIMION. For this simulation, bovine insulin (M.W. 5734) was chosen as the model compound, and only the transmission of MALDI-produced ions from the ion source into the quadrupole ion trap was considered (that is, no rf was placed on the ring electrode to study the trapping of the injected ions). The results for this simulation are shown in Figure 2-6, with the voltages used displayed above the lenses. The grid spacing for the simulation was set to 0.05 mm/grid (which allowed for the maximum resolution available), and an initial kinetic energy of 17 eV and an initial angle of 10 degrees were used. From Figure 2-6 it is clear that this source, used with much higher lens voltages, should be much better at focusing ions produced with a greater radial velocity (which is typically the case for MALDI-generated ions). This simulation demonstrated the feasibility of this instrument design.

Instrument Characterization

In order to characterize the performance of the MALDI QITMS instrument constructed for this research, a series of peptide standards were analyzed using a dihydroxybenzoic acid (DHB) matrix. A variety of peptides were chosen because of the mass range they covered and their availability: the synthetic tetrapeptide MRFA (M.W. 523.65); Angiotensin II (M.W. 1046.2); Bradykinin (M.W. 1060.2); Angiotensin I (M.W. 1296.5); Substance P (M.W. 1347.6); Dynorphin B (M.W. 1570.9); and Melittin

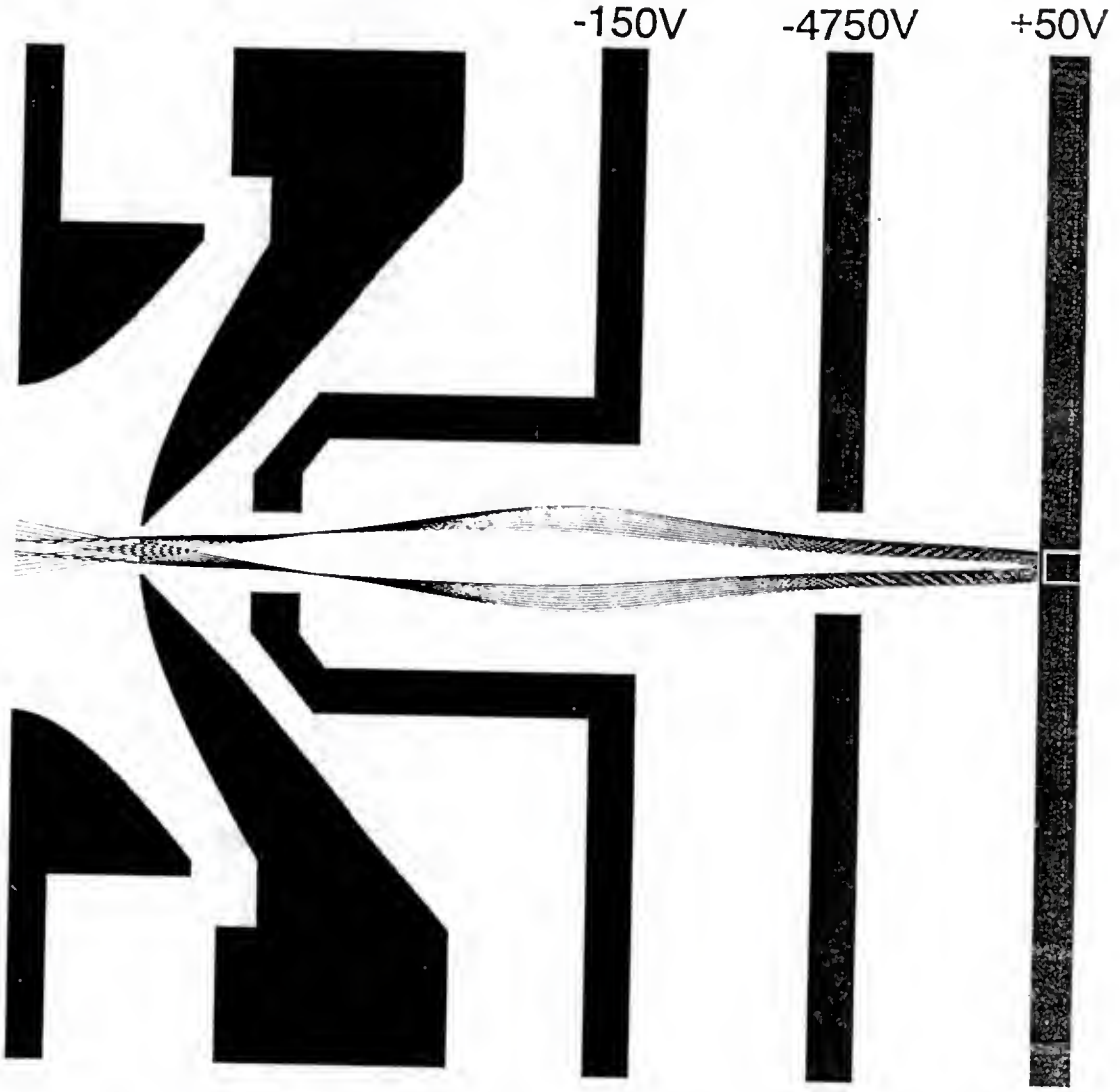

Figure 2-6. SIMION simulation for bovine insulin using the design for the MALDI QITMS instrument built for this research.

(M.W. 2847.5). Two of the peptides analyzed during this characterization are presented in this dissertation as being representative of the ability of the MALDI QITMS instrument to analyze these types of compounds.

Primary standards for these peptides were prepared at $1x10^{-3}$ M in deionized water. Working standards were prepared at $2x10^{-5}$ M in deionized water. The DHB matrix solution was prepared by adding 0.125 g of DHB to 1 mL of 50:50 (v/v) deionized water and acetonitrile. Equal amounts of the working peptide standards and the DHB solution (10 μL each) were mixed in a 100 μL microcentrifuge vial, and 1 μL of this mixture was placed on the mass spectrometer probe tip and allowed to air dry.

MALDI QITMS of a synthetic tetrapeptide (MRFA)

MALDI quadrupole ion trap mass spectrometry was first performed on the synthetic tetrapeptide MRFA (Met-Arg-Phe-Ala) because it has a molecular weight (523.65 amu) accessible to the standard quadrupole ion trap instrument. During this stage of instrument characterization, proper lens voltage settings were obtained by varying the voltages and observing the effect they had on the MALDI QITMS spectrum for this compound. The settings determined for MRFA worked equally well for all of the compounds analyzed for this dissertation. The setting used are

L1 (sample plate lens) = +20 V

L2 (focusing lens) = -700 V

L3 (ion trap entrance lens) = -63 V

L4 (ion trap exit lens) = -500 V

For all of the MALDI QITMS spectra acquired for this dissertation, no offset voltage was applied to the ion trap (that is, the ion trap was not floated), and an electron multiplier voltage of -1600 V and a dynode voltage of -3 kV was used. The helium buffer gas pressure was set to 2.5×10^{-5} torr (uncorrected for helium) as read on a Bayard-Alpert type ion gauge (Granville Phillips) mounted above the diffusion pumps used to achieve the high vacuum needed for this system. This corresponds to approximately 1.8×10^{-3} torr within the ion trap when conductance limits and ion gauge correction factors are accounted for.

The MALDI quadrupole ion trap spectrum for 20 pmol of MRFA is shown in Figure 2-7. This spectrum shows the $[M + H]^+$ ion at m/z 524 as the base peak along with an intense $[M + Na]^+$ ion typical of biopolymers. Also present is the $[M + CO]^+$ ion which is routinely seen in MALDI mass spectrometry and is produced from attachment of photofragments from the matrix[38]. This spectrum shows the unit mass resolution attainable by using a quadrupole ion trap as the mass analyzer for performing MALDI analyses. The presence of adduct peaks in the mass spectrum seen here is typically observed in MALDI mass spectra, and requires excellent mass resolution in order to determine correct mass assignments. The mass resolution required to resolve these mass peaks, especially in the low mass region, is very difficult for a time-of-flight mass spectrometer to achieve. A comparison of the analysis of MRFA on the MALDI QITMS instrument built for this dissertation and on a Finnigan LaserMAT linear time-of-flight mass spectrometer (which has a 0.5 m flight tube) is shown in Figure 2-8. Whereas the TOF instrument gives a broad peak at m/z 524 with a high-mass tail, the QITMS instrument resolves these peaks into the $[M + H]^+$ peak, the ^{13}C isotopes associated with the $[M + H]^+$ peak, the $[M + Na]^+$ and $[M + K]^+$ peaks, and the $[M + CO]^+$ adduct peak.

The scan function used to produce this spectrum is shown in Figure 2-9, and is listed in Table 2-1. At the start of the scan function, the rf level is set so that the [M +

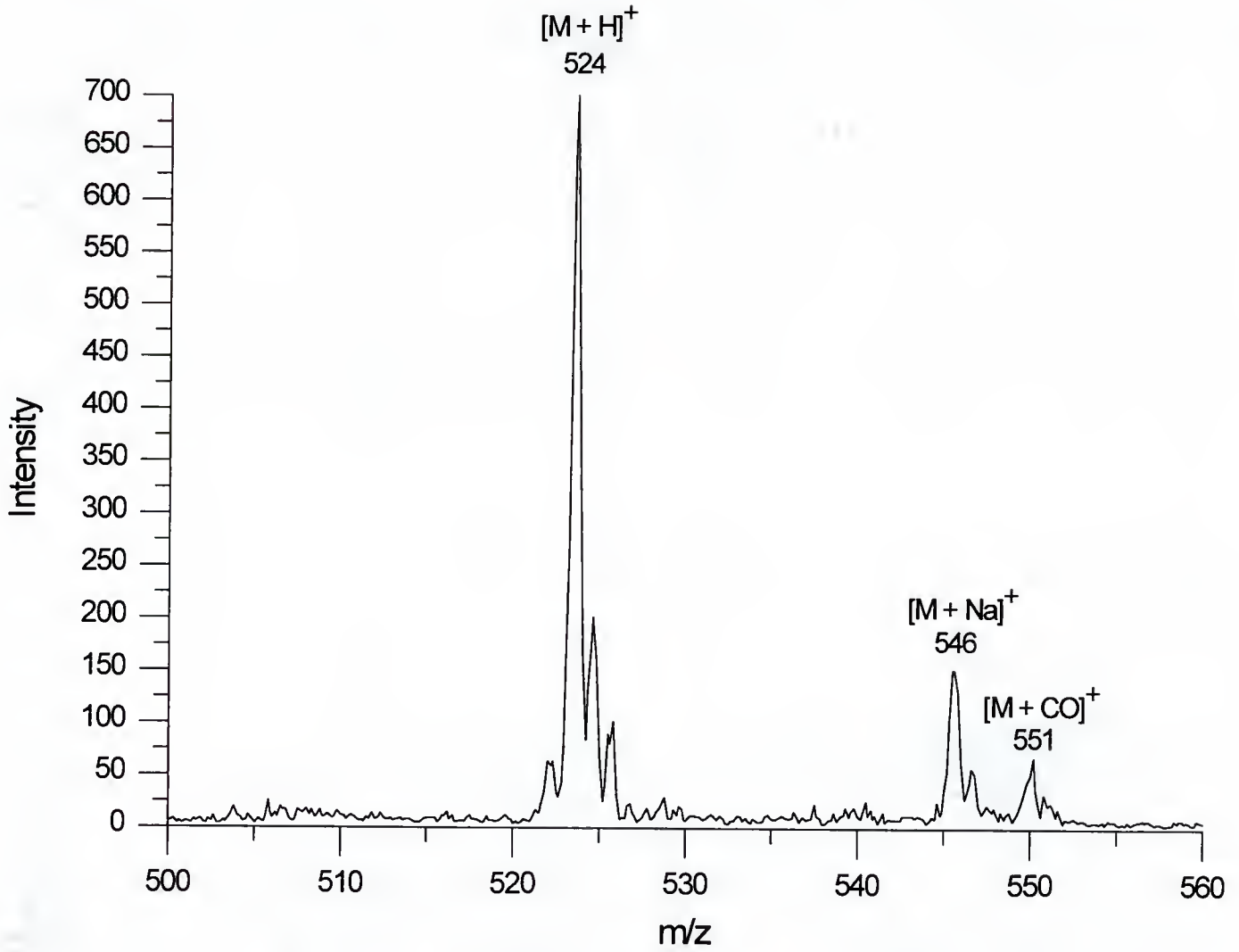

Figure 2-7. MALDI QITMS spectrum for 20 pmol of the synthetic peptide MRFA.

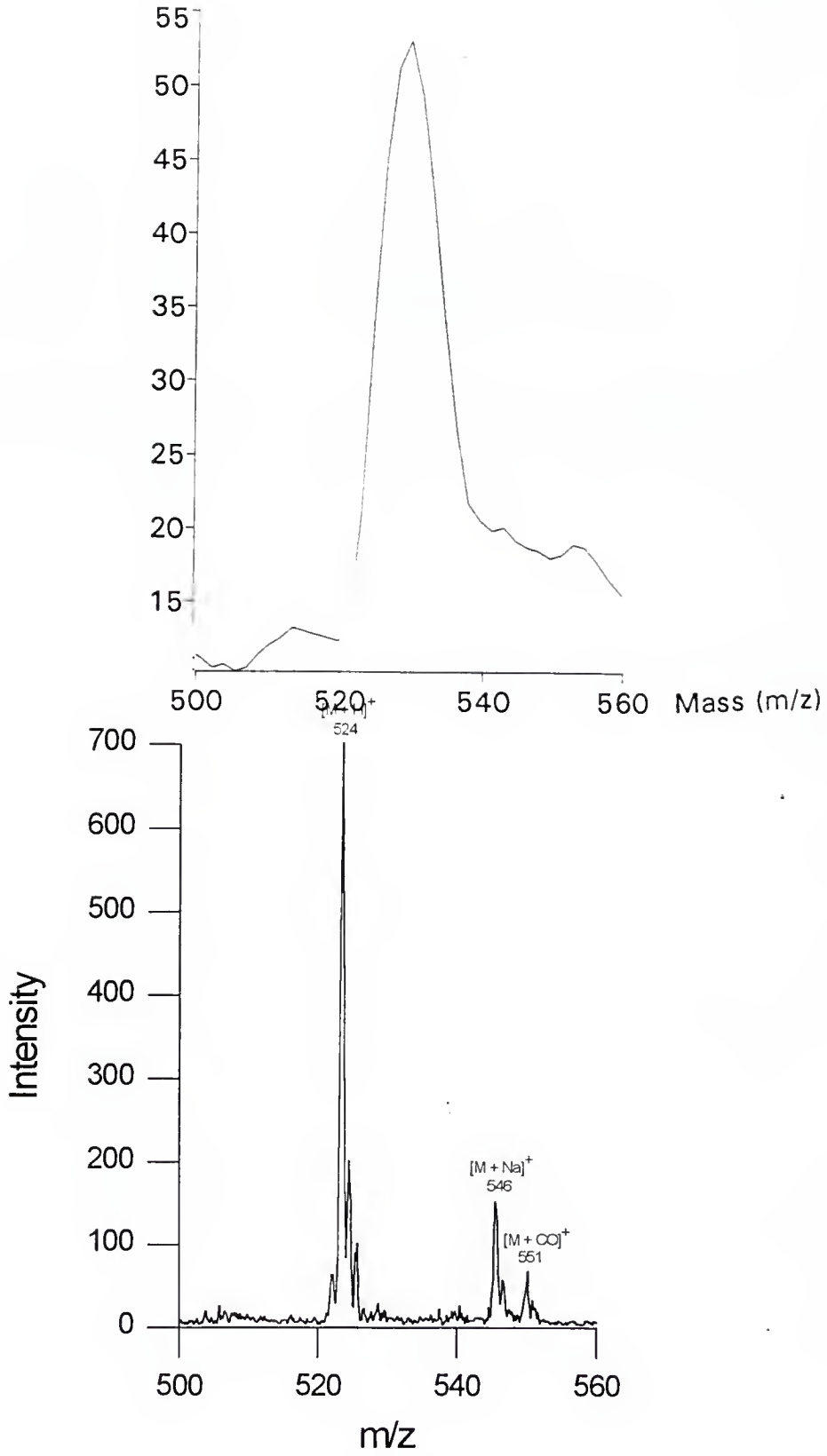

Figure 2-8. Comparison of the MALDI analysis of MRFA on a). a Finnigan LaserMAT TOF MS instrument and b). on the MALDI QITMS instrument constructed for this research.

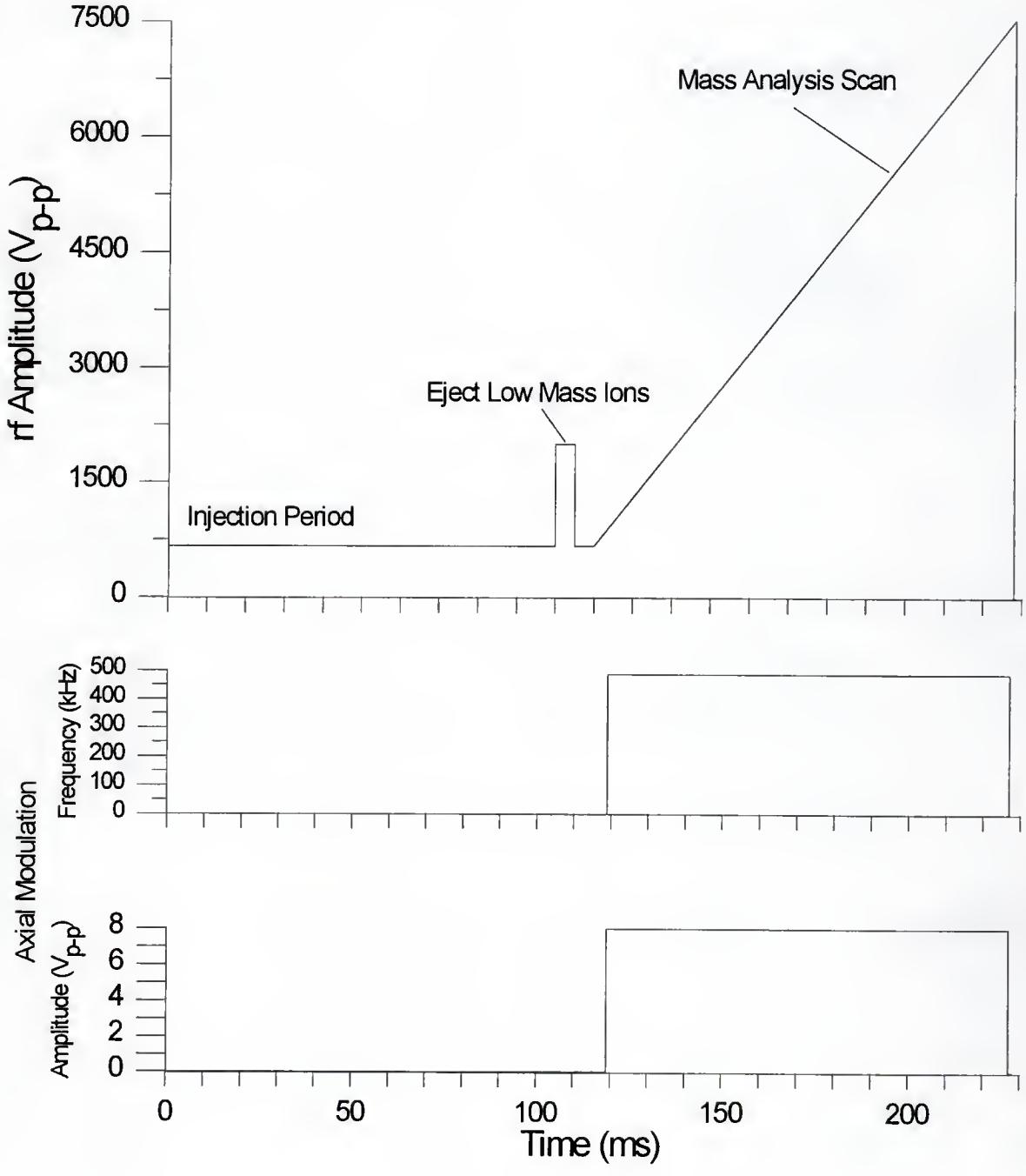

Figure 2-9. Scan function used for the MALDI QITMS analysis of the synthetic tetrapeptide MRFA.

Table2-1. Scan table listing for the MALDI QITMS analysis of the synthetic peptide MRFA.

#	Scan Table	rf Voltage Start	rf Voltage End	Axial Modulation Freq. (kHz)	Axial Modulation Amp (V)	Time (ms)
1	First Table	1328	1328			0.5
2	Ionize	1328	1328			0.001
3	Cool	1328	1328			50
4	Ionize	1328	1328			0.001
5	Cool	1328	1328			50
6	Eject Low Mass Ions	3985	3985			5
7	Prescan	1328	1328			5
8	Acquire	1328	15000	485	8	108
9	Empty Trap	0	0			2

$H]^+$ ion for this compound (m/z 524) is injected at a q of 0.1 (scan table 1). This corresponds to an rf voltage of 664 $V_{0\text{-}p}$. The next table (scan table 2) is used to trigger the nitrogen laser, which has a pulse width of 3 ns (FWHM) in the triggered mode. Next, a cool time of 50 ms (scan table 3) is used to allow the ions that are injected into the ion trap to have sufficient time to be buffered by the helium gas present. The laser trigger and cool tables are then repeated (scan tables 4 and 5) to give a total of two laser shots per scan function, which increases the number of ions present in the ion trap. The ability of this system to store ions from multiple ionization events to increase the sensitivity of the analysis is not available on a time-of-flight mass spectrometer, where each ionization event (defined by the laser pulse) defines the start of the timing cycle to determine the flight time of the ions (and thereby the mass of the ion). The rf is then increased (scan table 6) to eject low mass ions (primarily produced from the DHB matrix) from the ion trap. The mass analysis scan is then performed, in which the electron multiplier is turned on and the rf is ramped to scan out the ions present in the ion trap to produce a mass spectrum (scan table 8). This scan function was repeated 20 times (referred to as 20 microscans), and the mass assignment and sum of the ion signals were acquired as an ASCII text file (using Gatorware software). Mass assignments for this compound were made using the standard calibration software available with the ITS40 software.

MALDI QITMS of Angiotensin II

The next peptide analyzed was Angiotensin II (Asp-Arg-Val-Tyr-Ile-His-Pro-Phe, molecular weight 1046.2 Da). This octapeptide is one of the major components of the renin-angiotensin system of renal hypertension and acts on the adrenal gland to stimulate the release of aldosterone.[39] Since the mass of this compound is greater than the maximum m/z achievable with the standard quadrupole ion trap instrument, the axial

modulation frequency was decreased during the mass analysis scan to increase the mass range of the ion trap. For this analysis, an axial modulation frequency of 210.75 kHz was used, giving a q_{eject} of 0.533 and a maximum attainable mass of 1100 Da (giving a mass range extension of 1.7x). Since the mass resolution is inversely related to the mass range extension factor,[40] the maximum attainable mass is usually set to just above the maximum mass for the ion of interest (in this case, m/z 1046).

The MALDI quadrupole ion trap spectrum for 20 pmol of this compound is shown in Figure 2-10. The scan function used to produce this spectrum is the same as the one used for MRFA (Figure 2-9), except that the rf voltage which corresponds to a q_{inject} of 0.1 is 2655 V. This spectrum shows the $[M + H]^+$ ion at m/z 1047 as the base peak along with lower mass ions resulting from cleavage of the amide bonds along the peptide backbone. These fragment ions, typically seen when performing MALDI using ion trap instruments (e.g. FTMS and quadrupole ion traps)[41,42] but not with time-of-flight instrument, are produced by collision-induced dissociation (CID) with helium and other background gases present in the ion source and quadrupole ion trap, by surface-induced dissociation, SID, with ion optic surfaces or the ion trap electrodes, or by metastable decay, and can be very useful in sequencing the peptide.[43] The mechanism for the formation for the y- and b-ions (following the product ion nomenclature of Roepstorff and Fohlman[44]) seen in this spectrum is shown in Figures 2-11 and 2-12, respectively. Formation of y-type ions (e.g. the y_7^+ ion, Figure 2-11) involves cleavage of the amide bond along the peptide backbone, with the charge being retained on the amide nitrogen. The fragment shown in Figure 2-11 is termed y_7 because it contains seven amino acid residues from the original peptide structure (counting from the carboxy terminus). Formation of b-type ions (e.g. the b_6^+ ion, Figure 2-12) occurs by β-cleavage and charge migration to the carbonyl end of the amino terminus fragment. The fragment shown in

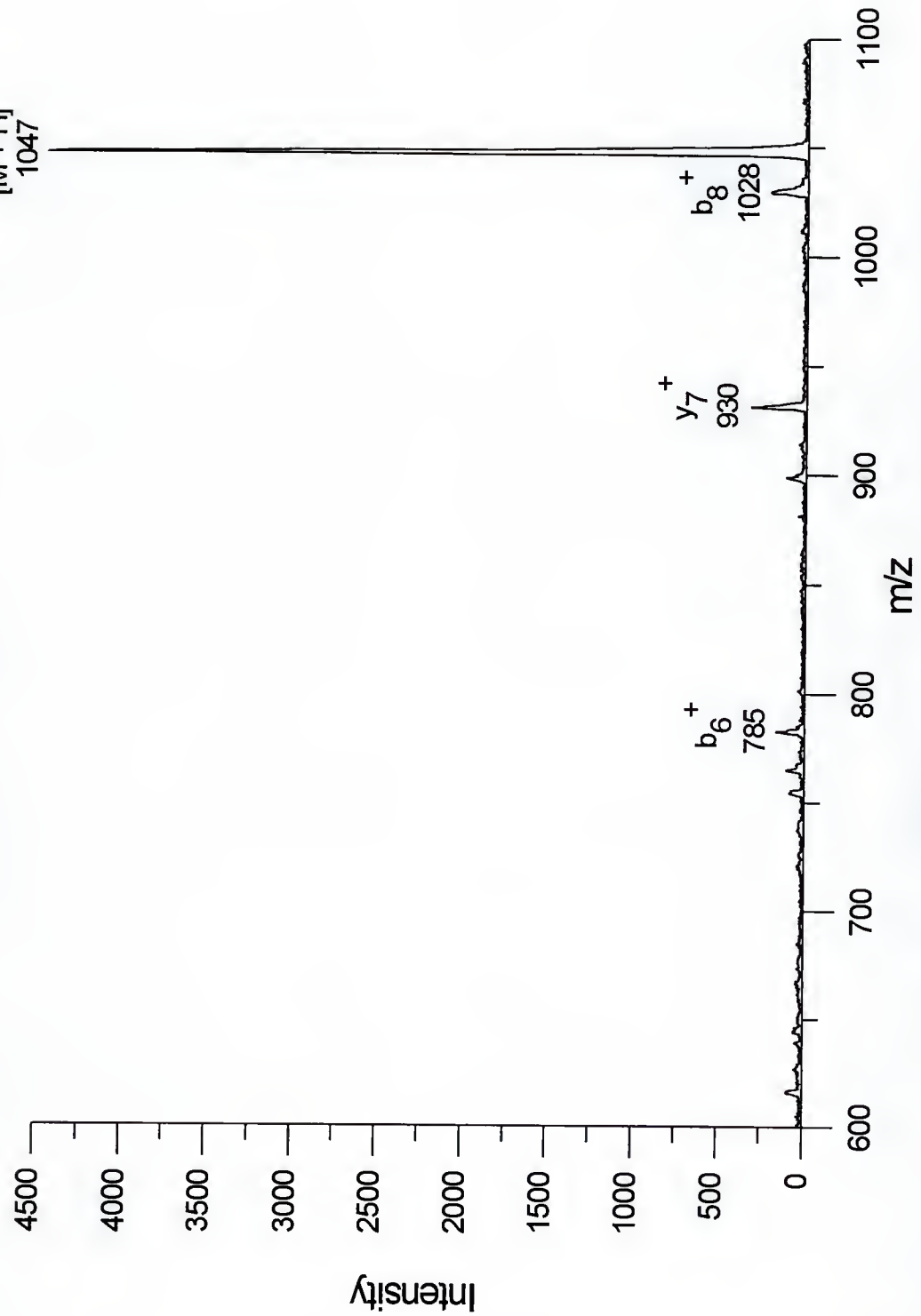

Figure 2-10. MALDI QITMS spectrum for 20 pmol of Angiotensin II.

ANGIOTENSIN II

R_8 = Asp
R_7 = Arg
R_6 = Val
R_5 = Tyr
R_4 = Ile
R_3 = His
R_2 = Pro
R_1 = Phe

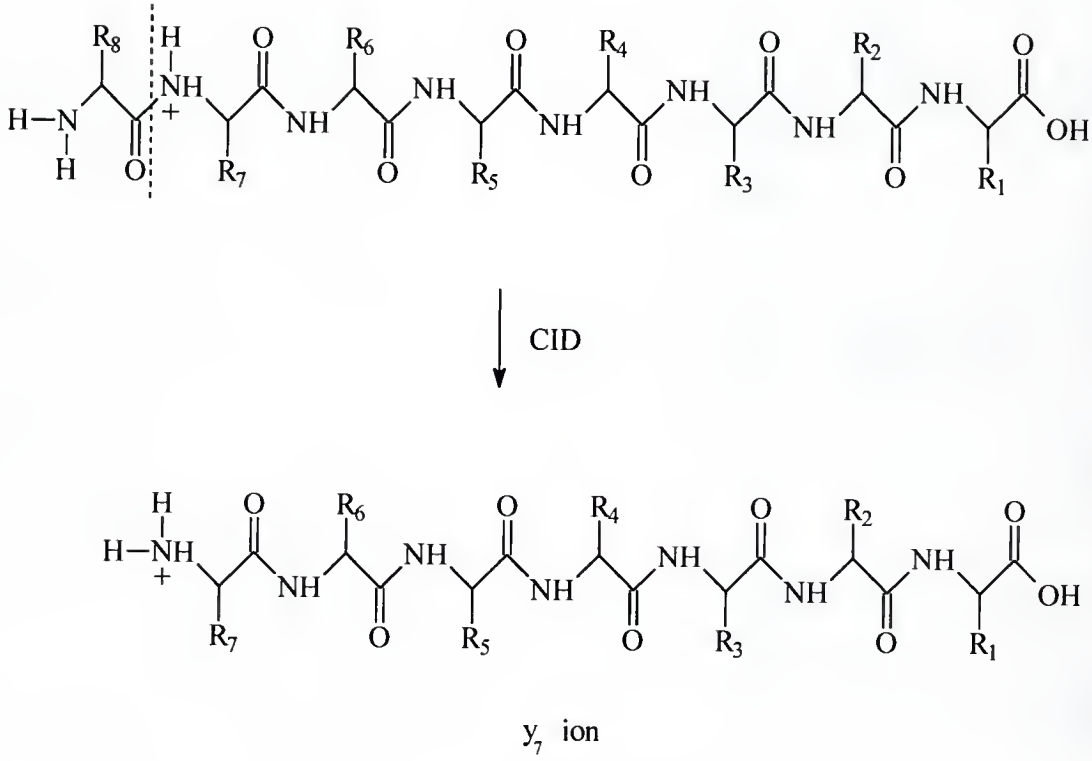

y_7 ion

Figure 2-11. Mechanism for the formation of the y_7^+ ion for angiotensin II.[58]

ANGIOTENSIN II

R_1 = Asp
R_2 = Arg
R_3 = Val
R_4 = Tyr
R_5 = Ile
R_6 = His
R_7 = Pro
R_8 = Phe

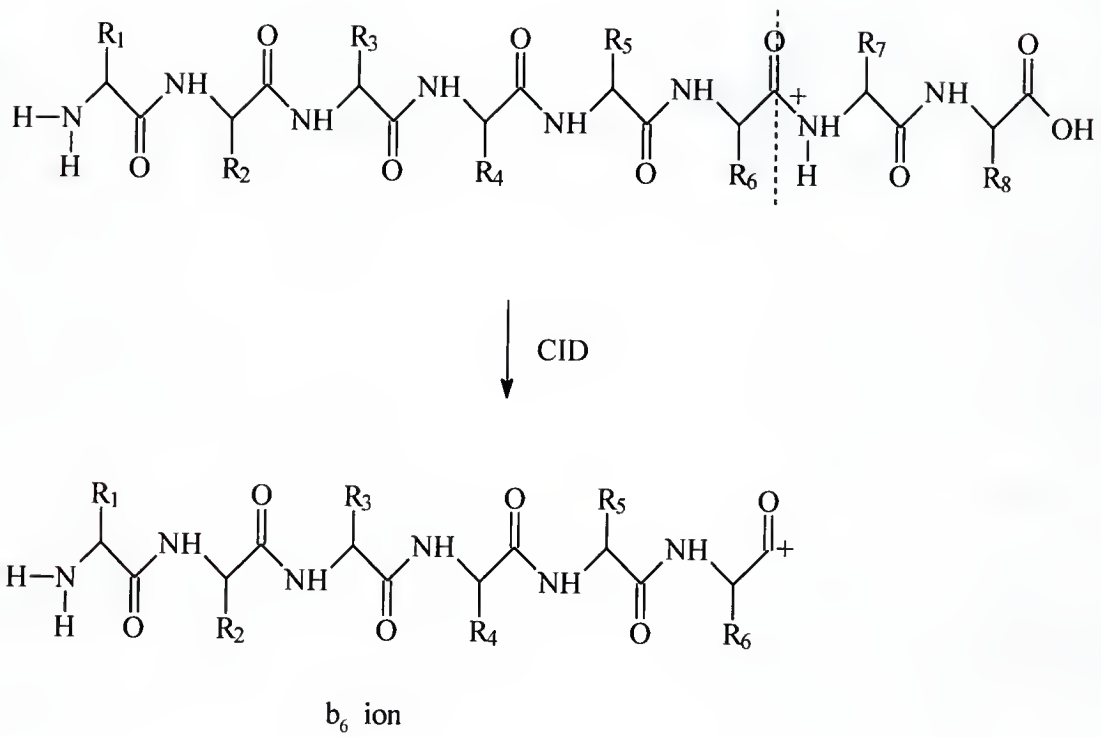

Figure 2-12. Mechanism for the formation of the b_6^+ ion for angiotensin II.[58]

Figure 2-12 is termed b_6 because it contains six amino acid residues from the original peptide structure (counting from the amino terminus).

Although fragment ions produced during the injection process can be used to help sequence a peptide, this is only the case when the analyte is present as the sole constituent in the sample (since it is impossible to tell which fragment ion came from which $[M + H]^+$ ion in a mixture of unknowns). When a mixture is present, MS/MS must be performed. When performing MS/MS using a quadrupole ion trap, the ion of interest must be isolated from the remainder of the ions present in the ion trap prior to resonance excitation. A number of techniques have been successfully used to isolate ions using a quadrupole ion trap, including apex,[45-46] two-step,[47,48,49] SWIFT (stored-waveform inverse Fourier transform),[50,51] random noise,[52] FNF (filtered noise field),[53] and forward-and-reverse scanning.[54,55] For the MS^n results for Angiotensin II shown in this dissertation, the forward-and-reverse isolation technique as shown by Schwartz et al.[54,55] was used. Although apex and two-step isolation are effective, they can only isolate ions up to approximately m/z 600 on standard ion trap instruments because of the high dc voltages necessary to be applied to the ring electrode. The forward-and-reverse scanning technique, however, only requires differing frequencies and voltages to be applied to the endcap electrodes.

The scan program to implement this method of ion isolation is shown in Figure 2-13 and is listed in Table 2-2. After the ionization and cool steps (labeled as "Injection Period"), the axial modulation is turn on (210.75 kHz, 8 V) and the rf is ramped from a q of 0.1 to a q of 0.562 (which corresponds to an ion frequency just below that for the ion of interest). Since the axial modulation frequency and voltage used for isolation is the same as that used for mass analysis, the final q that will be ramped to is calculated based on the observed (rather than the actual) m/z for the ion of interest (that is, the final q that will be ramped to is varied until the corresponding mass, as displayed by the Gatorware

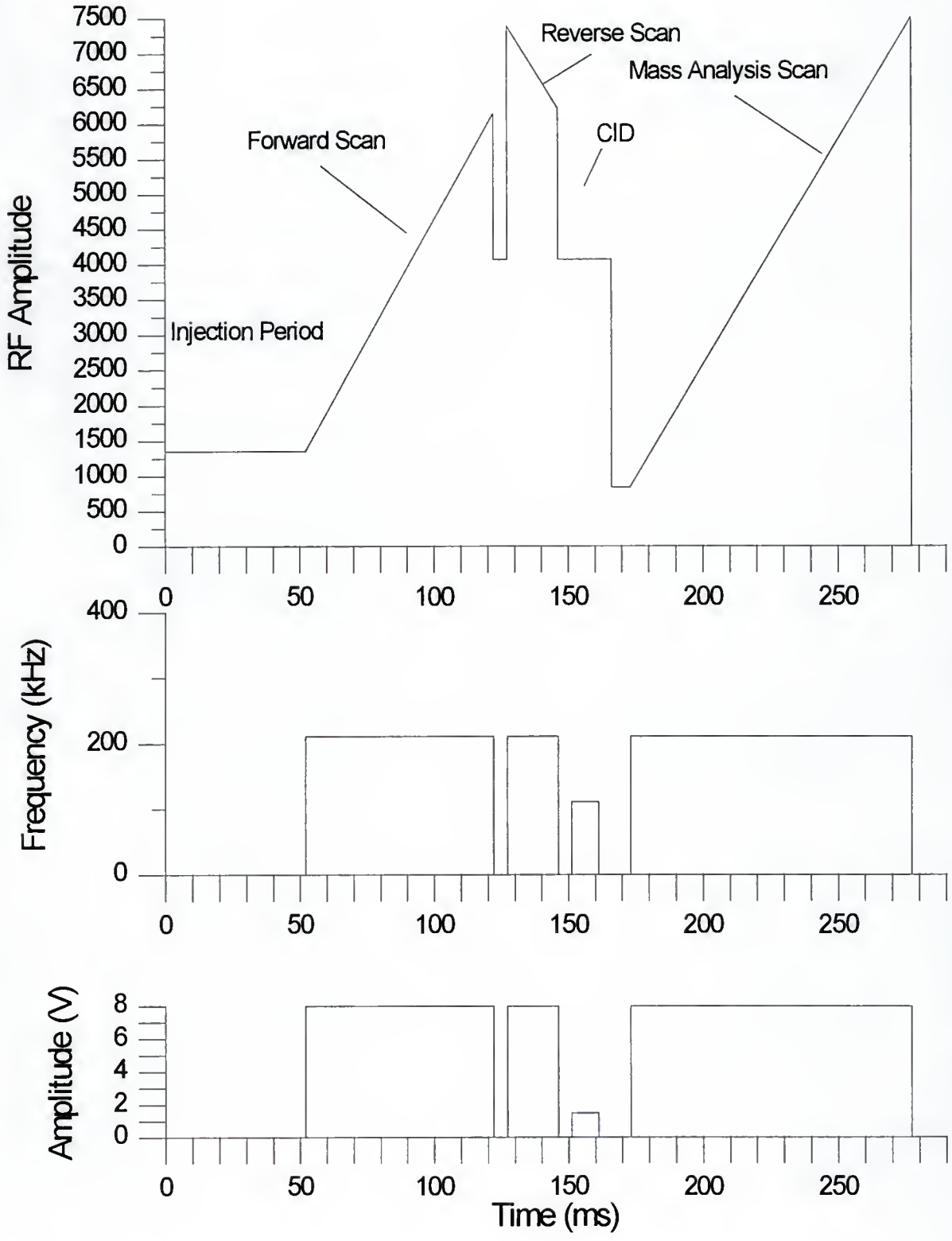

Figure 2-13. Scan function used for the MALDI QIT MS/MS analysis of Angiotensin II.

Table 2-2. Scan table listing for the MALDI QITMS analysis of angiotensin II.

#	Scan Table	rf Voltage Start	rf Voltage End	Axial Modulation Freq. (kHz)	Axial Modulation Amp (V)	Time (ms)
1	First Table	2655	2655			0.5
3	Ionize	2655	2655			0.001
4	Cool	2655	2655			50
5	Ionize	2655	2655			0.001
6	Cool	2655	2655			50
7	Forward Scan	2655	12274	210.75	8	70
8	Cool	10090	10090			5
8	Reverse Scan	15000	12444	210.75	8	19
9	Cool	7965	7965			5
10	MS/MS	7965	7965	115	2.8	10
11	Cool	7965	7965			5
12	Prescan	2655	2655			5
13	Acquire	2655	15000	210.75	8	108
14	Empty Trap	0	0			2

software, is set to just below the displayed mass for the ion of interest). As ions of increasing mass come into resonance with the supplementary field, they become excited and are ejected from the ion trap. Just before the ion of interest gets to this frequency, the axial modulation is turned off and the rf is set to cool the remaining ions in the ion trap. This is termed a "Forward Scan" because the rf is scanned in an increasing manner and ions of increasing m/z are ejected from the ion trap. The rf is then set to the maximum available (7500 $V_{0\text{-}p}$, q = 0.89) and the axial modulation is turned back on. The rf is then ramped down to just above that for the ion of interest (the rf is ramped from a q of 0.89 to a q of 0.570 in this case). This is termed a "Reverse Scan" since the rf is scanned in a decreasing manner. The axial modulation is then turned off and the rf is set to cool the remaining ions in the ion trap. The sequential steps involved in the forward-and-reverse scan isolation procedure is shown in Figure 2-14. At this point a narrow m/z range is isolated in the ion trap. In the case of the mass spectrum of Angiotensin II shown at the top of Figure 2-15, the mass analysis scan immediately follows the forward-and reverse scan. This gives the spectrum of the mass-isolated $[M + H]^+$ ion for Angiotensin II. To perform MS/MS on this ion, after the $[M + H]^+$ ion for Angiotensin II is isolated the rf is set to correspond to a q of 0.3 for the ion of interest and the axial modulation frequency is set to 115 kHz. The axial modulation voltage is varied until the mass-isolated ion (in this case the $[M + H]^+$ ion) begins to decrease and daughter ions begin to appear. If too much voltage is applied, resonance ejection takes place instead of resonance excitation and the signal is lost. If not enough voltage is applied, the spectrum remains unchanged. The daughter ion spectrum produced from the fragmentation of the $[M + H]^+$ ion of Angiotensin II using an axial modulation frequency of 115 kHz and voltage of 2.8 V is shown in the bottom spectrum of Figure 2-15. Along with residual $[M + H]^+$ ion, ions corresponding to the cleavage of amide bonds (y_7^+, b_8^+, and b_6^+ ions) are observed. Although these ions correspond well with those seen for the

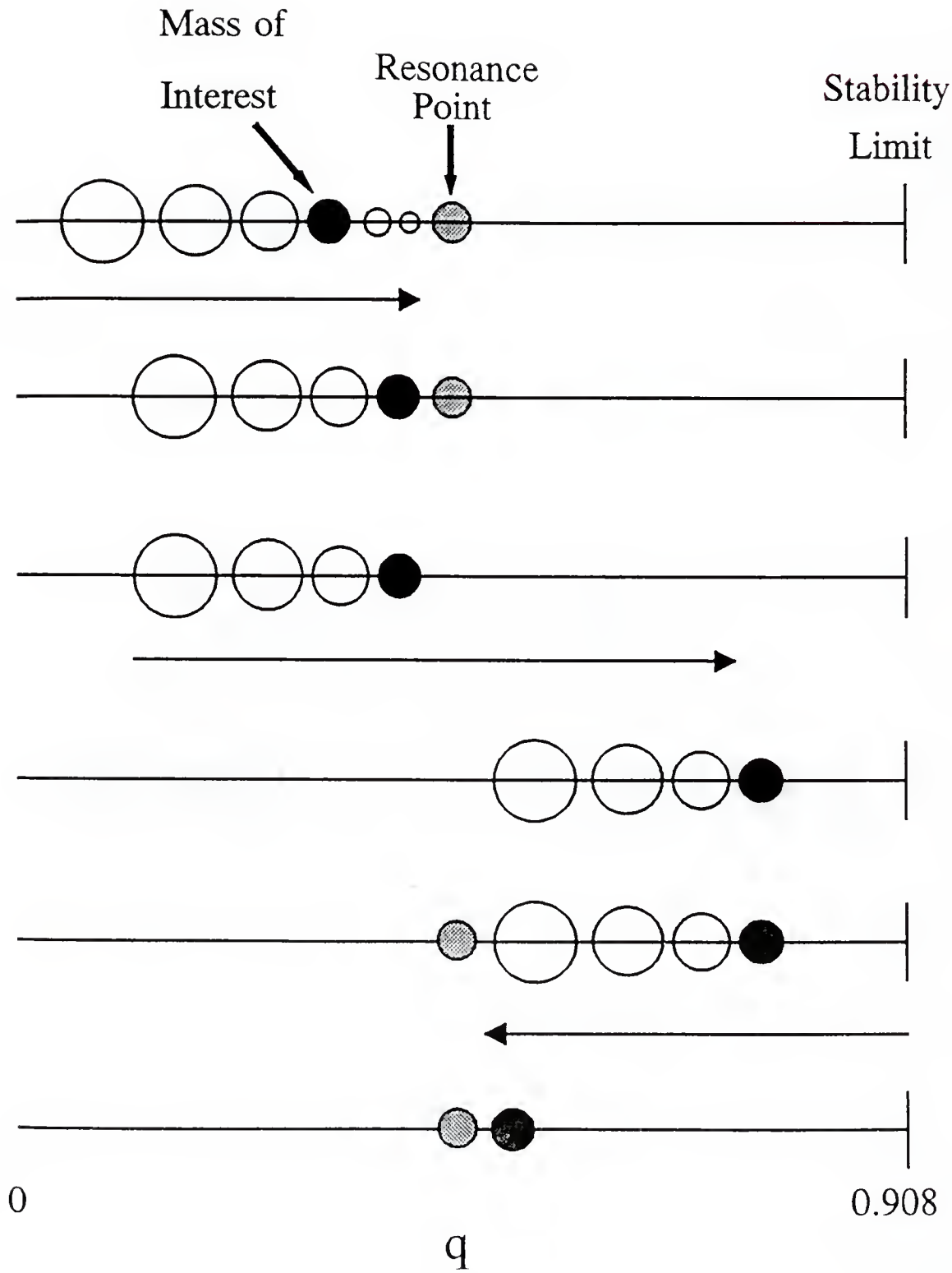

Figure 2-14. Sequential steps in the forward-and-reverse scan isolation procedure.[55]

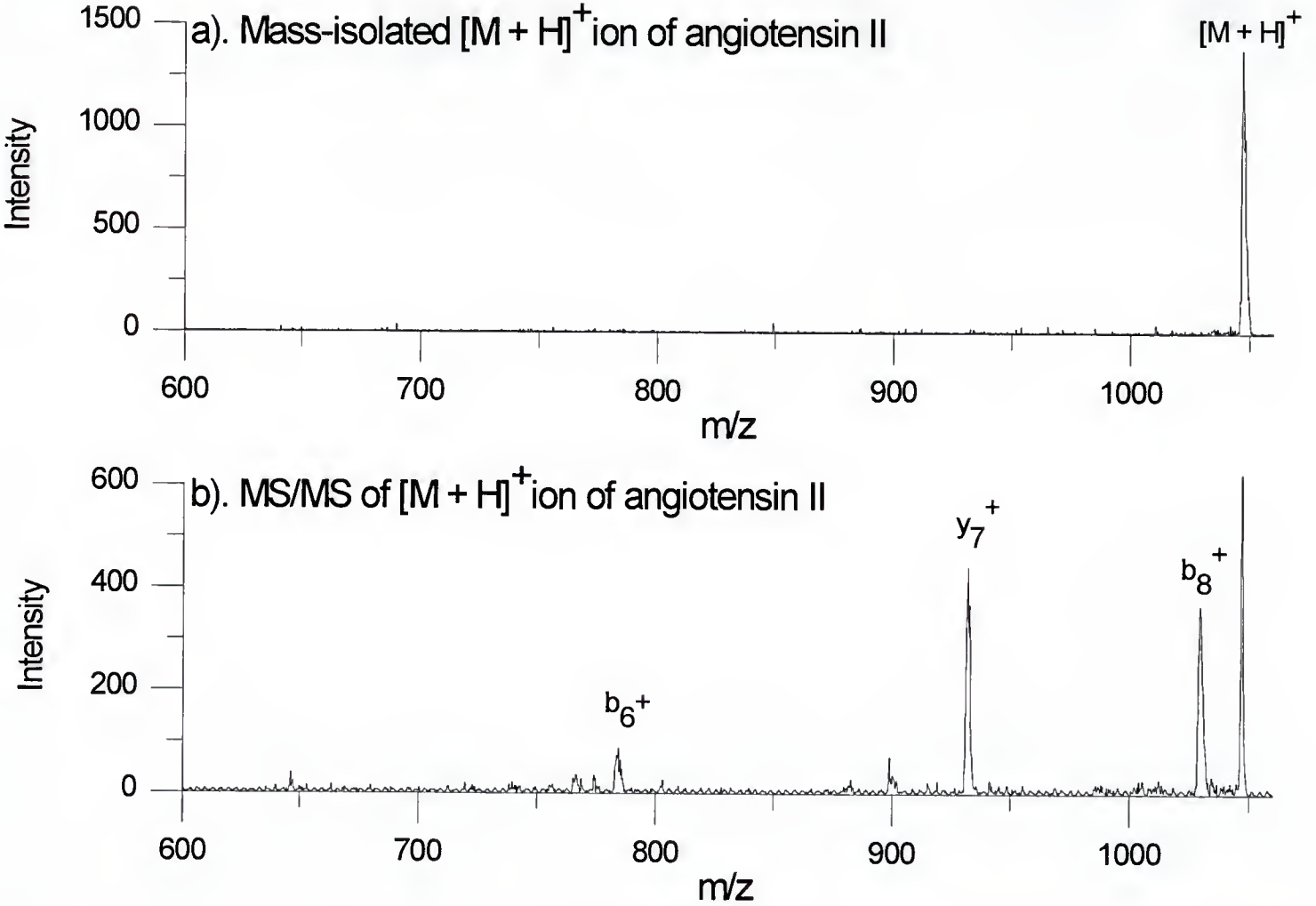

Figure 2-15. a). Mass isolated MALDI QITMS spectrum ($[M + H]^+$ ion) for 20 pmol of Angiotensin II, and b). MS/MS spectrum for this ion.

fragment ions produced during the injection process, the isolation and MS/MS process assures that these fragment ions are only produced for the ion of interest (in this case, the $[M + H]^+$ ion of Angiotensin II). It is also interesting to note the greater increase in intensity for these peptide backbone fragment ions. Although it is difficult to correlate separate MALDI spectra (due to a decrease in the signal intensity over time at a single spot due to ablation of the sample), the intensities of the MS and MS/MS spectra taken in Figure 2-15 can be roughly compared to estimate the MS/MS efficiency (defined as the fraction of ions collected that are product ions, and is given as the ratio of the sum of the intensities of the product ions divided by the intensity of the parent ion remaining following excitation and the sum of the intensities of the product ions[56]) since they were taken from the same laser spot and from back-to-back acquisitions. After 20 microscans were acquired for the MS spectrum (with 2 laser shots per microscan, giving a total of 40 laser shots summed for this spectrum), the resonance excitation frequency was turned on, and 20 microscans were acquired for the MS/MS spectrum (again with 2 laser shots per microscan). Another MS spectrum taken immediately after the MS/MS spectrum confirmed that the intensity had not decreased by more than 10% of its original value. Comparing these two spectra gives an MS/MS efficiency of approximately 50%.

MS/MS was then performed on the daughter ions produced by the fragmentation of the $[M + H]^+$ ion of Angiotensin II. This is termed MS^3, since three stages of MS are performed. As is the case with MS/MS, MALDI ions from Angiotensin II were injected and cooled, then the $[M + H]^+$ ion for Angiotensin II was isolated using the forward-and-reverse scanning technique. After fragmentation using resonance excitation, one of the daughter ion, the y_7^+ ion, was mass isolated (again using the forward-and-reverse scanning technique). The rf level was set to a q of 0.3 for the y_7^+ ion, and resonance excitation was performed (115 kHz, 2.5 V). The mass-isolated spectrum for Angiotensin II is shown in Figure 2-16a, the daughter ion spectrum for the $[M + H]^+$ ion is shown in

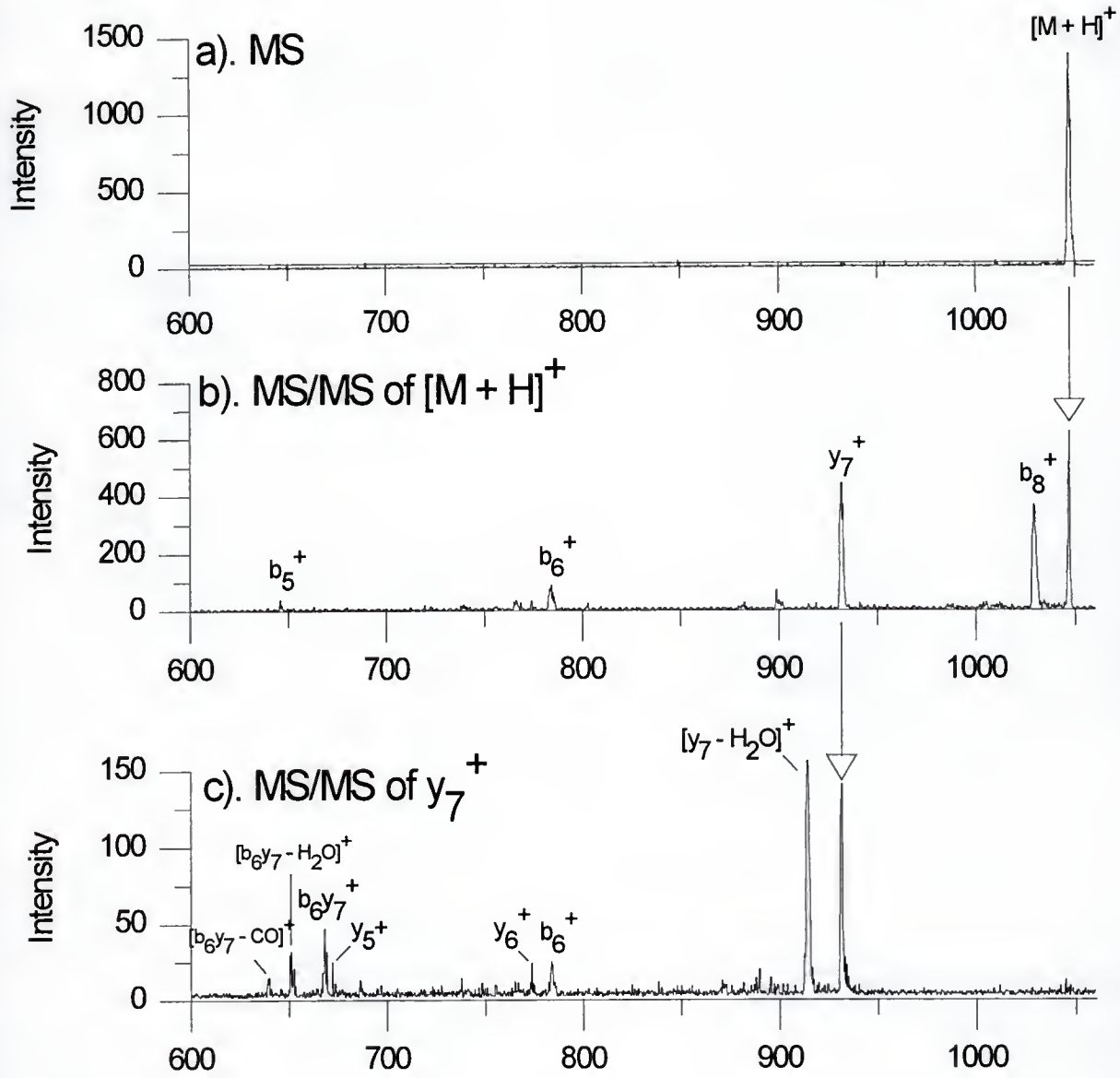

Figure 2-16. a). Mass isolated MALDI QITMS spectrum ($[M + H]^+$ ion) for 20 pmol of Angiotensin II, b). MS/MS spectrum for this ion, and c). MS/MS for the mass-isolated y_7^+ ion (MS^3 spectrum for the $[M + H]^+$ ion of Angiotensin II).

Figure 2-16b, and the daughter ion spectrum produced from the y_7^+ ion is shown in Figure 2-16c. This is also termed a granddaughter ion spectrum for the $[M + H]^+$ ion of Angiotensin II, since the y_7^+ ion is the daughter of the $[M + H]^+$ ion and the resulting ions for the MS/MS of the y_7^+ ion are daughter ions of that ion. Besides the $[y_7 - H_2O]^+$ ion, which is typically seen in MS^3 analysis of peptides,[57] y- and b-ions due to further peptide backbone cleavages are observed along with the internal sequence fragment ion $b_6y_7^+$ (which corresponds to the amino acid sequence Arg-Val-Tyr-Ile-His produced from the center of the intact peptide) and ions due to the loss of water and carbon monoxide from the internal fragment ion. The internal sequence fragment ion is most likely driven by the presence of the highly basic proline residue on the seventh amino acid of this peptide.[58] The presence of the proline residue at this position also leads to a lack of a b_7^+ ion in this spectrum.

In addition to performing MS^2 of the y_7^+ ion, MS^2 of the b_8^+ ion was also performed. The mass-isolated spectrum for Angiotensin II is shown in Figure 2-17a, the daughter ion spectrum for the $[M + H]^+$ ion is shown in Figure 2-17b, and the daughter ion spectrum produced from the b_8^+ ion is shown in Figure 2-17c. The scan function for the MS^2 of the b_8^+ ion was identical to the one used for the MS^2 of the y_7^+ ion, except that the rf levels used for the mass isolation and resonance excitation steps are set to correspond to the different ion of interest. In contrast to the previous MS^3 data, the only easily identifiable peak in this MS^3 mass spectrum is the neutral loss of ammonia from the b_8^+ ion. The lack of backbone fragments in this spectrum is due to the presence of the proline residue as the first amino acid of the b_8^+ ion. The very high basicity of this residue leads to cyclization rearrangements, making identification of these mass peaks very difficult.

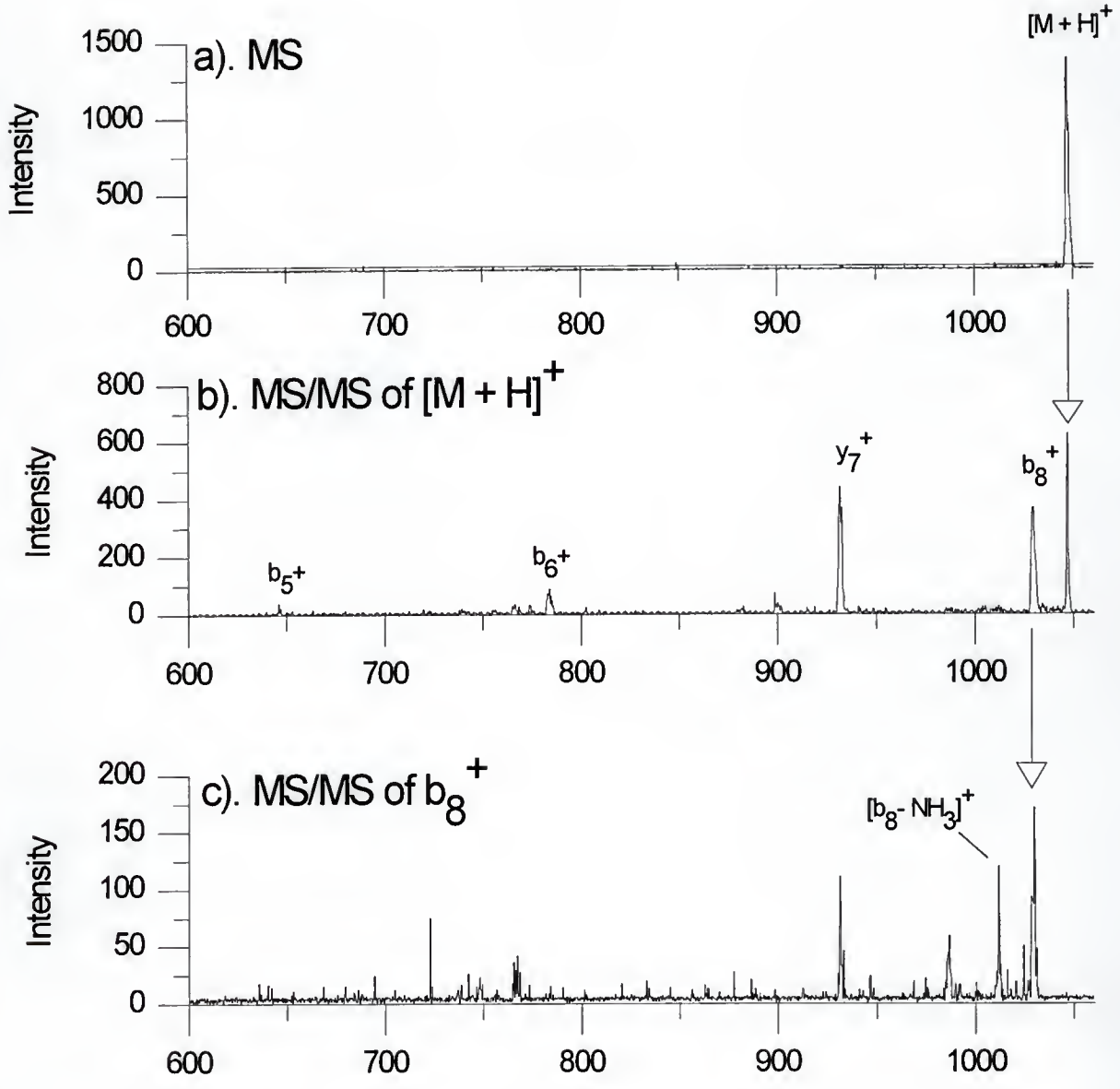

Figure 2-17. a). Mass isolated MALDI QITMS spectrum ($[M + H]^+$ ion) for 20 pmol of Angiotensin II, b). MS/MS spectrum for this ion, and c). MS/MS for the mass-isolated b_8^+ ion (MS^3 spectrum for the $[M + H]^+$ ion of Angiotensin II).

Summary

This chapter described the design, construction, and characterization of a MALDI QITMS instrument. The commercially-available MALDI time-of-flight mass spectrometer used as the basis for this instrument provided a MALDI ion source optimized for the analysis of proteins and polymers, and also allows for the potential of imaging the sample probe. The instrument was constructed by placing the quadrupole ion trap directly behind the MALDI ion source, with a continuous dynode detector installed in place of the flight tube of the time-of-flight mass spectrometer. Simulations of the instrument design showed that the MALDI ion source should be much better at focusing ions produced with a radial velocity than previously used MALDI ion sources. In order to characterize the instrument, two peptides were analyzed: the synthetic tetrapeptide MRFA and an octapeptide, Angiotensin II. Both peptides showed $[M + H]^+$ ions as base peaks, along with fragment ions observed from either collisions with background gases, surface-induced dissociation, or metastable decay. MRFA was chosen because the m/z for its $[M + H]^+$ ion is within the mass range of the standard quadrupole ion trap, while Angiotensin II has an m/z for its $[M + H]^+$ ion greater than the standard mass range and required mass range extension using axial modulation. Tandem mass spectrometry (MS^2 and MS^3) was also performed for Angiotensin II. Ion isolation was accomplished using the forward-and-reverse scanning technique, and resonance excitation was performed to produce daughter ions. The results from these two peptides demonstrate that this instrument is capable of performing MS and MS^n on MALDI-generated ions.

CHAPTER 3
THE ANALYSIS OF PHARMACEUTICAL COMPOUNDS USING A MALDI QUADRUPOLE ION TRAP MASS SPECTROMETER

Introduction

Tandem mass spectrometry plays an important role in the analysis of pharmaceutical compounds because of its ability to provide structural information for unknown compounds and its ability to allow for the detection of targeted compounds in complex matrices. These two features of tandem mass spectrometry using the MALDI QITMS instrument built for this research were explored for a number of compounds. In this chapter two examples are presented: the MS^6 analysis of spiperone and the MS^2 analysis for the identification of taxol in a liver sample.

MALDI QITMS for the Structural Determination of Spiperone.

Tandem mass spectrometry using the MALDI QITMS instrument constructed for this research was performed to demonstrate the ability of this technique to provide structural information for a compound. Spiperone (Figure 3-1), an antipsychotic drug developed by Bristol-Myers Squibb, was used for this analysis. The MALDI quadrupole ion trap spectrum for 20 pmol of this compound (using a DHB matrix) is shown in Figure 3-2. This spectrum shows the $[M + H]^+$ ion at m/z 396 as the base peak along with peaks due to the DHB MALDI matrix (m/z 138 and 154) and fragment ions due to CID with helium and other background gases present in the ion source and quadrupole

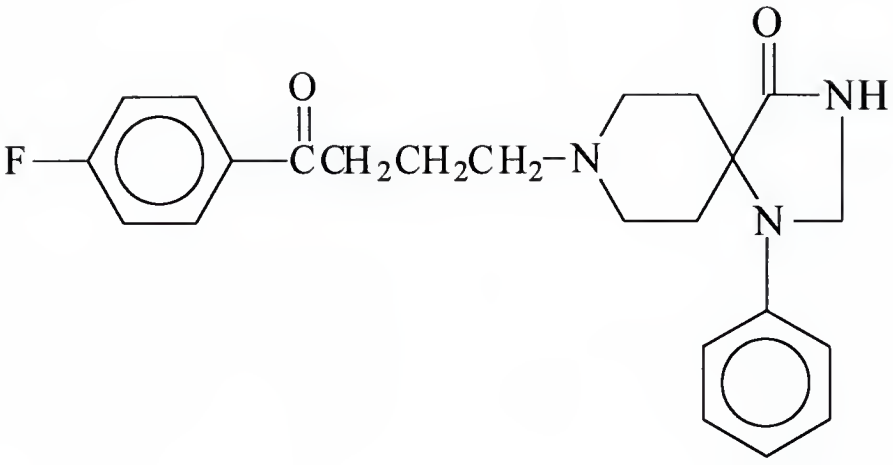

Figure 3-1. Spiperone, M.W. 395.

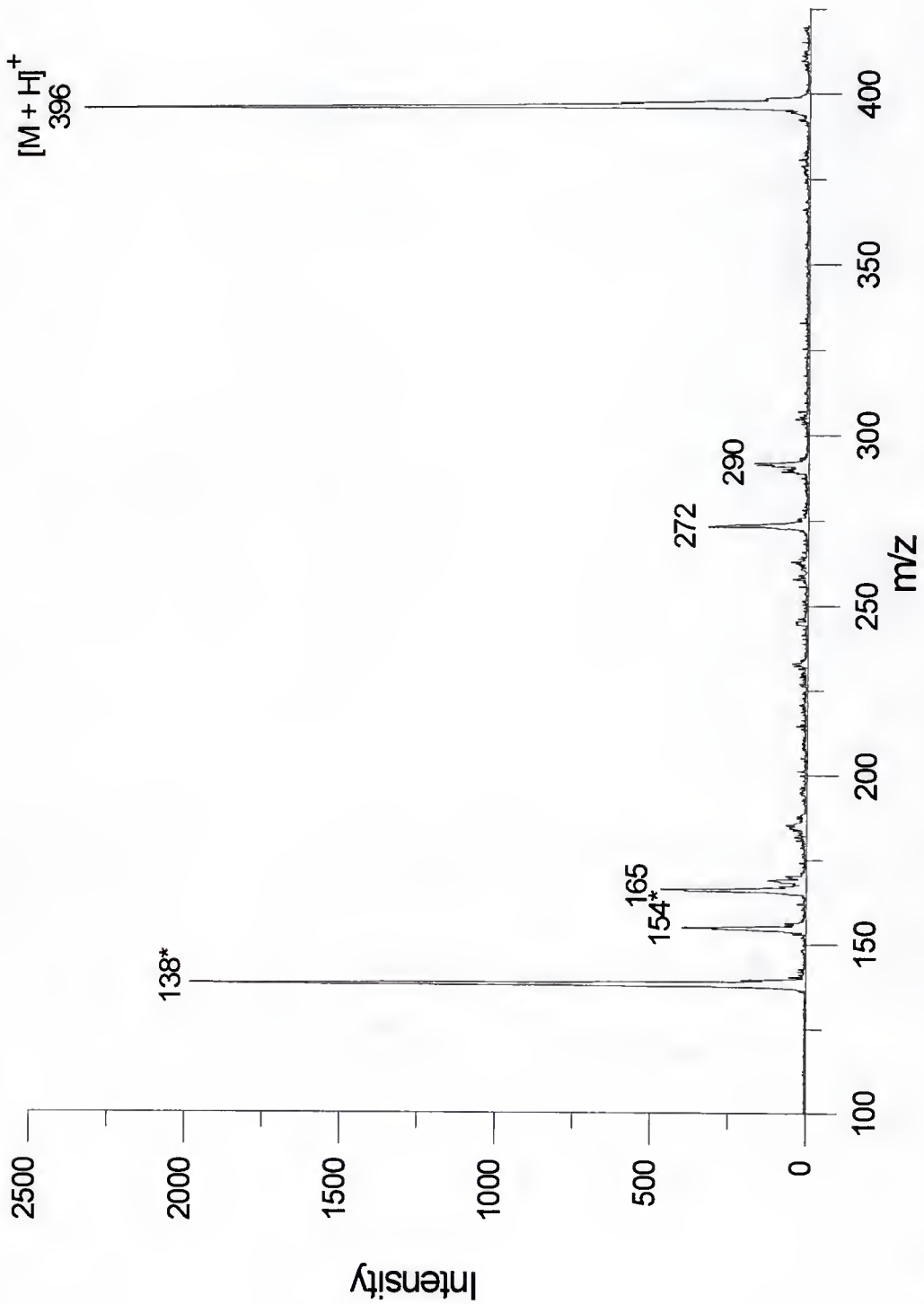

Figure 3-2. MALDI QITMS spectrum for 20 pmol of spiperone.

ion trap, SID with ion optic surfaces or the ion trap electrodes, or by metastable decay. The scan function used to produce this spectrum is the same as the one used for MRFA (Figure 2-9), except that the rf voltage which corresponds to a q_{inject} of 0.1 is 843 V.

To identify the fragment ions observed in this spectrum, tandem mass spectrometry (MS^2) was performed by first using the two-step isolation technique as shown by Yates et al.[59] The scan program to implement this method of ion isolation is shown in Figure 3-3, and is listed in Table 3-1. After the ionization and cool steps, the RF level positions m/z 396 (which is the $[M + H]^+$ ion for spiperone) at a $q_z = 0.70$ on the ion trap stability diagram (Figure 3-4). Next, a DC potential of 466 V is applied to the ring electrode during scan table 9. This positions m/z 396 at a working point of $a_z = -0.23$ and $q_z = 0.70$ on the stability diagram (point H in Figure 3-4). At this point, all ions with a m/z greater than 396 are ejected from the ion trap. Next, the DC voltage is returned to 0 V and the RF level is increased to position m/z 396 at $a_z = 0.0$ and $q_z = 0.85$ (scan tables 9). The DC is then set to -142 V to eject all ions with a m/z less than 394 (scan table 10) (point L in Figure 3-4). At this point a narrow m/z range from 394 to m/z 397 has been isolated in the ion trap. The mass spectrum for the isolation of the $[M + H]^+$ ion of spiperone is shown in the top spectrum of Figure 3-5. After the isolation steps, MS/MS is performed by setting the q to 0.3, and applying a supplemental frequency of 115 kHz (2.8 V) for 10 ms across the endcap electrodes. The daughter ion spectrum for the $[M + H]^+$ ion of spiperone is shown in the bottom spectrum of Figure 3-5. The possible fragments that produce the ions seen in this daughter ion spectrum are shown in Figure 3-6.

Further stages of mass spectrometry (MS^n) were performed to create a fragmentation map for this compound. The results for this MS^n analysis of spiperone are shown in Figure 3-7, with the identity of the neutral lost at each stage of CID (along with the mass of this neutral) shown on each resulting isolated mass spectrum. Starting with

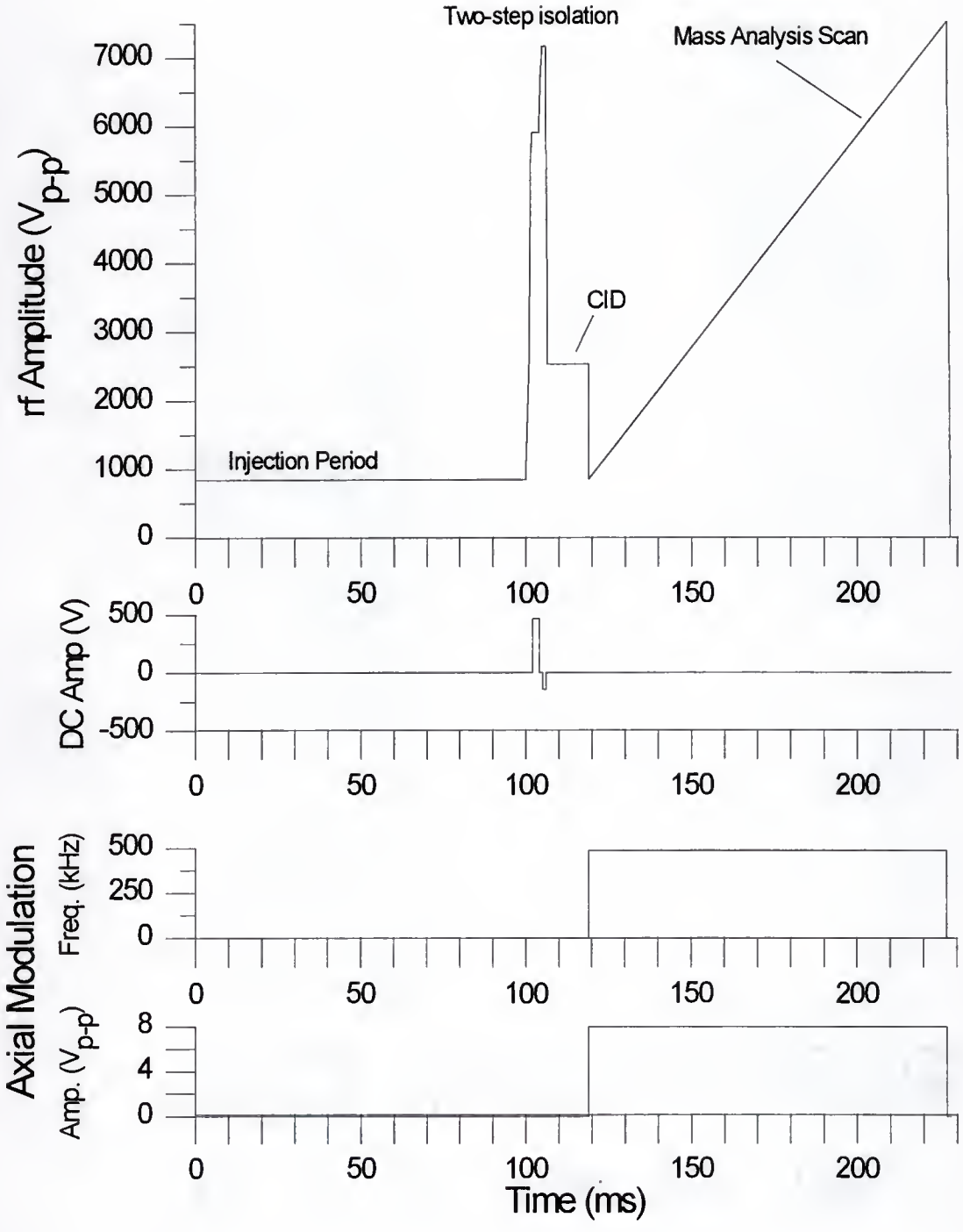

Figure 3-3. Scan function used for the MALDI QIT MS/MS analysis of spiperone.

Table 3-1. Scan table listing for the MALDI QIT MS/MS analysis of spiperone.

		rf Voltage		dc Voltage		Axial Modulation		Time
#	Scan Table	Start	End	Start	End	Freq. (kHz)	Amp (V)	(ms)
1	First Table	1004	1004					0.5
3	Ionize	1004	1004					0.001
4	Cool	1004	1004					50
5	Ionize	1004	1004					0.001
6	Cool	1004	1004					50
7	RF Ramp #1	1004	6525					0.5
8	RF Ramp #2	6525	7028					0.5
8	Eject High Masses	7028	7028	466	466			5
9	RF Ramp #3	7028	8534					0.5
10	Eject Low Masses	8534	8534	-142	-142			5
11	Cool	3012	3012					5
12	MS/MS	3012	3012			115	2.8	10
13	Cool	3012	3012					5
14	Prescan	1004	1004					5
15	Acquire	1004	15000			486	6	108
16	Empty Trap	0	0					2

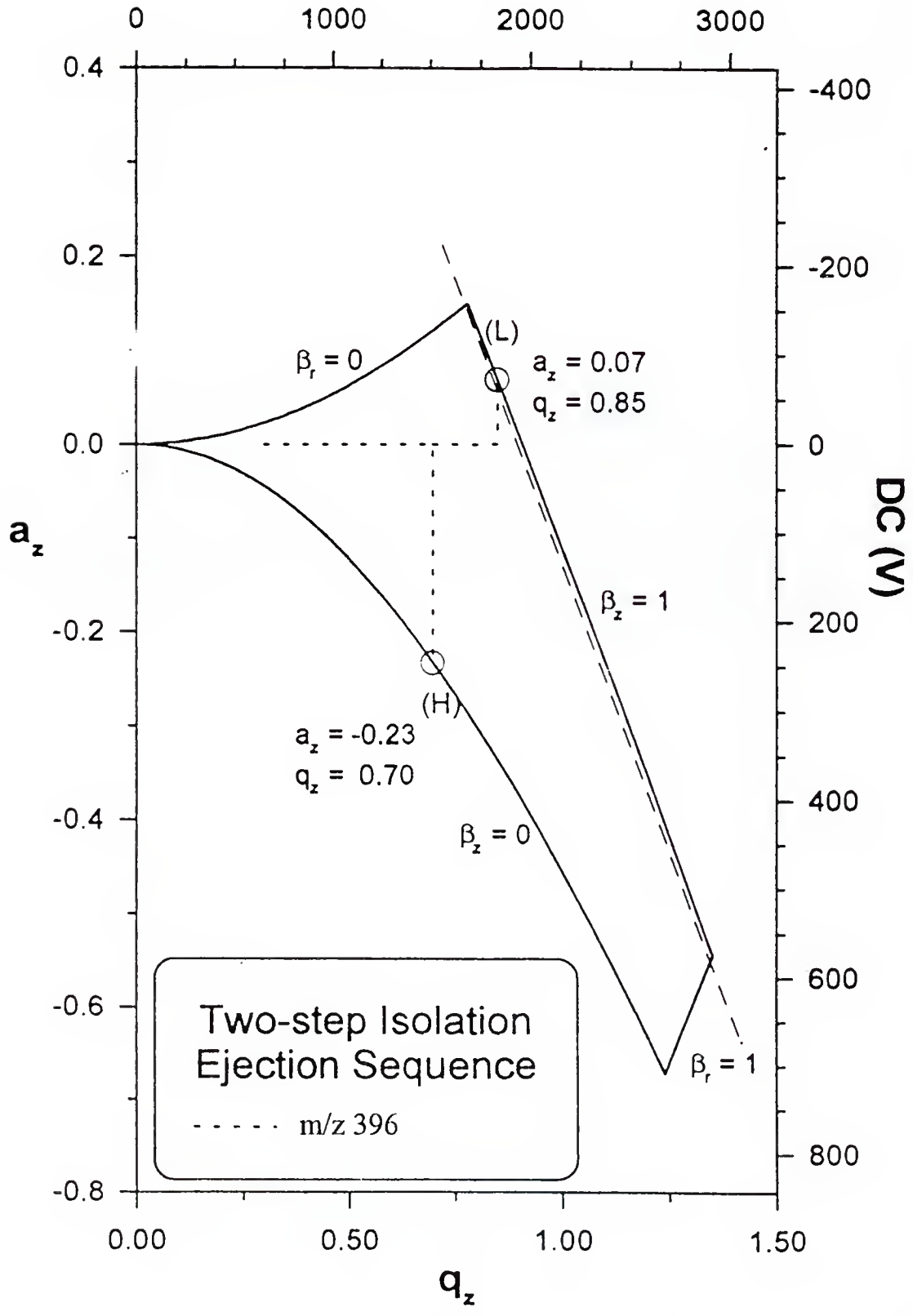

Fig 3-4. Stability diagram showing the path (-----) taken by the $[M + H]^+$ ion of spiperone during the two-step isolation sequence.

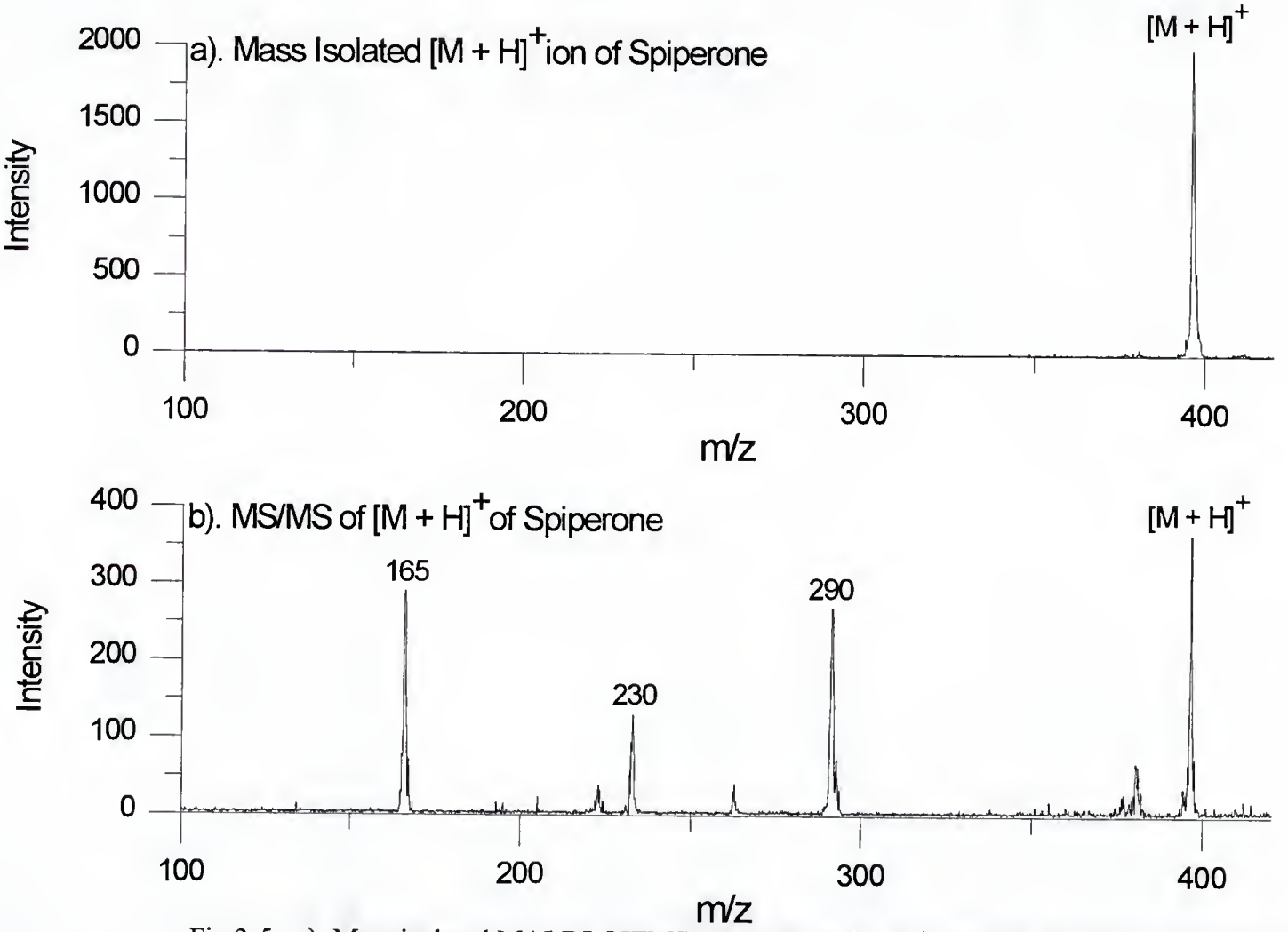

Fig 3-5. a). Mass isolated MALDI QITMS spectrum ($[M + H]^+$ ion) for 20 pmol of spiperone, and b). MS/MS spectrum for this ion.

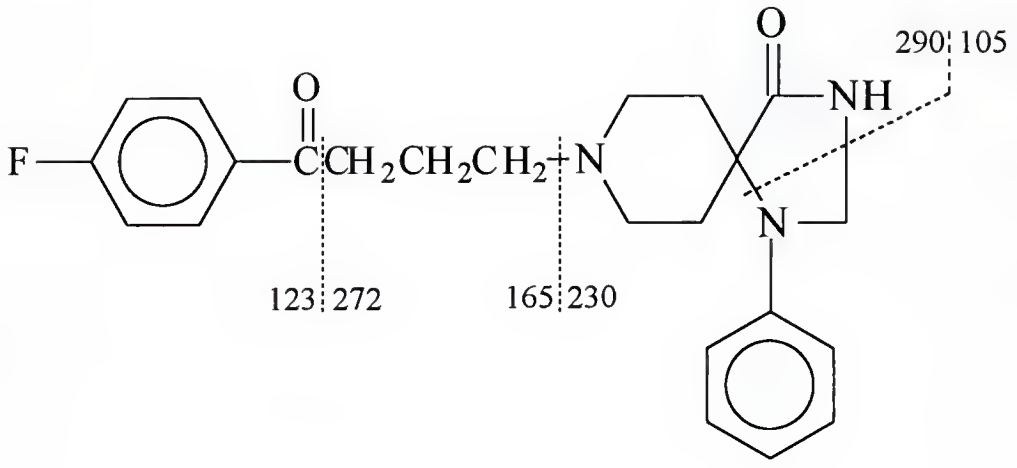

Figure 3-6. Possible fragments that produce the daughter ions seen in the spectrum for spiperone.

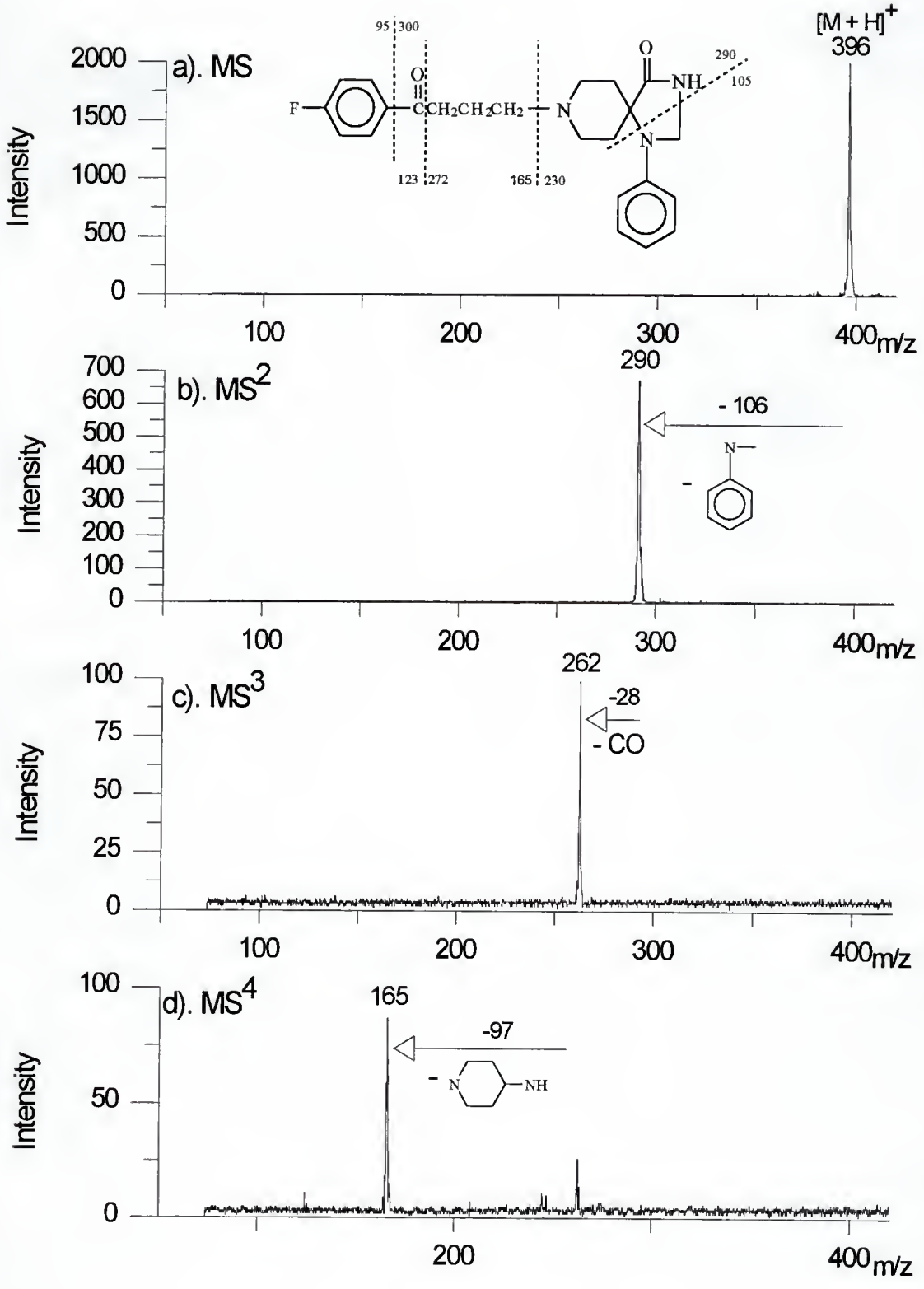

Figure 3-7. Series of mass-isolated spectra from the MS^n analysis of spiperone.

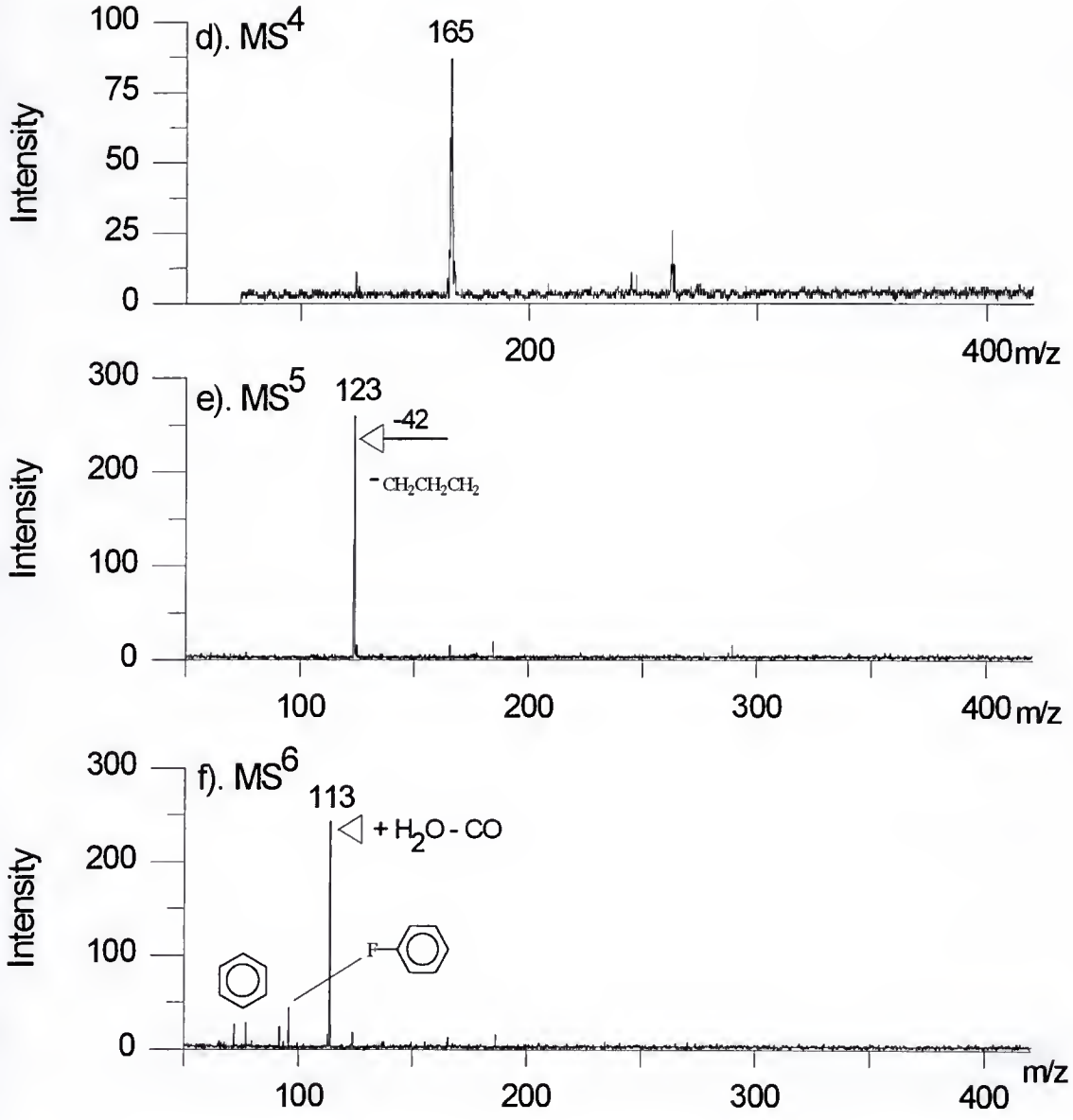

Figure 3-7, continued. Series of mass-isolated spectra from the MS^n analysis of spiperone.

the isolated $[M + H]^+$ ion of spiperone (m/z 396) (Figure 3-7a), MS/MS was performed as described above. One of the daughter ions (m/z 290) was then mass isolated using the two-step isolation technique (Figure 3-7b). MS/MS of this ion was then performed, and one of the daughter ions produced from the fragmentation of the m/z 290 ion (m/z 262) was mass isolated (Figure 3-7c). This ion is the great-granddaughter ion of the $[M + H]^+$ ion of spiperone. After the m/z 262 ion was mass isolated, MS/MS was performed, and one of the daughter ions produced from this fragmentation (m/z 165) was mass isolated (Figure 3-7d). MS/MS was then performed on the m/z 165 ion, and one of the daughter ions produced from this fragmentation (m/z 123) was mass isolated (Figure 3-7e). Finally, MS/MS was performed on the m/z 123 ion (Figure 3-7f). For this final stage of mass spectrometry, a mass peak of 113 is achieved, resulting from the addition of water and subsequent loss of carbon monoxide. The proposed structure of the fragment ions produced at each stage of MS are shown in Figure 3-8.

Taxol (paclitaxel) and Cancer

Ovarian cancer is a very deadly disease that accounts for about 5 percent of all cases of cancer among women. Since there are generally no symptoms until the cancer has advanced into later stages, about 70 to 75 percent of cases of ovarian cancer are diagnosed after the cancer has spread beyond the pelvic area and into the abdominal cavity. In 1995, about 26,600 new cases of ovarian cancer were diagnosed among American women, and about 14,500 died from this disease.[60]

Taxol is the registered trademark name for paclitaxel (Figure 3-9) as produced by the Bristol-Myers Squibb Company. This compound contains a complex taxane ring linked to an oxetan ring at position C4-5, and contains an ester side chain at position C-13. It is believed that the ester side chain is responsible for the cytotoxicity of this drug.[61] Paclitaxel's antitumor activity was discovered in the 1960s during a National

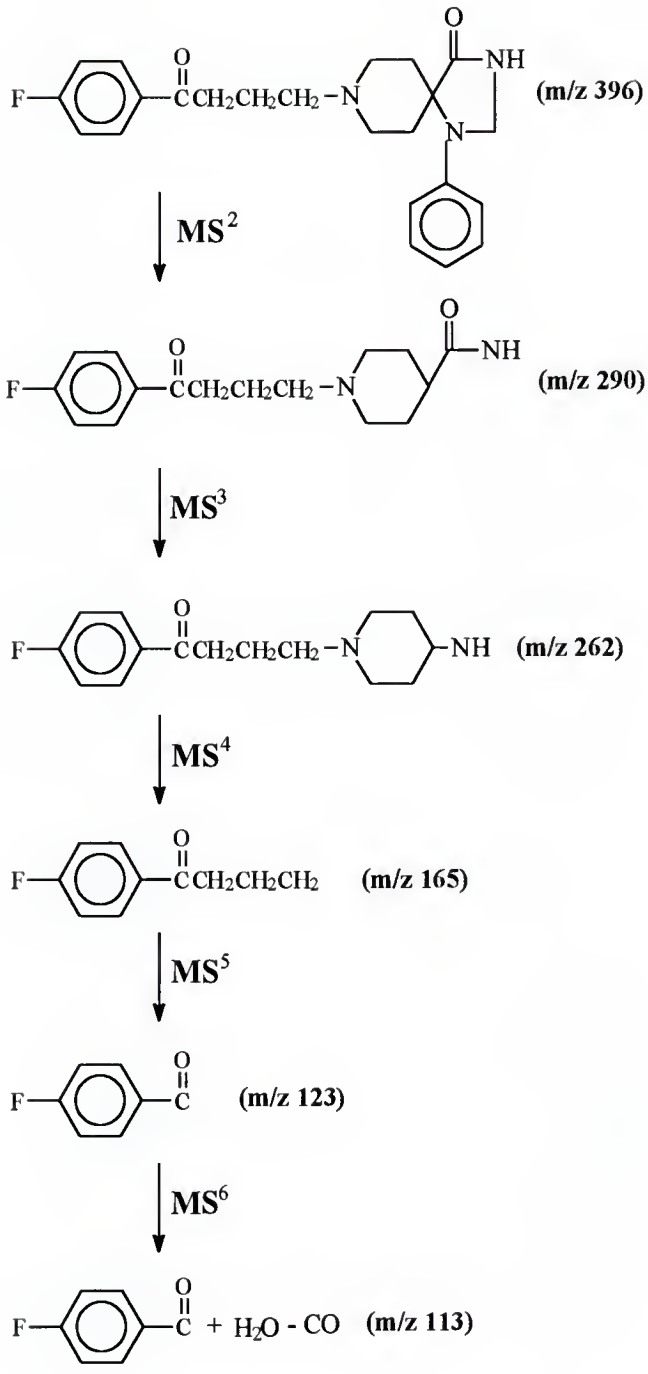

Figure 3-8. Possible fragment ions produced from the MS^n analysis of spiperone.

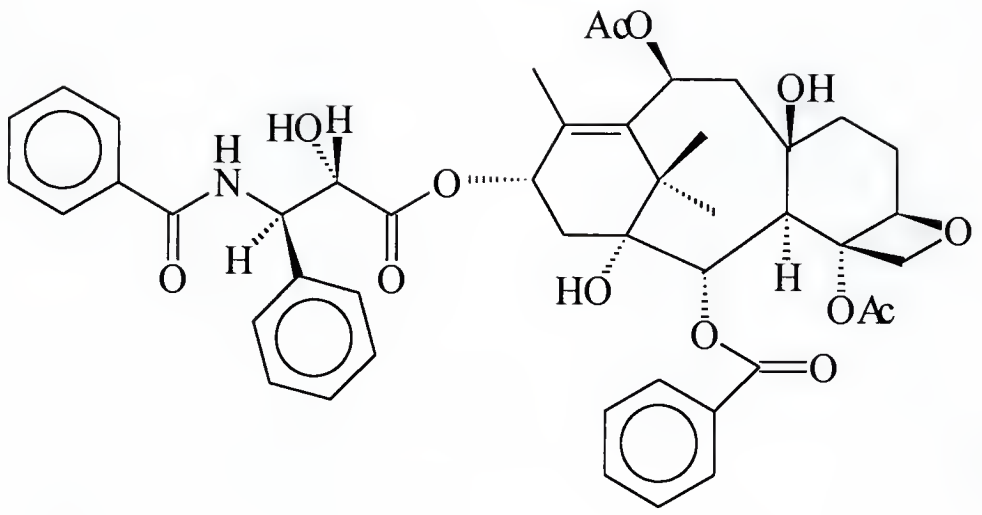

Figure 3-9. Taxol, M.W. 853.

Cancer Institute large-scale plant-screening program. Interest in developing the drug increased in 1979 after scientists found that paclitaxel has a unique mechanism for preventing the growth of cancer cells.

Paclitaxel is one of a class of drugs called taxans which bind to the protein tubulin (M.W. 100,000), the major constituent of microtubules that serve as part of the skeletal system for cells.[62] For cell division (mitosis) to occur, the microtubule skeleton of the cell must disassemble, reform into spindles across which duplicate sets of DNA material line up, again disassemble, and finally reform into skeletal systems for the two new cells. In binding to the tubulin, taxol stabilizes the structure of the intracellular microtubules, thereby preventing them from breaking down at the end of cell division. Cancer cells, which attempt to divide frequently, become so clogged with microtubules that they cease to grow and divide.

The National Cancer Institute began conducting clinical trials on the safety and effectiveness of paclitaxel against various types of cancer in 1983. In 1989, NCI-supported investigators at The Johns Hopkins Oncology Center reported that the drug produced shrinking or disappearance of tumors in 30 percent of previously treated patients with advanced ovarian cancer. In December 1992, the United States Food and Drug Administration (FDA) approved the use of paclitaxel for treatment-resistant ovarian cancer, and in April 1994, approved its use for breast cancer that has recurred within 6 months after the completion of initial chemotherapy and for metastatic breast cancer that is not responding to combination chemotherapy. Trials to test the effectiveness of paclitaxel against many other types of cancer, including leukemia, lymphoma, and cancers of the lung, head and neck, and colon, are currently in progress.

Paclitaxel was originally extracted from the bark of the Pacific yew tree (Taxus brevifolia). This type of yew is found only in old-growth forests of the North American Pacific Northwest, and grow very slowly (about 8 inches per year). Since it takes the

bark of about three trees to treat one patient, there has been a great deal of research activity to produce the compound by alternative processes. The first total synthesis of taxol was published independently in 1994 by R. A. Holton of Florida State University and by K.C. Nicolaou and R. K. Guy of the Scripps Research Institute and the University of California, San Diego.[63,64] Taxol is currently obtained via a semi-synthetic process from the precursor 10-deactylbaccatin III, which is isolated from the needles of the European yew tree (taxus baccata). Because the tree continues growing after the branches providing needles have been harvested, this type of yew tree provides a renewable source of the precursor.

Although taxol can be effective as an antitumor agent, it has side effects as do most other cancer drugs. Its most significant toxic effect is depression of bone marrow, which causes a reduction in the body's ability to produce the blood cells that fight infection. Reversible hair loss is also a common result of paclitaxel treatment, and gastrointestinal problems, nerve damage, and other adverse effects sometimes occur. Two major problems in using taxol are paclitaxel's limited aqueous solubility and the toxicity of the compounds thus used as the drug vehicle (polyoxyethylated castor oil and dehydrated alcohol).[65]

MALDI QITMS and MS^2 of Taxol

Taxol was obtained as a pure white crystalline powder from Bristol-Myers Squibb. For this analysis, 1 mg of taxol was mixed with 10 mL of methanol. 1 uL of this 100 pmol/μL taxol solution was mixed with 1 uL of the DHB matrix solution on the probe tip and allowed to air dry. The MALDI quadrupole ion trap spectrum for 20 pmol of taxol (using a DHB matrix) is shown in Figure 3-10. This spectrum shows the $[M + K]^+$ ion at m/z 892 as the base peak along with fragment ions due to either collisions with

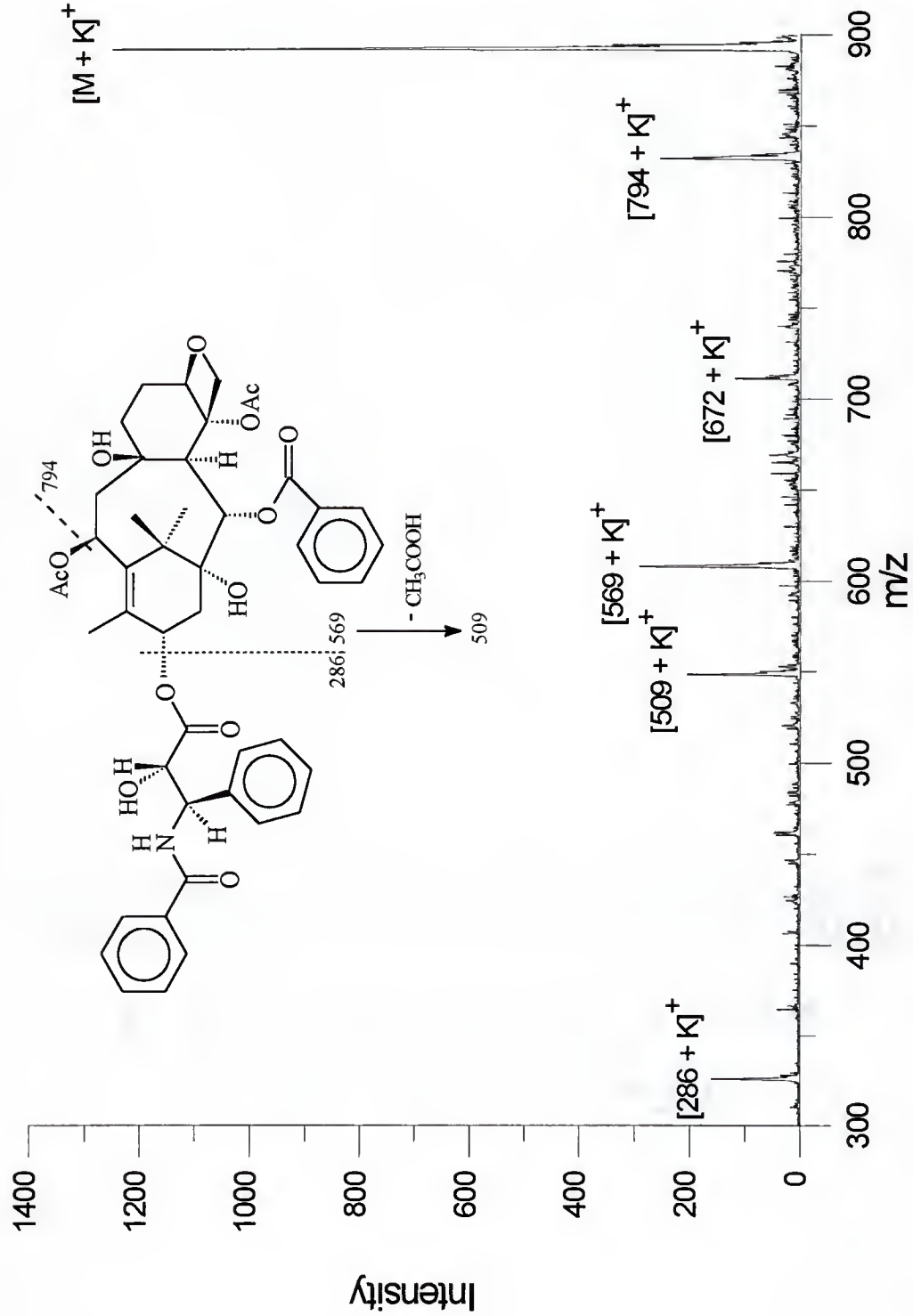

Fig 3-10. MALDI QITMS spectrum for 20 pmol of Taxol.

background gases, surface-induced dissociation, or metastable decay. The fragment ions seen in this spectrum correspond well with those published by Lee et al.[66] for the tandem mass spectrometry of the $[M + NH_4]^+$ ion of this compound using an ionspray LC/MS system. The appearance of the potassiated or sodiated molecule instead of a protonated molecule is very common in biological samples, which often contain a large concentration of salts. The scan function used to produce this spectrum is the same as the one used for Angiotensin II (Figure 26), except that the rf voltage were changed to correspond to the difference in mass of these two compounds. Since the m/z of $[M + K]^+$ ion for this compound is greater than the maximum m/z achievable with the standard quadrupole ion trap instrument, the axial modulation frequency was decreased during the mass analysis scan to increase the mass range of the ion trap. For this analysis, an axial modulation frequency of 250.861 kHz was used, giving a q_{eject} of 0.6172 and a maximum attainable mass of 950 amu.

MS/MS was next performed on the $[M + K]^+$ ion of this compound. This ion was isolated using the forward-and-reverse isolation technique, since its mass was greater than 600 amu and the two-step isolation technique used for spiperone could not be used (due to the limited dc voltage that can be placed on the ring electrode of the ion trap). The scan program to implement this method of ion isolation is the same as that used for Angiotensin II (Figure 2-7), with the rf voltages used for the injection, isolation, and CID of the taxol ions changed to reflect the m/z of these ions. The isolated $[M + K]^+$ ion of taxol is shown in the top spectrum of Figure 3-11, while the daughter ion spectrum produced from the fragmentation of the $[M + K]^+$ ion of taxol (115 kHz, 1.1 V) is shown in the bottom spectrum of this figure. The fragment ions seen in this daughter spectrum are the same as those in the MALDI QITMS spectrum (Figure 3-10).

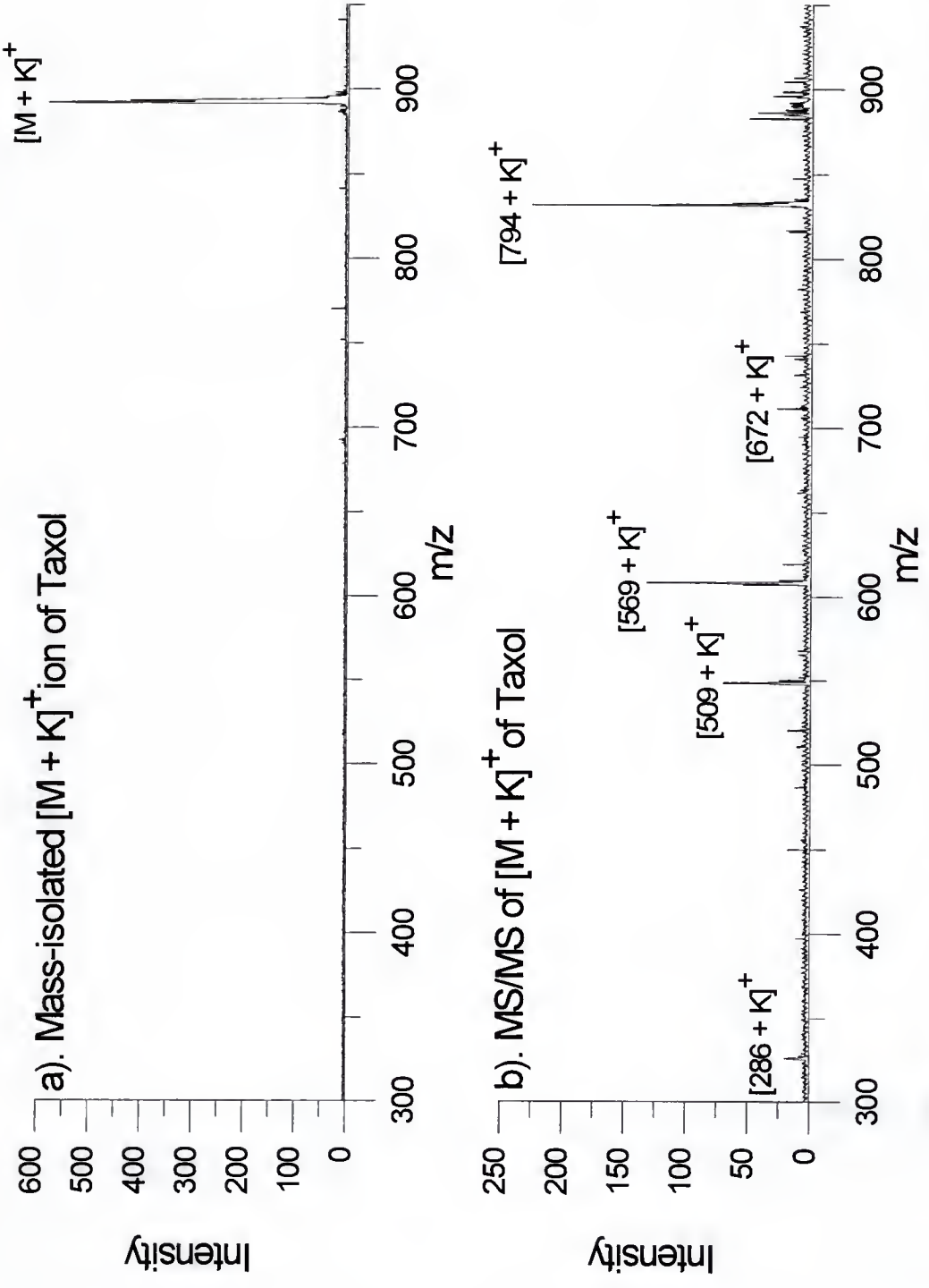

Fig 3-11. a). Mass isolated MALDI QITMS spectrum ($[M + H]^+$ ion) for 20 pmol of Taxol, and b). MS/MS spectrum for this ion.

MALDI QITMS for the Determination of Taxol in Rat Liver Tissue.

Tissue samples are a very complex matrix. This is especially true of samples taken from the liver, since this organ has functions which involves many biological compounds. Some of the functions of the liver are to produce and store proteins, regulate and control the by-products of protein metabolism, remove metabolic waste products generated by other tissues from the blood (by converting these compounds into ones which can be excreted via the urine or feces) and to detoxify biologically active compounds such as drugs, hormones, and poisons.[67]

The use of tandem instrumental methods gives the selectivity required to detect for the presence of a compound at trace levels in the presence of interferents.[68] In an analytical method, as the number of stages of analysis is increased, the absolute level of both the signal and noise decrease. In the case where the additional stages increase the selectivity of the technique, the "chemical" noise (which consists of the signal due to any interfering analytes) will decrease more rapidly than the signal for the targeted analyte, and if the chemical noise (rather than electrical noise) dominates, an overall improvement in the S/N ratio will result. When using multiple stages of mass spectrometry (tandem mass spectrometry), for a mixture component to interfere with the detection of an analyte it must produce the same m/z parent ion/daughter ion pair, which means that it must be ionized to form the same parent ion m/z as the analyte, which then must undergo collision-induced dissociation (CID) to form a fragment ion (daughter ion) of the same m/z as the analyte.

In order to evaluate the use of tandem mass spectrometry for the identification of taxol in tissue samples, a thin slice (approximately 1 mg) of rat liver tissue was incubated for one hour in a 1 mL solution containing 100 ng of taxol. After the incubation period, the tissue was taken out of the taxol solution and repeatedly washed with deionized

water, then placed onto the tip of the MALDI probe. The DHB MALDI matrix (2 uL) was then pipetted onto the top of the tissue sample and allowed to dry, then placed into the vacuum system of the instrument. The MALDI quadrupole ion trap spectrum for this tissue sample is shown in Figure 3-12. This spectrum shows the very complex nature of this liver tissue sample. Although mass peaks can be observed in this spectrum that may correspond to taxol, it is impossible to say with any confidence that taxol is present. This can be seen better by displaying a blow-up of the mass regions for four characteristic ions ($[509 + K]^+$, $[569 + K]^+$, $[794 + K]^+$, and $[M + K]^+$) of taxol in the liver tissue sample (top spectrum) and in the standard (bottom spectrum) as shown in Figure 3-13.

MS/MS was next performed on the rat liver tissue sample. A wide region around the m/z 892 ion (± 10 amu) was isolated using the forward-and-reverse isolation technique exactly as it was for the taxol standard, and the m/z 892 ion was resonantly excited. The MALDI QITMS spectrum for the liver sample incubated with taxol is shown in the top spectrum in Figure 3-14, and the daughter ion spectrum produced from the fragmentation of the $[M + K]^+$ ion of taxol (115 kHz, 1.1 V, 10 ms) is shown in the bottom spectrum of this figure. A comparison of the MS/MS results from taxol in both the standard and the incubated liver tissue sample is shown in Figure 3-15. These two figures show that whereas it is not possible to identify taxol present in the MALDI QITMS spectrum of the rat liver tissue, the MS/MS data for this sample unequivocally shows the presence of this compound.

Summary

This chapter presented the analysis of two pharmaceutical compounds using the MALDI QITMS instrument described in chapter 2 of this dissertation. Spiperone was analyzed in standard samples using MS and MS^n (up to MS^6). Since the structure of

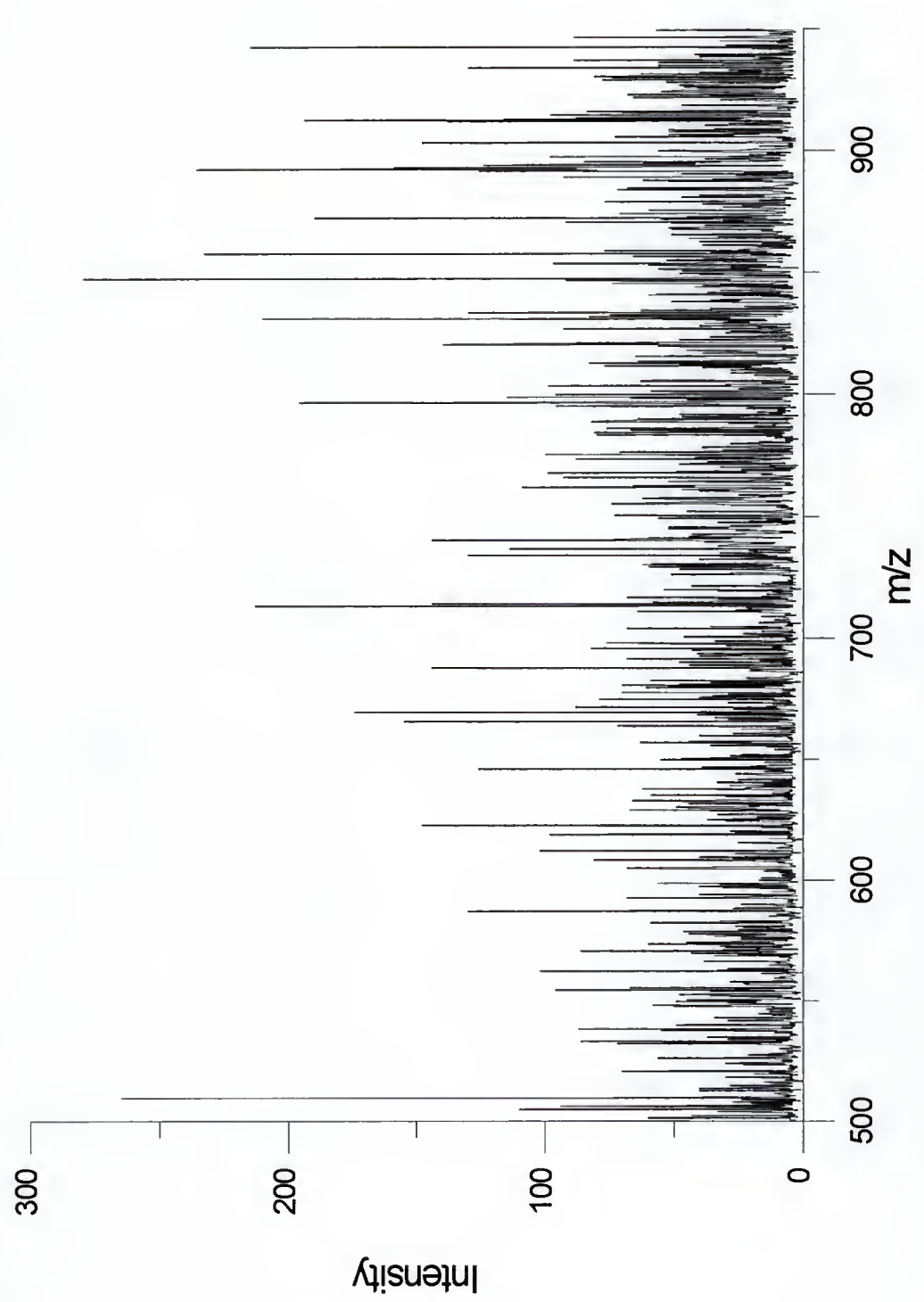

Fig 3-12. MALDI QITMS spectrum for a thin slice of rat liver tissue incubated with Taxol.

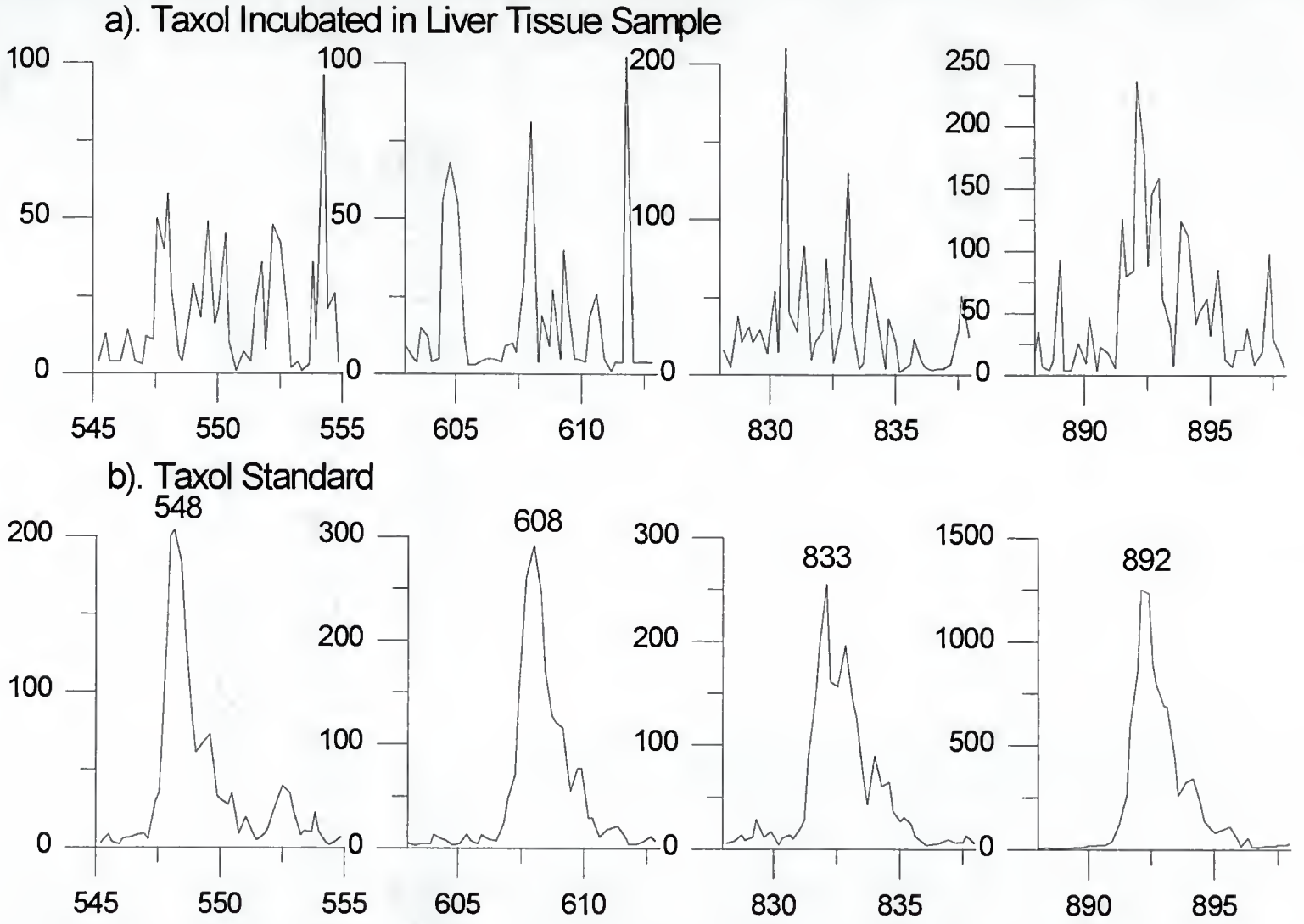

Fig 3-13. Blow-up of four regions for the MALDI QITMS spectrum for a). a thin slice of rat liver tissue incubated with Taxol and b). 20 pmol Taxol standard.

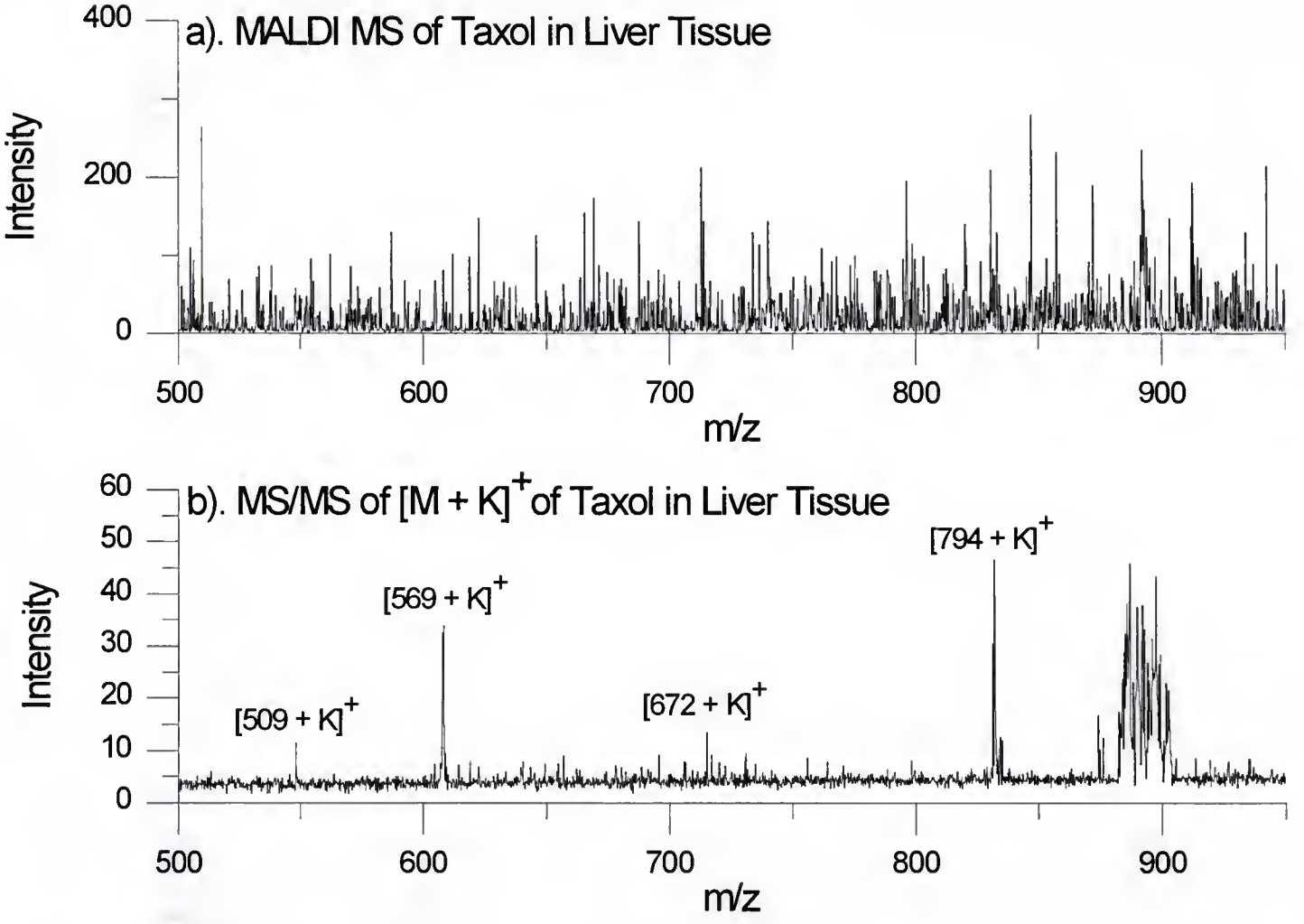

Fig 3-14. a). The MALDI QITMS spectrum and b). MS/MS spectrum of Taxol incubated in a thin slice of rat liver tissue.

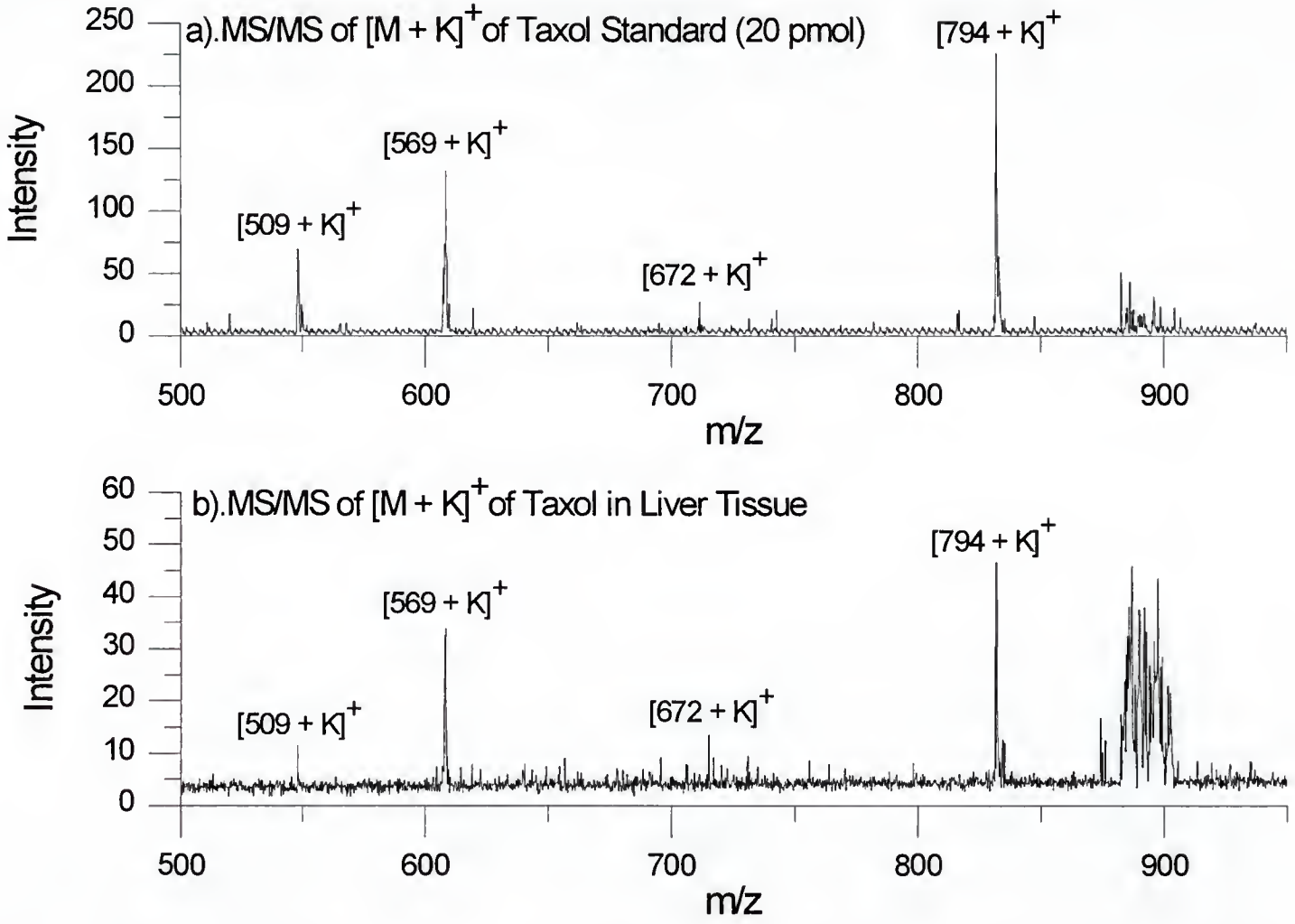

Fig 3-15. MALDI QITMS spectrum of Taxol in a). a standard and b). a thin slice of rat liver tissue incubated with Taxol.

spiperone is already known, this MS^6 analysis does not provide any new information, but was used to confirm the identity of the fragment ions seen in the mass spectrum of this compound and to demonstrate the usefulness of MS^n for compound elucidation.

Taxol, a very powerful anticancer drug currently being used to combat ovarian and breast cancer, was analyzed in standard samples and in incubated rat liver tissue. The daughter spectrum of the $[M + K]^+$ ion in the MALDI QIT MS/MS analysis of a standard of this drug compared well with that obtained for MS/MS of the $[M + NH_4]^+$ ion using ionspray on a triple quadrupole mass spectrometer. The analysis of Taxol in the liver sample showed that whereas it was difficult to identify this compound in the complex liver matrix using MS, the MS/MS data for this sample provided for the unequivocally detection of this compound.

CHAPTER 4
CONCLUSIONS AND FUTURE WORK

This research entailed the design and construction of a MALDI quadrupole ion trap mass spectrometer. This instrument consisted of the mating of two separate commercially-available instruments: the ion source from a Vestec ResearcH™ MALDI Time-of-Flight mass spectrometer and a Finnigan ITS40™ quadrupole ion trap mass spectrometer. The advantages of using an ion trap as the mass analyzer for MALDI-generated ions is that it allows for excellent mass resolution in the low mass range and tandem mass spectrometry (MS^n) for structural determination and the identification of trace quantities of analytes in complex matrices. The novel use of an ion source specifically designed for MALDI analyses allows for the better focusing of ions leaving the sample probe tip with significant radial velocities and the potential for imaging of the sample.

This instrument was characterized using a variety of peptides, including MRFA and Angiotensin II. These peptides were chosen to determine the proper conditions for the MALDI QITMS instrument (lens voltages, axial modulation frequencies and voltages and helium buffer gas pressure) and the MS and MS^n performance of the instrument. These compounds demonstrated the excellent resolution and MS/MS efficiency of this instrument, providing results comparable to other ion trap instruments (using both internally- and externally-generated MALDI ions).

The real power of the MALDI QITMS instrument designed and constructed for this dissertation lies in its ability to perform tandem mass spectrometry (MS^n) on MALDI

generated ions. This feature was demonstrated by the analysis of spiperone using MS^6 and the detection of Taxol in a liver sample using MS^2.

The research presented in this dissertation showed the first results for the detection of Taxol directly from a tissue sample. Since the tissue samples used in this study were only incubated with the drug of interest (Taxol), the next step is to administer the drug to rats, then analyze thin liver slices for the presence of this compound along with any metabolites that will be present. As is the case with the parent drug, standards containing different metabolites of Taxol can be analyzed to determine the appropriate MS/MS scan functions (e.g. CID frequencies and voltages). In the case where there may be no standard available for a suspected metabolite, a range of voltages can be attempted (setting the CID frequency so that the q of the expected metabolite is set to 0.3), and the expected fragments monitored.

One of the ultimate goals of this project is to develop a microprobe instrument for the imaging of pharmaceutical compounds and their metabolites in a tissue samples. A next generation instrument is currently being built, and will consist of a MALDI source coupled to a quadrupole ion trap, with an octopole ion guide used to transmit ions from the source to the ion trap. This instrument will also use a microscope objective to view the tissue sample, which will allow for accurate positioning of the point where the nitrogen laser hits the sample. A tissue sample will be microtomed to give a thin slice, then placed onto the MALDI probe tip. The DHB matrix will then be electrosprayed onto the tissue sample to produce a thin, even coat of matrix. As an alternative to this technique, the DHB matrix will first be electrosprayed onto the probe tip, then the microtomed tissue sample will be laid on top of it. This second method should allow for better imaging of the tissue sample, but the sample must be thin enough so that the laser will ablate both the sample and the underlying DHB matrix. In order to provide a means to quantitate the amount of targeted compounds present in the tissue, labeled analogues

of the compounds that are to be monitored will be added to the DHB prior to the electrospraying process.

In conclusion, this work demonstrates that the MALDI QITMS instrument designed and constructed for this dissertation has the potential to become an invaluable tool for pharmaceutical analysis. Further work should enable the extension of this MALDI QIT MS/MS method to detect the presence of metabolites, and then for the imaging of tissue samples.

REFERENCE LIST

1. Spengler, B.; Kaufmann, R. *Analusis*, **1992**, *20*, 91-101.

2. Hillenkamp, F.; Karas, M.; Beavis, R.C.; Chait, B.T. *Analytical Chemistry,* **1991**, *63*, 24.

3. Bornsen, K.O.; Schar, M.; Gassmann, E.; Steiner, V. *Biological Mass Spectrometry*, **1991**, *20*, 471-478.

4. Karas, M.; Bachmann, D.; Bahr, U.; Hillenkamp, F. *International Journal of Mass Spectrometry and Ion Processes*, **1987**, *78*, 53.

5. Karas, M.; Hillenkamp, F. *Analytical Chemistry,* **1988**, *60*, 2299.

6. Karas, M.; Bahr, U.; Gissmann, U. *Mass Spectrometry Reviews.* **1991**, *10*, 335-357.

7. Beavis, R.C.; Chait, B.T. *Analytical Chemistry,* **1990**, *62*, 1836.

8. Strupart, K.; Karas, M.; Hillenkamp, F. *International Journal of Mass Spectrometry and Ion Processes*, **1991**, *111*, 89-102.

9. Beavis, R.C.; Chait, B.T. *Proceedings of the National Academy of Science. USA.* **1990**, *87*, 6873.

10. Karas, M.; Bahr, U.; Hassenburger, A.; Ingendoh, A.; Overberg, A.; Stahl, B.; Strupat, K.; Hillenkamp, F.; Giessmann, U. in *Proceedings of the 39th ASMS Conference on Mass Spectrometry and Allied Topics*, Nashville, TN, **1991**, 356-357.

11. Nelson, R., Vestal, M., in *Proceedings of the 39th ASMS Conference on Mass Spectrometry and Allied Topics*, Nashville, TN, **1991**, 332-333.

12. LaserMAT User Guide, Finnigan MAT, Hemel Hempstead, U.K. **1991**.

13. Cotter, R.J. *Analytical Chemistry,* **1992**, *64*, 1027A-1039A.

14. Carr, S.A.; Hemling, M.E.; Bean, M.F.; Roberts, G.D. *Analytical Chemistry,* **1991**, *63*, 2802-2824.

15. Jardine, I. *Methods in Enzymology*, **1991**, *193*, 441-455.

16. Hillenkamp, F.; Karas, M.; Beavis, R.C.; Chait, B.T. *Analytical Chemistry,* **1991**, 63, 1193A.

17. "*Time-of-Flight Mass Spectrometry*", R.J. Cotter, Ed.; ACS Symposium Series 549, American Chemical Society, Washington, DC **1994**.

18. White, M.A.; Strobel, F.H.; Russell, D.H. in *Proceedings of the 39th ASMS Conference on Mass Spectrometry and Allied Topics*, Nashville, TN, **1991**, 334-335.

19. Beavis, R.C.; Chait, B.T. *Chemical. Physics Letters,* **1991**, *181*, 479.

20. Mamyrin, B.A.; Karatajev, V.J.; Shmikk, D.V.; Zagnlin, V.A. *Soviet Physics* JETP, **1973**, *37*, 45-48.

21. Dawson, P.H.; Whetten, N.R. "Three-Dimensional Mass Spectrometer and Gauge", British Patent 1,225,272, **1971**.

22. March, R.E.; Hughes, R.J. *Quadrnpole Storage Mass Spectrometry* (Wiley, New York, **1989**).

23. Wuerker, R.F.; Shelton, H.; Langmuir. R.V. *Journal of Applied Phyics*, **1959**, *30*, 342.

24. Kaiser, R.E., Jr., Cooks, R.G., Stafford, G.C., Jr., Syka, J.E.P., Hemberger, P.H. *International Jonrnal of Mass Spectrometry and Ion Processes*, **1991**, *106*, 79.

25. Weber-Grabau, M.; Kelly, P.E.; Bradshaw, S.C.; Hoekman, D.J. *Proceedings of the 35th ASMS Conference on Mass Spectrometry and Allied Topics,* Denver, CO, **1987**, 263.

26. Ingendoh, A.; Karas, M.; Hillenkamp, F.; Giessmann, U. *International Journal of Mass Spectrometry and Ion Processes*, **1994**, *131*, 345-354.

27. Spengler, B.; Kirsch, D.; Daufmann, R. *Rapid Communications in Mass Spectrometry,* **1991**, *5*, 198-202.

28. Heller, D.N.; Lys, I.; Cotter, R.J.; Uly, O.M. *Analytical Chemistry,* **1989**, *61*, 1083.

29. Chambers, D.M.; Goeringer, D.E.; McLuckey, S.A.; Glish, G.L. *Analytical Chemistry,* **1993**, *65*, 14.

30. Chambers, D.M.; Goeringer, D.E.; McLuckey, S.A.; Glish, G.L. in *Proceedings of the 40th ASMS Conference on Mass Spectrometry and Allied Topics*, Washington, DC, **1992**, 1747-1748.

31. Vargas, R.R.; Yost, R.A. in *Practical Aspects of Ion Trap Mass Spectrometry, Volnme II. Ion Trap Instrumentation,* R.E. March, ; J.F.J. Todd, ed. CRC Press, Boca Raton, **1995**, 217.

32. Vargas, R.R. *Development and Application of a Laser Desorption Ionization/ Quadrupole Ion Trap Mass Spectrometer.* Ph.D. dissertation. Unversity of Florida, Gainesville, FL. **1993**.

33. Bier, M.E.; Schwartz, J.C.; Jardine, I.; Stafford, G. in *Proceedings of the 40th ASMS Conference on Mass Spectrometry and Allied Topics*, Washington, DC, **1992**, 1017-1018 .

34. Qin, J.; Steenvoorden, R.J.J.M.; Chait, B.T.; *Analytical Chemistry*, **1996**, *68*, 1784.

35. Dahl, D.A.; Delmore, J.E. SIMION; Idaho National Engineering Laboratory: Idaho Falls, ID, **1988**.

36. Luo, C.; Williams, P. in *Proceedings of the 41st ASMS Conference on Mass Spectrometry and Allied Topics*, San Francisco, CA, **1993**, 661.

37. Griffin, T.P.; Yost, R.A. in *Proceedings of the 43rd ASMS Conference on Mass Spectrometry and Allied Topics*, Atlanta, GA, **1995**, 986.

38. Gilfrich, N.L.; Brown, R.S. in *Proceedings of the 39th ASMS Conference on Mass Spectrometry and Allied Topics*, Nashville, TN, **1991**, 346-347.

39. Ganten, D.; Hermann, K.; Bayer, C.; Unger, T. *Science*, **1983**, *22*

40. Williams, J.D.; Cox, K.A.; Schwartz, J.C.; Cooks, R.G. High Mass, High Resolution Mass Spectrometry in *Practical Aspects of Ion Trap Mass Spectrometry, Volume II. Ion Trap Instrumentation.* R.E. March, ; J.F.J. Todd, ed. CRC Press, Boca Raton, **1995**, 25.

41. Covey, J.P.; Haas, J.; Sheng, L.-S.; Weigt, D.; Campana, J.E. in *Proceedings of the 41st ASMS Conference on Mass Spectrometry and Allied Topics*, San Francisco, CA, **1993**, 651.

42. Qin, J.; Steenvoorden, R.J.J.M.; Chait, B.T. in *Proceedings of the 42nd ASMS Conference on Mass Spectrometry and Allied Topics*, Chicago, IL, **1994**, 687.

43. McLuckey, S.A.; Van Berkel, G.J.; Glish, G.L.; Schwartz, J.C. in *Practical Aspects of Ion Trap Mass Spectrometry, Volume II. Ion Trap Instrumentation.* R.E. March, ; J.F.J. Todd, ed. CRC Press, Boca Raton, **1995**, 101.

44. Roepstorff, P.; Fohlman, *J. Biomedical Mass Spectrometry*, **1984**, *11*, 601.

45. Todd, J.F.J.; Bexon, J.J.; Smith, R.D.; Weber-Grabau, M.; Kelly, P.E.; Syka, J.E.P.; Stafford, G.C.; Bradshaw, S.C. in *Proceedings of the 16th Meeting of the British Mass Spectrometry Society,* York, U.K., **1987**, 206-209.

46. Tucker, D.B.; Hameister, C.H.; Bradshaw, S.C.; Hokeman, D.J.; Weber-Grabau, M. in *Proceedings of the 36th ASMS Conference on Mass Spectrometry and Allied Topics*, San Francisco, CA, **1988**, 662-663.

47. Gronowska, I.W.; Paradisi, C.; Traldi, P.; Vettori, U. *Rapid Communications in Mass Spectrometry,* **1990**, *4*, 306-313.

48. Yates, N.A.; Yost, R.A.; Bradshaw, S.C.; Tucker, D.B. in *Proceedings of the 39th ASMS Conference on Mass Spectrometry and Allied Topics*, Nashville, TN, **1991**, 132-133

49. Eades, D.M.; Yates, N.A.; Yost, R.A. in *Proceedings of the 39th ASMS Conference on Mass Spectrometry and Allied Topics*, Nashville, TN, **1991**, 1491-1492.

50. Yates, N.A.; Griffin, T.P.; Yost, R.A. in *Proceedings of the 41st ASMS Conference on Mass Spectrometry and Allied Topics*, San Francisco, CA, **1993**, 444.

51. Soni, M.H.; Cooks, R.G. *Analytical Chemistry,* **1994**, *66*, 2488-2496.

52. McLuckey, S.A.; Goeringer, D.E.; Glish, G.L. *Analytical Chemistry,* **1992**, *64*, 1455-1460.

53. Kelly, P.E.; Hoekman, D.J.; Bradshaw, S.C., in *Proceedings of the 41st ASMS Conference on Mass Spectrometry and Allied Topics*, San Francisco, CA, **1993**, 453.

54. Schwartz, J.C., Jardine, I. *Rapid Communications in Mass Spectrometry,* **1992**, *6*, 313-317.

55. Kaiser, R.E.; Cooks, R.G.; Syka, J.E.P.; Stafford, G.C.; *Rapid Communications in Mass Spectrometry,* **1990**, *4*, 30.

56. Yates, N.A. *Methods for Gas Chromatography - Tandem Mass Spectrometry on the Quadrupole Ion Trap.* Ph.D. dissertation. Unversity of Florida, Gainesville, FL. **1994**, 187.

57. Huang, Y.; Pasa-Tolic, L.; Kim, H.S.; Guan, S.; Marshall, A.G. in *Proceedings of the 42nd ASMS Conference on Mass Spectrometry and Allied Topics*, Chicago, IL, **1994**, 687.

58. Hunt, D.F.; Yates, J.R. III; Shabanowitz, J.; Winston, S.; Hauer, C.R. *Procreedings o the National Academy of Sciences of the United States of America,* **1986**, *83*, 6233-6237.

59. Yates, N.A., Yost, R.A., Bradshaw, S.C., Tucker, D.B. in *Proceedings of the 39th ASMS Conference on Mass Spectrometry and Allied Topics*, Nashville, TN, **1991**, 1489-1490.

60. American Cancer Society Annual Report, **1995**.

61. Kingston, D.; Samaranayake, G.; Ivey, C. *Journal of Natural Products*, **1990**, *53*, 1-12.

62. Rowinsky, E.; Donehower, R. *Pharmcol. Ther.* **1991**, *52*, 35-84.

63. Holton, R.A.; Somoza, C.; Kim, H.-B.; Liang, F.; Biediger, R.J.; Boatman, P.D.; Shindo, M.; Smith, C.C.; Kim, S.; Nadixadeh, H.; Suzuki, Y.; Tao, C.; Vu, P.; Tang, S.; Zhang, P.; Murthi, K.K.; Gentile, L.; Liu, J. *Journal of the American Chemical Society*, **1994**, *116*, 1597.

64. Nicolaou, K.C.; Yang. Z.; Liu, J.J.; Ueno, H.; Nantermet, P.G.; Guy, R.K.; Clairborne, C.F.; Paulvannan, K.; Sorensen, E.J.; *Nature*, **1994**, *367*, 630.

65. Gumoleu, P.; Chevallier, B.; Kerbrat, P. Proceedings of the American Society of Clinical Onocology, **1993**, *12*, 56.

66. Kerns, E.H.; Volk, K.J.; Hill, S.E.; Lee, M.S. *Journal of Natural Products*, **1994**, *57*, 1399.

67. *The New Lexicon Illustrated Medical Encyclopedia*, (8th ed.), R.E. Rothenberg, Ed. Lexicon Publications, Inc., New York, **1988**, 323.

68. Johnson, J.V.; Yost, R.A. *Analytical Chemistry,* **1985**, 51, 758A-768A.

BIOGRAPHICAL SKETCH

Matthew M. Booth, son of Richard L. and Mary Ann Booth, was born in Warren, Michigan, on June 16, 1960. He graduated from Salesian Preparatory High School in 1978. From 1978 to 1982 he attended Purdue University in West Lafayette, Indiana, where he graduated with a Bachelor of Science degree in chemistry (ACS accredited). He then attended Eastern Michigan University in Ypsilanti, Michigan, from 1982 to 1984, graduating with a Master of Science in Chemistry degree. His research towards the MS degree consisted of analyzing ancient Roman coins using a variety of techniques (X-ray fluorescence and atomic absorption at Eastern Michigan and neutron activation analysis at the nuclear reactor at the University of Michigan) under the direction of Dr. Giles F. Carter. During the second year of the MS program, Matthew took part in a cooperative education program offered by EMU (in order to gain some real-world experience), working at Clayton Environmental Laboratory in Detroit, Michigan. Upon graduation, he worked as a GC/MS analyst and technical supervisor at the Environmental Research Group in Ann Arbor, Michigan. He moved to Orlando Laboratories in Orlando, Florida, in 1986 as the GC/MS group leader and organics laboratory manager. He joined Finnigan Corp. in 1987 as a consulting chemist in their Chicago office, where he performed instrumentation demonstrations, technical support, and on-site training in the operation of Finnigan GC/MS systems for environmental analyses. In 1989 he was promoted to the position of environmental marketing specialist (serving as the defacto environmental marketing manager and damage-control specialist) and moved to the corporate offices of Finnigan in San Jose, California. He left Finnigan in 1991 to begin

his Ph.D. degree at the University of Florida under the direction of Dr. Richard A. Yost (realizing he enjoyed creating and breaking instruments- in particular ion trap mass spectrometers- far more than he enjoyed marketing them). While working toward the Ph.D. degree, he married Pauline R. Schneider, started a family with the birth of their son, Christopher, and purchased a home in Gainesville, Florida. During the last three years of the Ph.D. program, he was working full-time as the Air Toxics Group Leader at Environmental Science and Engineering (ESE) in Gainesville.

Upon completion of his Ph.D. degree, Matthew plans on working as a reasearch associate in the laboratory of Dr. Yost, and will be consulting with ESE as part of their Air Toxics Laboratory.

I certify that I have read this study and that in my opinion it conforms to acceptable standards of scholarly presentation and is fully adequate, in scope and quality, as a dissertation for the degree of Doctor of Philosophy.

Richard A. Yost, Chairman
Professor of Chemistry

I certify that I have read this study and that in my opinion it conforms to acceptable standards of scholarly presentation and is fully adequate, in scope and quality, as a dissertation for the degree of Doctor of Philosophy.

James D. Winefordner
Graduate Research Professor of Chemistry

I certify that I have read this study and that in my opinion it conforms to acceptable standards of scholarly presentation and is fully adequate, in scope and quality, as a dissertation for the degree of Doctor of Philosophy.

Robert T. Kennedy
Associate Professor of Chemistry

I certify that I have read this study and that in my opinion it conforms to acceptable standards of scholarly presentation and is fully adequate, in scope and quality, as a dissertation for the degree of Doctor of Philosophy.

Nigel G. Richards
Associate Professor of Chemistry

I certify that I have read this study and that in my opinion it conforms to acceptable standards of scholarly presentation and is fully adequate, in scope and quality, as a dissertation for the degree of Doctor of Philosophy.

Sheldon M. Schuster
Professor, Biochemistry and Molecular Biology

This dissertation was submitted to the Graduate Faculty of the Department of Chemistry in the College of Liberal Arts and Sciences and to the Graduate School and was accepted as partial fulfillment of the requirements for the degree of Doctor of Philosophy.

December, 1996

_____

Dean, Graduate School

LD
1780
1996
.B725

UNIVERSITY OF FLORIDA
3 1262 08557 0298